Award Number: **W81XWH-05-2-0027**

TITLE: IMPACT: Imaging and Molecular Markers for Patients with Lung Cancer: Approaches with Molecular Targets, Complementary/Innovative Treatments, and Therapeutic Modalities"

PRINCIPAL INVESTIGATOR: George Simon, M.D.

CONTRACTING ORGANIZATION:
The University of Texas M.D. Anderson Cancer Center
Houston, TX 77030

REPORT DATE: April 2016

TYPE OF REPORT: Final Report

PREPARED FOR: U.S. Army Medical Research and Materiel Command
Fort Detrick, Maryland 21702-5012

REPORT DOCUMENTATION PAGE

Form Approved
OMB No. 0704-0188

1. REPORT DATE *(DD-MM-YYYY)*	**2. REPORT TYPE**	**3. DATES COVERED** *(From - To)*
April 2016	Final Report	1 Feb 2005- 31 Jan 2016

4. TITLE AND SUBTITLE

IMPACT: Imaging and Molecular Markers for Patients with Lung Cancer: Approaches with Molecular Targets, Complementary/Innovative Treatments, and Therapeutic Modalities"

5a. CONTRACT NUMBER
W81XWH-05-2-0027

5b. GRANT NUMBER

5c. PROGRAM ELEMENT NUMBER

6. AUTHOR(S)
George Simon, M.D.

email: gsimon@mdanderson.org

5d. PROJECT NUMBER

5e. TASK NUMBER

5f. WORK UNIT NUMBER

7. PERFORMING ORGANIZATION NAME(S) AND ADDRESS(ES)

The University of Texas M.D. Anderson Cancer Center
Houston, TX 77030

Email: gsimon@mdanderson.org

8. PERFORMING ORGANIZATION REPORT NUMBER

9. SPONSORING / MONITORING AGENCY NAME(S) AND ADDRESS(ES)
U.S. Army Medical Research and Materiel Command
Fort Detrick, Maryland 21702-5012

10. SPONSOR/MONITOR'S ACRONYM(S)

11. SPONSOR/MONITOR'S REPORT NUMBER(S)

12. DISTRIBUTION / AVAILABILITY STATEMENT
Approved for public release; distribution unlimited

13. SUPPLEMENTARY NOTES

14. ABSTRACT

The projects in this proposal specifically target several signal transduction pathways known to be critical for NSCLC pathogenesis including the EGFR pathway and the more downstream ras/raf/Mek/ERK pathway. These projects combine targeted approaches using molecular and imaging techniques to validate activity against a target and monitor response using imaging modalities specific to the receptor using either small molecules or targeted peptide approaches. This document serves as the final report for this grant, and details the results of the clinical trial that was the central focus of the last active project (Project 2)as well as provides summaries of the final reports for each of the other projects and cores that completed aims in previous years.

15. SUBJECT TERMS
Lung cancer, molecular markers, molecular imaging, targeted therapy

16. SECURITY CLASSIFICATION OF: Unclassified			**17. LIMITATION OF ABSTRACT**	**18. NUMBER OF PAGES**	**19a. NAME OF RESPONSIBLE PERSON**
a. REPORT U	**b. ABSTRACT** U	**c. THIS PAGE** U	UU	88	USAMRMC
					19b. TELEPHONE NUMBER *(include area code)*

Standard Form 298 (Rev. 8-98)
Prescribed by ANSI Std. Z39.18

TABLE OF CONTENTS

IMPACT: Imaging and **M**olecular Markers for **P**atients with **L**ung **C**ancer: **A**pproaches with Molecular Targets, **C**omplementary, Innovative and **T**herapeutic Modalities

INTRODUCTION

Lung cancer is the most prevalent cancer worldwide and the leading cause of cancer-related mortality in both men and women in the United States. Conventional multimodality therapies (surgery, radiation and chemotherapy) have reached a therapeutic ceiling in improving the five-year overall survival rate of non-small cell lung cancer (NSCLC) patients, clinically in large part due to chemo- and radiation-resistant locoregional and metastatic spread but ultimately due to poor understanding of the disease and its resistance to the therapy.

Lung cancer is a heterogeneous disease, resulting from accumulated genetic abnormalities over years, which thus requires a coordinated attack in a truly integrated fashion on multiple altered signal pathways. Emerging targeted therapy aims to target key molecular abnormalities in cancer and has succeeded in some tumor types such as chronic myeloid leukemia (CML) (Druker et al., 2004; Druker and Sawyers et al., 2001; Druker and Talpaz et al., 2001), gastrointestinal stromal tumor (Demetri et al., 2002), colon cancer (Hurwitz et al., 2003), and breast cancer (Howell et al., 2005). Thus, the incorporation of targeted therapy into conventional treatments appears to be a new promising approach to treatment of lung cancer.

The program project IMPACT has proposed to integrate targeted therapy in the lung cancer research program when initial clinical results showed disappointing response rates and survival benefit of epidermal growth factor receptor (EGFR) inhibitor gefitinib (Iressa™) for non-selected lung cancer patients (Herbst et al., 2002, 2003, 2004; Herbst, 2004; Kris et al., 2003; Giaccone et al., 2004). It aims to validate molecular mechanisms of targeted agents alone and in combination with chemo- and/or radiation therapies in preclinical and clinical settings. It also aims to develop effective molecular imaging and cancer cell-targeted peptide-based delivery tools to help improve efficacy of the targeted agents. Specifically, our objectives are:

- To validate preclinically and clinically several key signaling pathways and their agents for therapeutic potentials alone or in combination with each other or with chemo and /or radiotherapy
- To explore applications of molecular imaging for targeted therapy and identify cancer cell-targeted peptides for systemic delivery of therapeutic and imaging agents
- To discover and evaluate new molecular abnormalities and therapeutic predictors in lung cancer
- To develop an educational program for teens and young adults for smoking risk and resultant lung cancer occurrence.

IMPACT is composed of 6 research projects, 1 Biostatistics Core, 1 Molecular Pathology Core, 1 Molecular Imaging Core, 2 career development projects, and 2 developmental research projects. We note that a number of no-cost extensions for this grant have been approved to allow final completion of the clinical activities proposed for Project 2 in this report.

Project 1: Targeting epidermal growth factor receptor signaling to enhance response of lung cancer to therapeutic radiation.

(PI and co-PI: Raymond E. Meyn, Ph.D., Ritsuko Komaki, M.D.)

In spite of significant technical advances including intensity-modulated radiation therapy (IMRT) and chemoradiation, locally advanced lung cancer continues to have a dismal prognosis as many patients' tumors appear to be resistant to radiation therapy. The molecular basis for radiation resistance is not fully understood, but tumor cells have an enhanced survival response that involves increased capacity for DNA repair and suppressed apoptosis. Both apoptosis propensity and DNA repair capacity are thought to be partly controlled by the upstream signal transduction pathways triggered by EGFR activation, which is constitutively activated in many NSCLCs, and its activation leads to a radiation-resistant phenotype. We hypothesize that the response of NSCLC to radiation can be improved through the use of inhibitors of EGFR signaling.

Aim 1 To test the combination of external beam radiation and the selective EGFR-tyrosine kinase inhibitor erlotinib (Tarceva) in locally advanced NSCLC.

Summary of Research Findings

Feb 2011 Report: The clinical trial completed accrual with a total of 48 patients between November 2007 and July 2010. Seventeen patients were female (37%), the median age was 64 years, ranging from 46 years to 81 years. All patients had stage III medically or surgically (53%) inoperable lung cancer. Twenty-three patients (48%) had adenocarcinoma. All patients had good performance status of KPS 80 or higher (ECOG 0 or 1). Sixty percent of these patients were former- and 12.5% were never-smokers.

At present time, 46 patients have completed the entire treatment and they are evaluable for their response. These patients have an 80% response rate (CR 30% and PR 50%), with 9% of patients with stable disease or progressive disease, based on RECIST.

Although follow-up time is still short, with median follow-up 11 months for patients treated, overall survival of this trial is promising compared to chemoradiotherapy alone. The comparison was made for stage III NSCLC patients who were treated with 63 Gy in 7 weeks radiotherapy and concurrent weekly taxol and carboplatin, the same chemoradiation regimen as ID 2005-1023 but without Tarceva that was added to the regimen for this trial. Overall survival (at one year) is 85% in ID 2005-1023 (Taxol/Carboplatin and concurrent RT with Tarceva) compared to the historical control rate of 67% of patients who were treated by weekly Taxol/Carboplatin and concurrent RT without Tarceva (P=0.03).

Toxicity

Toxicity data is available for 46 patients either having completed therapy, or who are presently receiving treatment. There have been no treatment-related deaths (Grade 5), although one patient died of pulmonary emboli which could not be differentiated from treatment-related or disease-related. Severe acute toxicities (grade 3 or higher according to CTC.3) related to treatments were recorded as the following events:

- Treatment skin reaction: Grade 2 in 6 patients and Grade 3 in 6 patients
- Acne, Grade 2 in 24 patients
- Acne, Grade 3 in 2 patients
- Diarrhea, Grade 2 in 4 patients
- Diarrhea, Grade 3 in 2 patient

- Pneumonitis, Grade 3 in 2 patients; Grade 4 in 1 patient
- Leukopenia, Grade 3 in 12 patients, Grade 4 in 1 patient
- Neutropenia Grade 3 in 5 patient, Grade 4 in 2 patients
- Thrombocytopenia, Grade 3 in 1 patient
- Hypomagnesemia, Grade 3 in 1 patient
- Hypokalemia, Grade 3 in 2 patient
- Pneumonia, Grade 3 in 7 patients
- Dehydration, Grade 3 in 3 patients.

Once the clinical trial reached the target patient accrual, we elected to extend the project to test whether EMT may govern the radiosensitizing abilities of EGFR antagonists and may also directly regulate tumor cell radiosensitivity itself. We hypothesized that these relationships extend to NSCLC patients treated with EGFR inhibitors, e.g., erlotinib, in combination with radiation and to patients treated with radiotherapy alone. To do this, we enlisted the expertise of Dr. Ignacio Wistuba (Core C) to analyze the biopsy specimens from the phase II clinical trial for biomarkers associated with response to EGFR TKI and tumor's epithelial or mesenchymal status and correlate the results with patient response. Tumor response in this trial was 14 (30%) CR, 23 (50%) PR, and 9 (20%) stable or progressive disease. Five in 41 pts (12%) had EGFR mutation (EGFR-M), all adenocarcinoma with 2 females, compared to none with squamous histology (p=0.05). At present time, 39.1% (18/46) of patients are alive without any evidence of disease, 34.8% (16/46) of patients are alive with disease, and 26.1% (12/46) of patients are dead. The median overall survival (OS) and progressive-free survival (PFS) were 25.8 months & 13.6 months, respectively. One-year & 2-year OS rates were 84% & 75%, respectively, and 1- and 2-year PFS rates were 54% & 32%, respectively. We plan to analyze the pre-treatment biopsy specimens and correlate findings with response as well as with patterns of failure outside the scope of this project.

Aim 2 To test the hypothesis that activation of the EGFR pathway leads to radiation resistance in NSCLC cells due to an enhanced capacity for repairing DNA lesions.

Summary of Research Findings

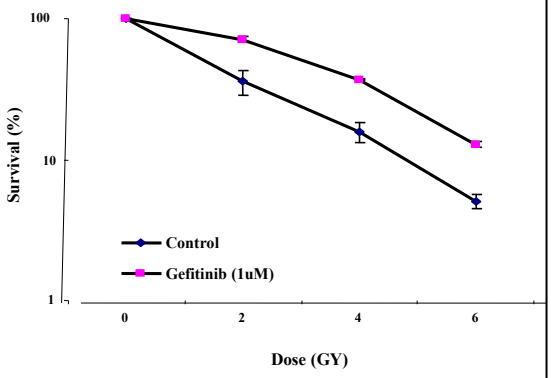

Figure 1: Gefitinb has a radioprotective effect on some NSCLC. H322 cells were treated with gefitinib (1 μM for 24 h) and assessed for radiosensitization by clonogenic cell survival. Average of three independent experiments each plated in triplicate.

Feb 2009 Report: As reported previously, 2 NSCLC cell lines, A549 and H1299, displayed a significant radiosensitization by gefitinib correlating with a gefitinib-mediated inhibition of radiation-induced DNA double-strand breaks (DSBs). Since then, we have extended this analysis to other cell lines including additional NSCLC lines and normal cells as well. Although some other NSCLC cell lines are radiosensitized by gefitinib, we also discovered that some lines are rendered radioresistant by gefitinib treatment. For example, survival curves for H322 cells have shown that gefitinib induces a rather profound degree of radioresistance (Fig. 1). A similar effect is seen in several normal cell lines including normal human bronchial epithelial cells (HBECs) (Fig. 2).

Although we haven't analyzed all of these different cell lines for the effects of gefitinib on DSB repair, we have examined the results on the H322 line, and gefitinib appears to accelerate the repair of DSBs compared to the radiation alone case (Fig. 3). During this past year, we have begun an extensive investigation to uncover the basis for these differences in the ability of NSCLC cell lines to be radiosensitized by EGFR inhibitors. As will be presented in the next section, we hypothesize that this difference is related to whether the cell line is epithelial-like or mesenchymal-like.

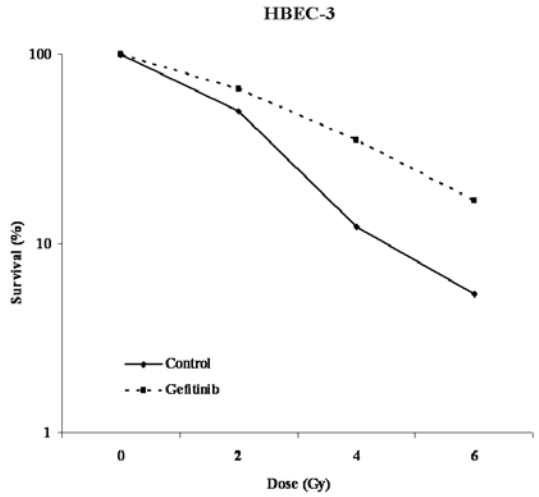

Figure 2. Effect of Gefitinib on radiosensitivity of normal cells. HBEC-3 cells were treated with gefitinib (1μM for 24 h) and assessed for radiosensitization by clonogenic cell survival immediately. Each data point represents the average of three independent experiments each plated in triplicate.

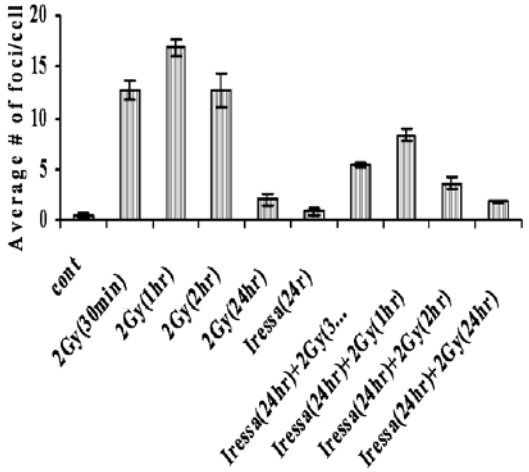

Figure 3. Gefitinib enhances the repair of radiation-induced DSBs detected on the basis of γ-H2AX foci. H322 cells growing on cover slips in 35 mm dishes were exposed to gefitinib (1μM) for 24 h, irradiated (2 Gy), and fixed at the specified times for analysis of nuclear γ-H2AX foci using immunofluorescence microscopy. Quantitative analysis of foci present in the cells following various treatments is presented. *Columns,* mean of three independent experiments. Bar: SE

Aim 3 To test the hypothesis that clinically useful inhibitors of EGFR signaling abrogate DNA repair capacity, restore apoptotic response and radiosensitize NSCLC cells.

Summary of Research Findings

Feb 2009 Report: Several recently published papers have reported that the sensitivity of NSCLC cells to antagonists of the EGFR correlates with whether they have undergone the epithelial-to-mesenchymal transition (EMT). Specifically, cells that have undergone EMT proved resistant to gefitinib or erlotinib as a single agent. We have now observed an EMT-related relationship amongst our NSCLC lines, some of which were the same lines as in these published reports. Cell lines that were reported to be epithelial-like (sensitive to gefitinib) were rendered radioresistant by the drug in our studies and cell lines reported to be mesenchymal-like (resistant to gefitinib) were radiosensitized by the drug in our experiments. This suggests that the activities of gefitinib for drug-induced cytotoxicity and drug-modulation of radiosensitivity are different. Based on the correlation between our observed results and reported results in the literature regarding the same cell lines, we decided to expand our panel of cell lines to include additional lines identified in those reports. Thus, we have now analyzed a total of 8 NSCLC cell lines for their response to a pre-irradiation treatment with 1 μM of gefitinib. Although complete clonogenic survival curves were generated for all 8 lines with and without gefitinib, we have summarized the results in Figure 4 where we present the SF_2 values for all of these survival curves (error bars omitted from Fig. 4). However, each value is the average of 3 independent experiments, each plated in triplicate. Statistical analysis indicated that the gefitinib treated vs. non-gefitinib treated value was significant at the $p<.05$ level for each cell line.

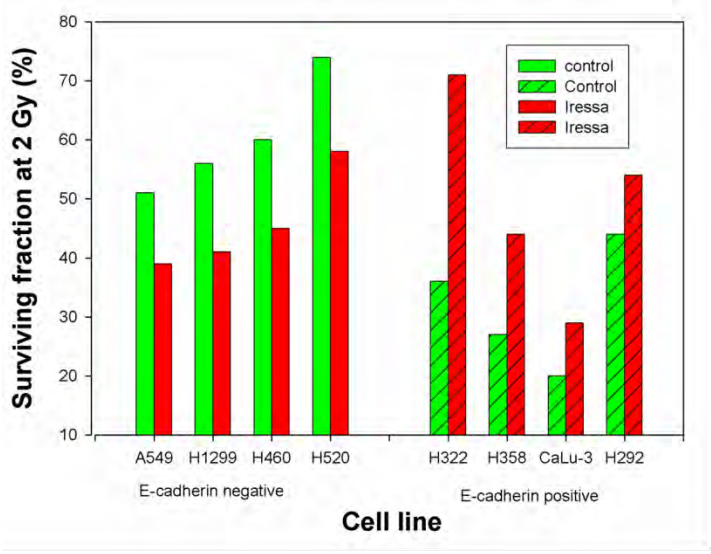

Figure 4. Comparison of SF2 values in E-cadherin positive versus E-cadherin negative cell lines following exposure to Gefitinib. Cells were exposed to Gefitinib (1μM) for 24 h following which they were assessed for radiosensitization by clonogenic cell survival.

The EMT is primarily indicated and, in at least some cases, dictated by the presence or loss of E-cadherin expression. To validate that the cell lines in our NSCLC panel had or had not undergone EMT, we performed immunoblot analysis of E-cadherin expression for all lines under study. The results indicated that, as reported for these same lines in the literature, the H322, H358, H292 and Calu3 lines express E-cadherin and the A549, H1299, H460, Calu6 and H520 lines do not (Fig. 5). The HBECs, as expected, express E-cadherin (not shown). Cells that have undergone EMT and have lost E-cadherin sometimes express mesenchymal markers such as vimentin, although this is not an absolute marker for EMT. We assessed vimentin in our panel of cell lines; all of the lines with the mesenchymal phenotype express vimentin except A549 cells, which express N-cadherin and fibronectin (2 other mesenchymal markers) instead. One cell line with epithelial phenotype also expresses vimentin, illustrating that this marker is not 100% specific compared to E-cadherin for EMT status.

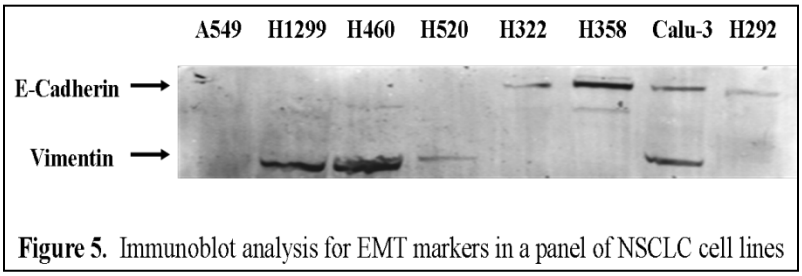

Figure 5. Immunoblot analysis for EMT markers in a panel of NSCLC cell lines

Although we have established the relationships of EMT status to tumor cell radiosensitivity in our panel of 8 NSCLC lines (the epithelial lines, H358, H322, CaLu-3 and H292, have SF_2 values of <0.45 and the mesenchymal lines, A549, H1299, H460 and H520, have SF_2 values of >0.50), this is an observed correlation and does not prove an absolute relationship between E-cadherin expression and cell sensitization. Therefore, we have begun a series of experiments to test whether restoring E-cadherin expression in the mesenchymal-like lines sensitizes them to radiation. We have transfected H1299 cells with a *CDH1*-expression vector and isolated clones based on drug-selection markers in the vector. Several clones were selected and analyzed for E-cadherin expression. One such clone, H1299-CDH1 (clone #1), has subsequently been tested for radiosensitivity compared to the parental line and the results are presented in Fig. 6. Although this experiment will have to be repeated and additional clones tested, this result suggests that restoration of E-cadherin expression in mesenchymal-like NSCLC cells produces a radiosensitizing effect.

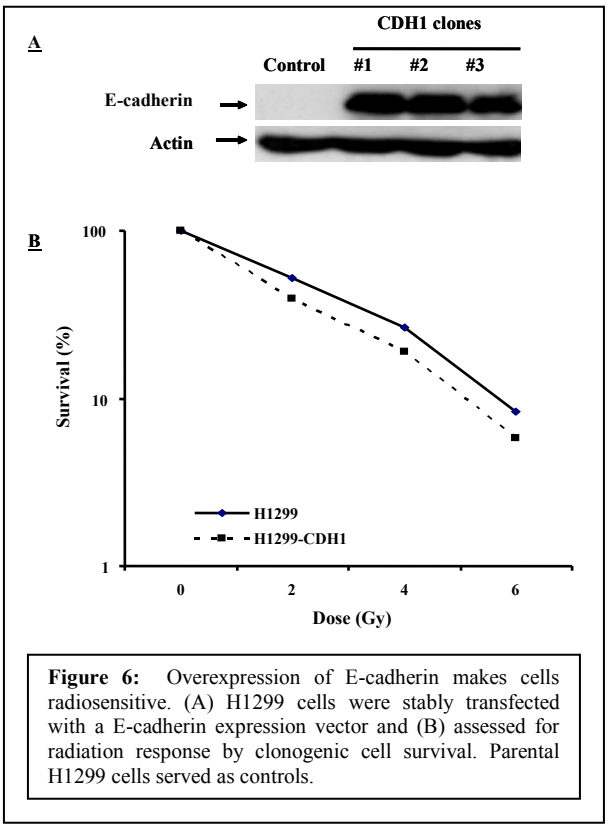

Figure 6: Overexpression of E-cadherin makes cells radiosensitive. (A) H1299 cells were stably transfected with a E-cadherin expression vector and (B) assessed for radiation response by clonogenic cell survival. Parental H1299 cells served as controls.

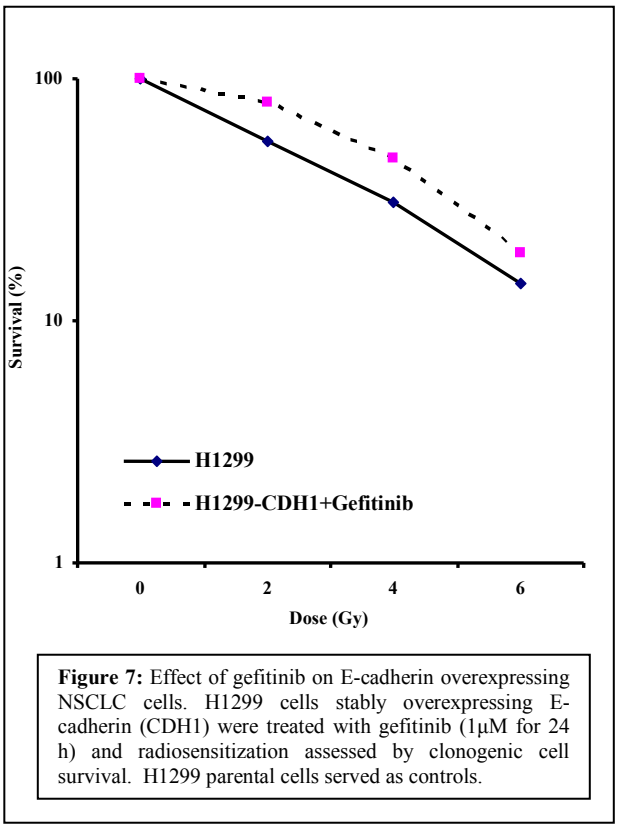

Figure 7: Effect of gefitinib on E-cadherin overexpressing NSCLC cells. H1299 cells stably overexpressing E-cadherin (CDH1) were treated with gefitinib (1μM for 24 h) and radiosensitization assessed by clonogenic cell survival. H1299 parental cells served as controls.

Using the same clone of H1299 cells with restored E-cadherin expression, described above, we tested the effects of a gefitinib pretreatment compared to parental cells. The results of this experiment indicate that instead of being sensitized to radiation, as shown for the parental cells in Figure 1, the same pretreatment with gefitinib exerts a radioprotective effect on these H1299-CDH1 cells (Fig. 7). Again, these experiments will have to be repeated and additional clones produced and analyzed. Moreover, this H1299-CDH1 clone was compared to parental cells in these experiments and we are in the process of making empty-vector control cell lines to use in further studies related to these questions. E-cadherin expressing clones of A549 cells have been produced and initial testing of one clone suggests that while gefitinib pretreatment does not render the A549-CDH1 cells radioresistant, it no longer induces a radiosensitizing effect compared to results in parental cells as shown in Figure 1 (data not shown).

Aim 4 To test the hypothesis that targeting both EGFR and its downstream signaling pathways will have at least an additive radiosensitizing effect on NSCLC.

Summary of Research Findings

Feb 2009 Report: It is now understood that resistance to EGFR inhibitors such as gefitinib and erlotinib may be due to compensatory signaling pathways. Two such pathways are now known: the c-Met and IGF1R mediated pathways. During this past funding period, we have continued to examine both of these pathways in order to understand why some cell lines are resistant to radiosensitization by inhibition of EGFR. For these experiments, we have used commercially available inhibitors of c-Met (e.g., SU11274) and of IGF1R (e.g., AG1024).

We examined the ability of both of these inhibitors to radiosensitize NSCLC cell lines. Last year, we reported that the c-Met inhibitor SU11274 has a significant radiosensitizing effect on H1299 cells, and we have extended this finding to H460 cells (Fig. 8). This finding is consistent with the emerging hypothesis that resistance to radiosensitization with EGFR inhibition may be due to compensatory signaling by the c-Met receptor, and that inhibition of c-Met signaling may be a useful strategy for radiosensitizing NSCLC cells either with or without combining with EGFR inhibitors. Similarly, we have shown that the H1299 and H358 cells are potentially radiosensitized by the IGF1R inhibitor, AG1024 (Fig. 9). Thus, inhibition of the IGF1R pathway may also be a viable strategy for enhancing the radiation response of NSCLC cells.

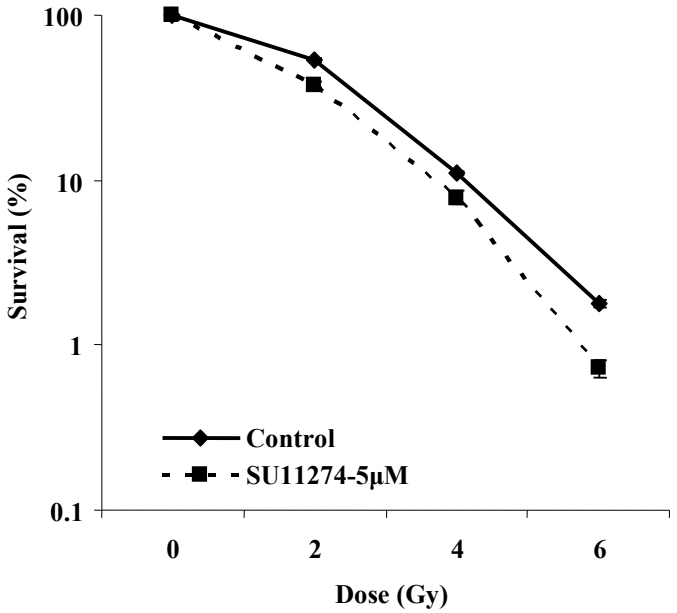

Figure 8: H460 cells are radiosensitized by a c-Met inhibitor. Cells were treated with SU11274 (5μM for 24 h) and assessed for radiosensitization by clonogenic cell survival immediately. Each data point represents the average of two independent experiments each plated in triplicate: solid line, control; dotted line, 5Bar; SE.

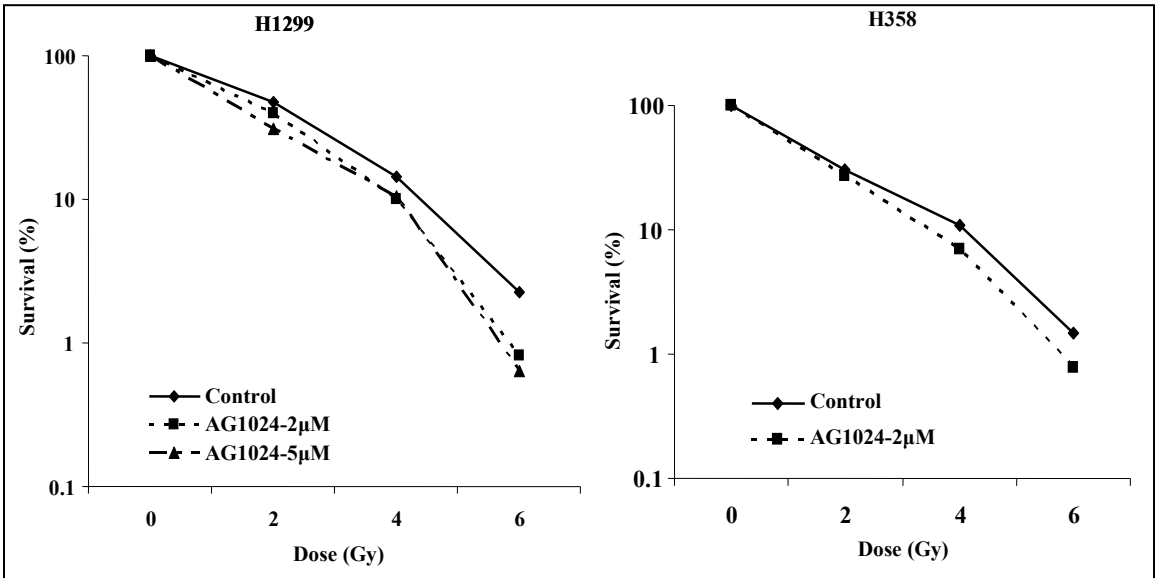

Figure 9: IGF-1R inhibitor radiosensitizes NSCLC cells. H129 and H358 cells were treated with AG1024 (2 or 5 μM for 24 h) and assessed for radiosensitization by clonogenic cell survival immediately.

Aim 5 To test whether the strategies developed in Specific Aims 2-4 have efficacy in a xenograft tumor model.

Summary of Research Findings

Feb 2009 Report: We also investigated the ability of erlotinib to mediate its radiosensitizing effect *in vivo*. Xenograft tumors were established by s.c. injection of 5 x 10^6 viable H1299 cells, suspended in PBS, into the hind legs of 6-8 week-old athymic nude mice (nu/nu; Charles River). Treatment was initiated when the tumors reached 100mm^3 with either erlotinib alone (60mg/kg daily for a total of nine doses), radiation alone (5 Gy), or erlotinib (60mg/kg daily) plus radiation. For *in vivo* radiation treatments, animals bearing xenograft tumors were irradiated while anesthetized using a ^{60}Co teletherapy unit. Radiation was given 24 h after the last injection of erlotinib. Tumor growth delay was assessed following treatment. Tumors were measured every other day in two orthogonal dimensions, and the tumor volume was estimated assuming an ellipsoid shape. Animals were sacrificed when the tumor volume reached 1000mm^3. A modest tumor growth delay was observed in the group that received erlotinib plus radiation treatment when compared with radiation or erlotinib treatments alone (Fig. 10).

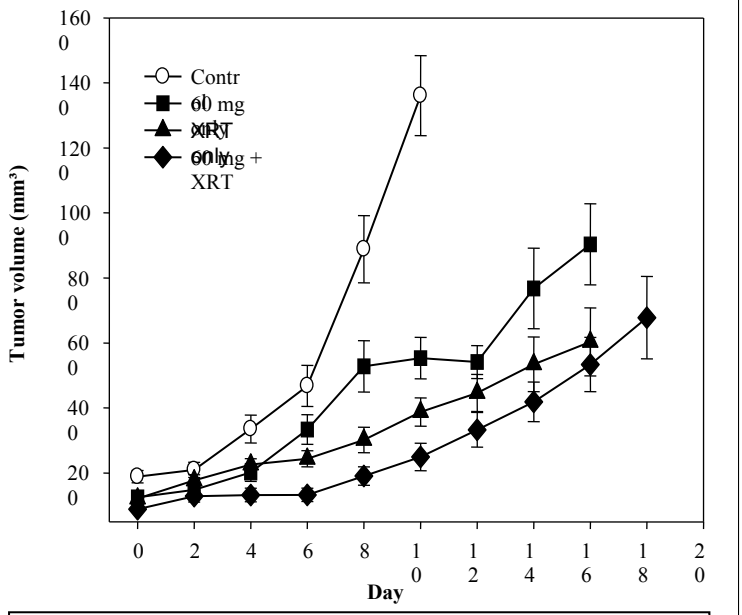

Figure 10: Response of H1299 xenograft tumors to erlotinib plus radiation.

Key Research Accomplishments

- Entered 22 patients onto the erlotinib (Tarceva) plus radiotherapy for locally advanced NSCLC trial and completed evaluation of 12 of these patients.
- Discovered relationship between the epithelial-to-mesenchymal transition and radiosensitivity of NSCLC cells.
- Demonstrated that pretreatment with gefitinib exerts a radioprotection of H1299-CDH1 cells.
- Demonstrated that small molecule inhibitors of both c-Met and IGF-1R produce a significant radiosensitizing effect on NSCLC cells.
- Completed an assessment of the combination of erlotinib (Tarceva) and radiation in a NSCLC xenograft tumor model.

Conclusions

We conclude that the epithelial-to-mesenchymal transition (EMT) plays a significant role in governing not just the intrinsic radiosensitivity of NSCLC cells, but also their sensitivity to inhibitors of the epidermal growth factor receptor (EGFR) and the ability of such inhibitors to radiosensitize these cells. It would be useful to assess the EMT status of patients treated with these combinations. In spite of this finding, results suggest that such combinations might be

useful in the clinic. In addition, we conclude that targeting other growth factor receptors such as the c-Met and IG-F1R receptors may be an alternative strategy to using EGFR inhibitors.

Project 2: Molecular Imaging of EGFR Expression and Activity in Targeting Therapy of Lung Cancer

(PI and co-PI: Juri Gelovani, M.D., Ph.D.; Roy Herbst, M.D., Ph.D.)

Aim 1 To synthesize novel pharmacokinetically optimized ^{124}I and ^{18}F-labeled IPQA derivatives for PET imaging of EGFR kinase activity and conduct *in vitro* radiotracer accumulation studies in tumor cells expressing different levels of EGFR activity.

Summary of Research Findings

Feb 2006 Report: This part of the project was conducted by the Imaging Core. As planned, we synthesized and investigated *in vitro* a number of different morpholino-derivatives of 2-iodo-4-(phenylamino)quinazoline-6-acrylamide (IPQA) derivatives with improved water solubility, which have been selected by additional *in silico* modeling of their structure-activity relationships with active EGFR kinase. Among these compounds, we narrowed the initial library of compounds to

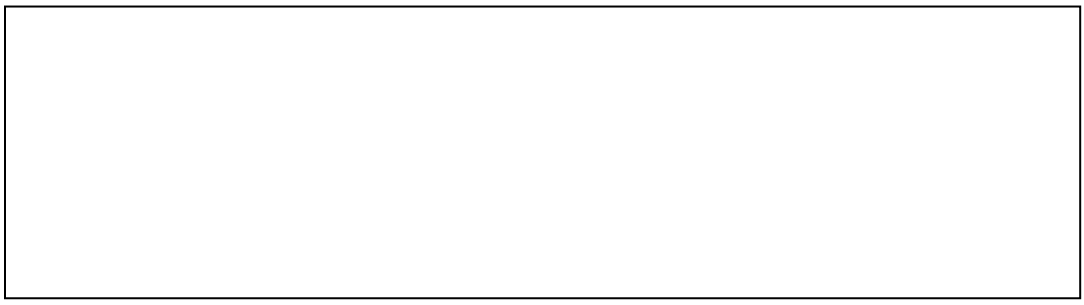

4 optimized lead compounds termed JGAP 1, 5, 11, and 13 (see Imaging Core D). Next, we studied the ability of these compounds to penetrate into tumor cells and inhibit their growth. For this study, we used four human NSCLC cells that express TGFα at different levels and express either the wild-type or mutant EGFR kinases (PC14, H441, H3255, H1975). All newly synthesized compounds demonstrated tumor growth inhibitory activities in low μM concentrations (Table 1), especially in H3255 expressing the L858R active mutant EGFR kinase. Based on these studies, we selected compounds JGAP-5 and JGAP-11 for further studies.

Currently, we are optimizing the radiolabeling procedure for production of [^{124}I]-JGAP-5. During the initial radiolabeling experiments, the [^{124}I]-JGAP-5 was produced at ~60% radiochemical yield. Our goal is to improve radio-iodination yield to >80%, which should be accomplished during the next 2 months.

In addition, we evaluated the uptake and retention of our original lead candidate, the [^{124}I]mIPQA, in the same NSCLC cells (PC14, H441, H3255, H1975). The results showed that [^{124}I]mIPQA rapidly accumulated and was efficiently retained in the H3255 cells and in H441 cells with wild-type EGFR and

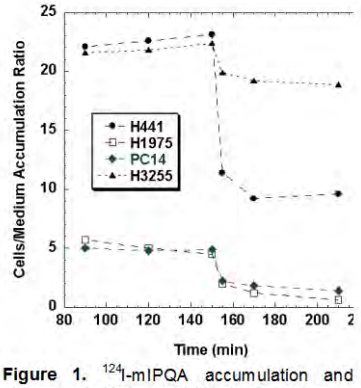

Figure 1. ^{124}I-mIPQA accumulation and clearance in different NSCLC cells in vitro.

high levels of TGFα that activates EGFR in an autocrine manner (Figure 1). The highest level of retention of [^{124}I]mIPQA was observed in H3255 cells, which is consistent with activated EGFR kinase expressed by the cells.
In contrast, low levels of accumulation and rapid washout of [^{124}I]mIPQA were observed in PC14 cells that express wild-type EGFR and in H1975 cells that carry both the activating L858R and resistance-inducing T790M mutations in EGFR kinase domain.

These data are consistent with sensitivity of different NSCLC cell lines to gefitinib (Table 1) and support our hypothesis that
imaging with [^{124}I]IPQA derivatives should allow for identification of tumors with increased EGFR signaling either through activating EGFR mutations or overexpression of TGFα.

Aim 2 **To assess the biodistribution (PK/PD) and tumor targeting by novel ^{124}I and ^{18}F-labeled EGFR kinase-specific IPQA derivatives using PET imaging in orthotopic mouse models of lung cancer and compare *in vivo* radiotracer uptake/retention with phospho-EGFR levels *in situ*.**

Summary of Research Findings

Feb 2010 Report: Differential sensitivity of NSCLC cell lines to EGFR kinase inhibition.
In vitro cell growth of different NSCLC cell lines was differentially inhibited by gefitinib (Iressa™) in a dose-dependent manner (Figure 2A). The most gefitinib-sensitive cell lines were the H3255 cells expressing L858R mutant EGFR, whereas the H1975 cells expressing both the L858R and T790M EGFR mutations were significantly more resistant. The H441 and PC14 cells expressing

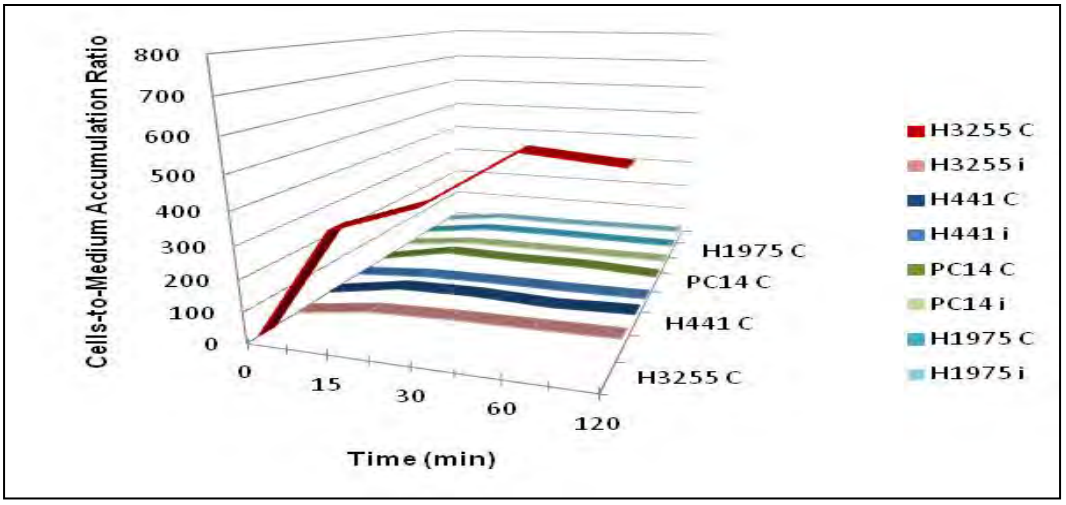

wild-type EGFR exhibited significant resistance to gefitinib.

Differential expression of EGFR in NSCLC cell lines.
The level of total EGFR expression under serum-starved conditions as measured by ELISA was similar in H3255 and H441 cells and significantly higher than levels in PC14 and H1975 cells (Figure 2B).

Preferential accumulation of ^{18}F PEG6-IPQA in NSCLC cells with L858R EGFR mutation.
All four cell lines demonstrated a rapid uptake of ^{18}F-PEG6-IPQA (Figure 2C) during the initial phase (first 20 min). Thereafter, the accumulation of ^{18}F-PEG6-IPQA reached a plateau in

H441, H1975, and PC14 cells at about 30-40 cells/medium concentration ratio. In contrast, in H3255 cells the accumulation of ^{18}F-PEG6-IPQA continued to increase up to one hour and thereafter reached a plateau at cells/medium concentration ratio of 400-600 (Figure 2D). The magnitude of ^{18}F-PEG6-IPQA accumulation in H3255 cells was more than 10-fold higher than in H441 cells, despite the similarity in levels of EGFR expression in the two cell lines, as measured by ELISA (Figure 2B). The "washout" study demonstrated a significant retention of ^{18}F-PEG6-IPQA in H3255 cells (at about 400 cell/medium concentration ratio), which accounted for about 65% of total accumulated radioactivity between 60 and 120 min of incubation.

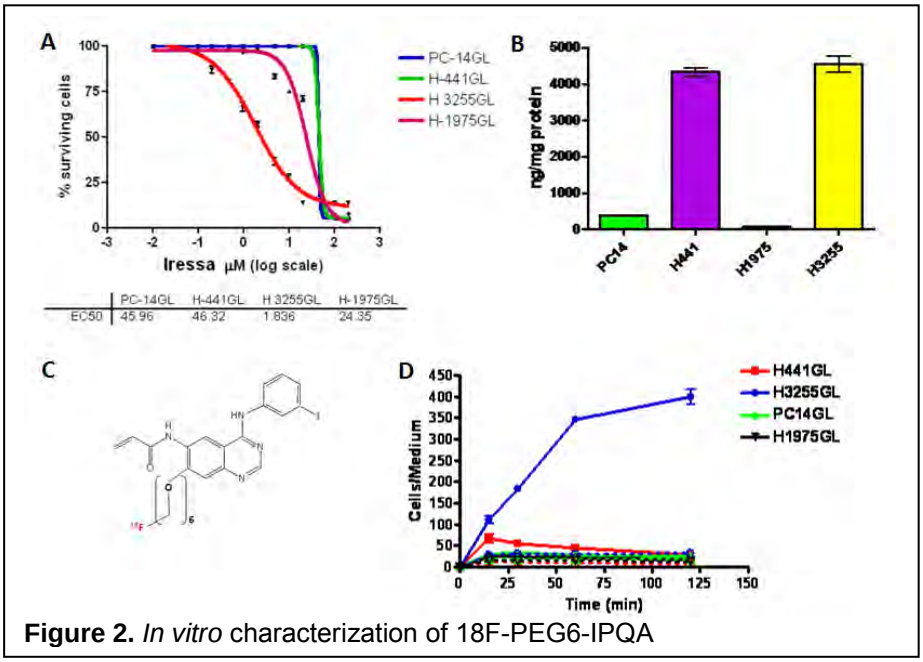

Figure 2. *In vitro* characterization of 18F-PEG6-IPQA

In contrast, almost 50% of ^{18}F-PEG6-IPQA radioactivity could be washed out from H441 cells, more than 60% from PC14 cells, and more than 70% from H1975 cells. After washout in PC14 and H1975 cells, the passive volume of ^{18}F-PEG6-IPQA distribution was less than 10. The magnitude of ^{18}F-PEG6-IPQA accumulation in all tested cell lines was significantly decreased in the presence of gefitinib at 100 μM/L in the culture medium.

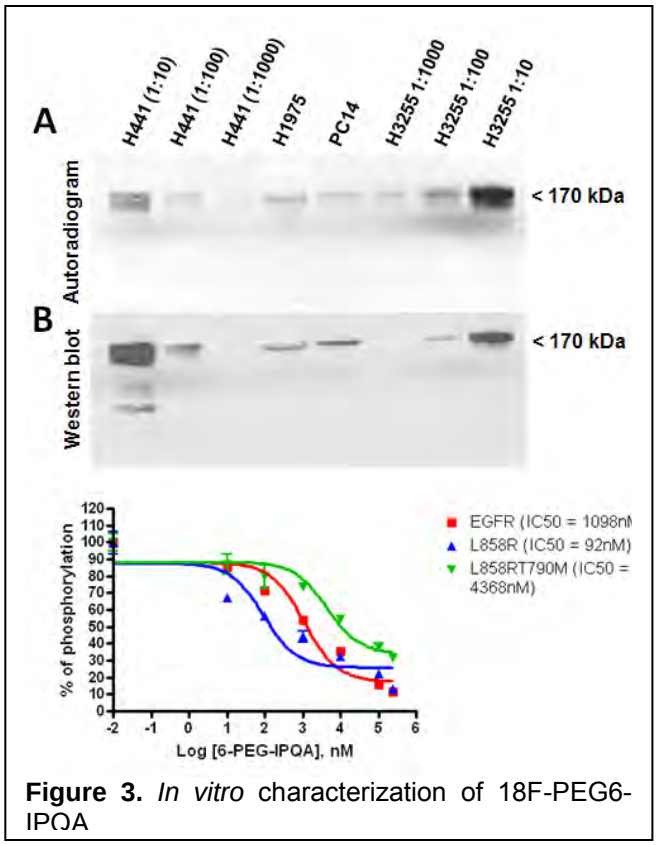

Figure 3. *In vitro* characterization of 18F-PEG6-IPQA

<u>Preferential and irreversible binding of ^{18}F-PEG6-IPQA to the L858R mutant EGFR kinase.</u> The autoradiograhic and Western blot analysis of electrophorograms of protein extracts from different NSCLC cells incubated with ^{18}F-PEG6-IPQA demonstrated preferential and irreversible covalent binding of ^{18}F-PEG6-IPQA to L858R mutant EGFR kinase domain, corresponding to 172 kD protein band (Figure 3). In H441 cells, the irreversible binding to wild-type EGFR kinase was significantly lower than in H3255 cells. This observation became more evident when comparing the intensity of radioactive bands (Figure 3A) and corresponding Western Blot bands (Figure 3B) of different dilutions of cellular protein extracts. In particular, the 1:10 dilution of H441 extract contained

significantly more EGFR protein than the 1:10 diluted extract from H3255 cells; however, the intensity of the radioactive band corresponding to 1:10 dilution of H3255 cells was significantly higher (at least a log order) than that in the 1:10 diluted extract of H441 cells. Autoradiographic detection was more sensitive than immunoblotting and chemiluminescent detection, as evidenced by the presence of a faint radioactive band in 1:1000 diluted extracts of H3255 cells, while the corresponding band on Western blot is not detectable. The irreversible covalent binding of ^{18}F-PEG6-IPQA to EGFR kinase domain was barely detectable in undiluted extracts of PC14 cells expressing low levels of wild-type EGFR and in undiluted extracts of H1975 cells expressing L858R/T790M dual mutant EGFR. More importantly, the enzyme inhibition studies demonstrated that cold (non-radiolabeled) F-PEG6-IPQA inhibits the recombinant L858R EGFR kinase a log order better than the recombinant wild-type EGFR kinase, and almost 50-fold better than the L858R/T790M dual mutant EGFR kinase (Figure 3C). Together with the results of *in vitro* radiotracer accumulation studies, these data confirm the selectivity of ^{18}F-PEG6-IPQA to active mutant L858R EGFR kinase.

Aim 3 Using selected ^{124}I or ^{18}F-labeled IPQA derivative, to conduct pre-clinical studies in animals with orthotopic models of lung cancer xenografts with different levels of EGFR expression/activity, and to assess the value of PET imaging as the inclusion criterion for therapy by EGFR inhibitors, as well as for monitoring the efficacy of treatment with EGFR-targeted drugs.

Summary of Research Findings

Feb 2009 Report: *In vivo* [^{18}F]fluoro-hexa-PEG-IPQA PET imaging of the H3255 subcutaneous tumor xenograft demonstrated superior binding of the tracer (Figs. 3 and 5). MicroPET images in mice provided the heterogeneous accumulation of [^{18}F]fluoro-hexa-PEG-IPQA in H3255 s.c. tumor xenografts. Hot spots and uptake layers could be identified in the central and peripheral regions of the tumor (Fig. 3, left middle panel, axial image at 60 min post-administration). The accumulation of [^{18}F]fluoro-hexa-PEG-IPQA displayed a one-phase exponential association kinetics in the first 10-15 minutes. The accumulation reached equilibrium at ~ 20 minutes (2.24 ± 0.11 %ID/g) after administration of radiotracer. Thereafter, the accumulation slowly increased till the last imaging time point (55-65 min). This seemed to indicate that the binding between [^{18}F]fluoro-hexa-PEG-IPQA and EGFR^{L858R} was on going during the entire imaging period. The optimal tumor-to-muscle concentration ratio was 2.07 ± 0.15 and tumor-to-blood ratio was 1.10 ± 0.21. We recorded a measurable difference between these results and the [^{18}F]fluoro-hexa-PEG-IPQA PET imaging of H441 tumor xenograft. Although H441 has the same magnitude of EGFR expression, it has lower EGFR activity as compared with H3255. H441 reached equilibrium in the first 3-6 minutes post injection at a level of 70 – 75% accumulation of that in H3255, and maintained a similar slow uptake over the subsequent period. PC14 and H1975, the negative controls in this study, showed much lower uptake ratio which is consistent with the results observed in cellular studies. In summary, the accumulation of H3255 was 1.4, 6.3 and 7.6 folds more than that of H441, PC14 and H1975 ($p < 0.001$; paired student t-test), respectively.

After treatment with Iressa, H3255, the most sensitive cell line, was significantly inhibited. The uptake ratio decreased from 2.27 before treatment to 0.65% ID/g (at 15 min post-administration) after treatment. Compared to H441 control group (1.89 %ID/g), there was only 15% uptake ratio left in H441-Iressa group (0.49 %ID/g). No significant difference was observed in the PC14 and H1975 before and after Iressa treatment.

The rate of [^{18}F]fluoro-hexa-PEG-IPQA accumulation by tumor xenografts in mice, *ki*, can be obtained from Patlak plot shown in Figure 4. The *ki* values were determined between 5-20

minutes (enzymatic phase) after radiotracer administration and they corresponded to the EGFR expression and activity.

Quantitative autoradiography (QAR)

QAR distribution was validated by whole-body quantitative autoradiography (Fig. 3, transverse section); high resolution QAR images demonstrated an impressive difference in the accumulation among the four s.c. tumor xenograft models (Fig. 3, left middle panel). H3255 (3.01± 0.84) had the highest tracer accumulation and it was followed by H441 (2.53 ± 0.15), H1975 (1.97 ± 0.80) and PC14 (1.59 ± 0.58). High levels of radioactivity were also observed in brown fat, skin, liver, bone marrow, but considered relatively lower in heart, skeletal muscle and spinal cord. In contrast, the Iressa-treated group presented approximately 4 times lower uptake in H3255 (from 3.01 to 0.78 %ID/g) and approximately 3 times lower in H441 (from 2.53 to 0.92 %ID/g). Similar accumulation was observed in PC14 and H1975 before and after treatment with Iressa (Fig. 3, lower middle panel).

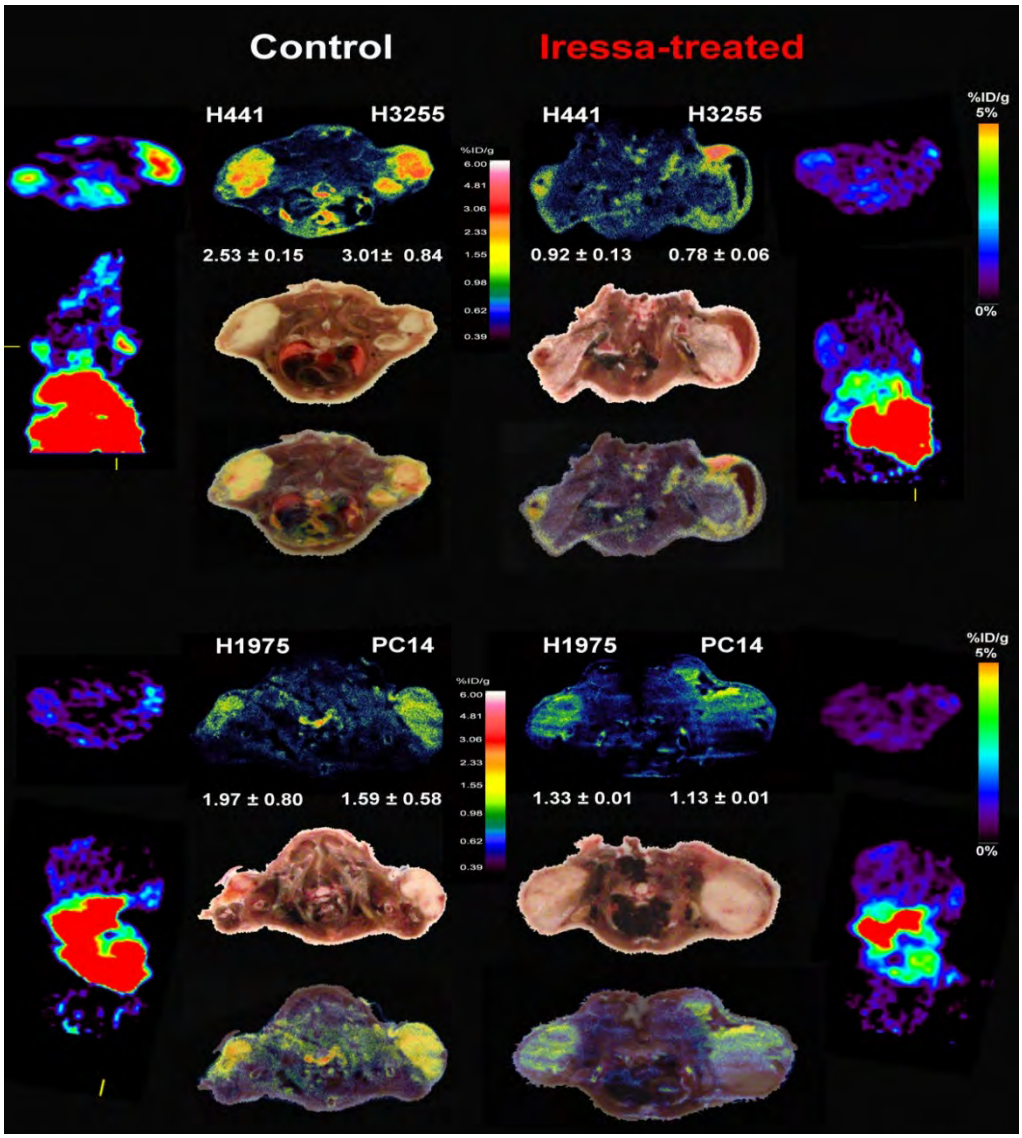

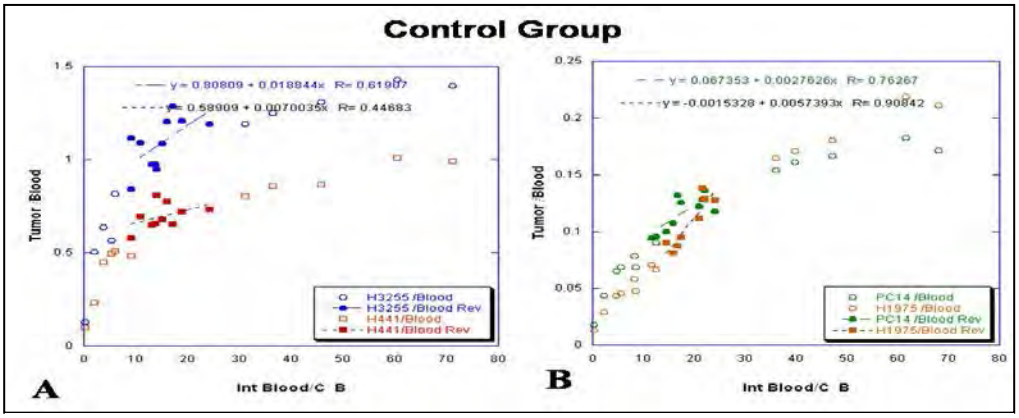

Figure 3: Representative PET and QAR images of [^{18}F]fluoro-hexa-PEG-IPQA in mice bearing different NSCLC cell lines.

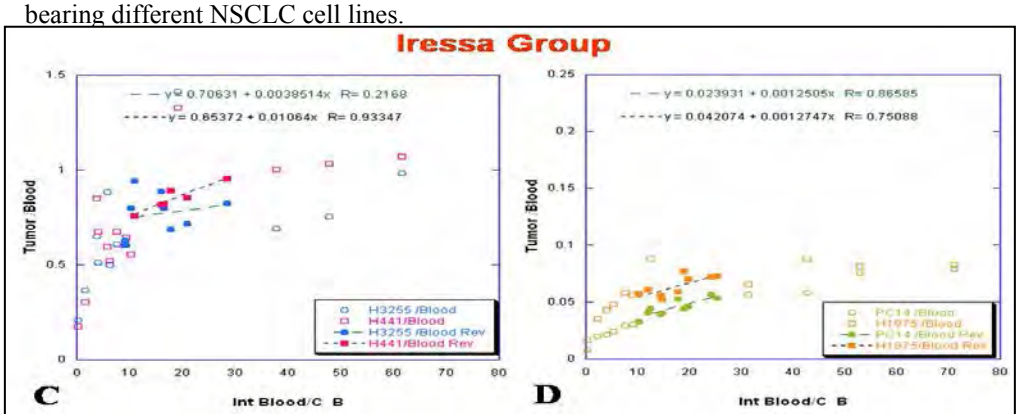

Figure 4. Patlak plots of [^{18}F]-PEG6-IPQA in mice bearing different NSCLC cell lines. The accumulation rate, *ki*, was calculated based on the input function obtained from blood.

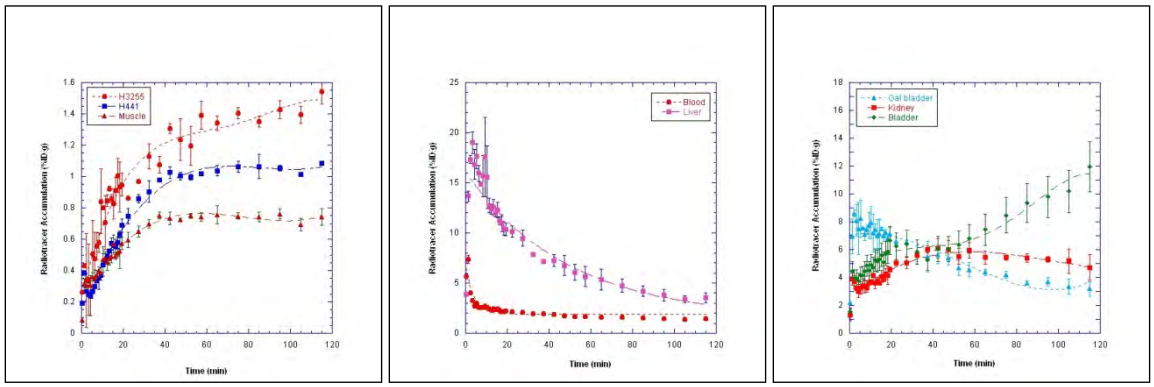

After 2 hours administration of [^{18}F]fluoro-hexa-PEG-IPQA, radioactivity was well distributed into organs (Table 1). The highest uptake was observed in small intestine (8.12 ± 0.13 %ID/g) and it was followed by kidneys (4.58 ± 0.82 %ID/g), liver (3.30 ± 0.28 %ID/g), and the lungs (3.25 ± 0.29 %ID/g). The distribution of tracer in different tumors also corresponded to the level and magnitude of EGFR expression and activity (H3255 2.55 ± 0.58, H441 2.20 ± 0.40, PC14 1.86 ±

0.39, H1975 1.86 ± 0.24 %ID/g). In the blocking study, an excess of Iressa was administered 1 hour before injection of radiotracer. We observed higher radioactivity in the majority of examined organs (Fig. 5).

	%ID/g (Average ± SD)	
Organ	Control	Iressa
Blood	1.99 ± 0.07	2.25 ± 0.07
Liver	3.30 ± 0.28	3.56 ± 0.07
Kidney	4.58 ± 0.82	6.23 ± 1.98
Small intestine	8.12 ± 0.13	5.11 ± 2.59
Large intestine	2.03 ± 0.03	2.01 ± 0.58
Spleen	1.88 ± 0.15	2.00 ± 0.30
Pancreas	1.27 ± 0.09	1.67 ± 0.24
Lung	3.25 ± 0.29	3.52 ± 1.84
Heart	1.60 ± 0.01	1.77 ± 0.24
Stomach	1.92 ± 0.15	1.78 ± 0.12
Brain	1.44 ± 0.01	1.29 ± 0.27
Bone	1.45 ± 0.29	1.14 ± 0.33
Muscle	1.29 ± 0.01	1.42 ± 0.20
Skin	1.48 ± 0.01	1.79 ± 0.34
H3255	2.55 ± 0.58	2.34 ± 0.36
H441	2.20 ± 0.40	2.62 ± 0.48
PC14	1.86 ± 0.39	2.42 ± 0.42
H1975	1.86 ± 0.24	1.36 ± 0.16

Table 1. Radioactivity levels (%ID/g) in different tissues at the end of PET imaging.

Study of pharmacokinetics, biodistribution, radiation dosimetry, and metabolites of [^{18}F]fluoro-hexa-PEG-IPQA in nonhuman primates

One of the most important pre-clinical studies for a novel PET imaging tracer in the development process is to evaluate the tracer in nonhuman primates. During this study, the pharmacokinetics, biodistribution, excretion pathway, metabolites, and radiation dosimetry of the tracer can be assessed. Based on these results, the dosimetry for the first cohort in human phase I can be calculated to improve the overall safety of the study. We have completed this study in six rhesus macaques. Results of the study constitute an important part in the investigational new drug (IND) application to the Food and Drug Administration (FDA) for their approval of our phase I study.

Six healthy rhesus macaques were injected intravenously with [^{18}F]fluoro-hexa-PEG-IPQA (5mCi/animal). Dynamic imaging was performed on a PET/CT scanner for the first 30 minutes covering the thoracic-abdominal area, and it was followed by whole-body static imaging at 30, 60, 90, 120, and 180 minutes. The biodistribution and radiation dosimetry estimates were obtained from blood sampling and volume of interest analysis (VOI) data measured on PET/CT images.

Based on data from the first six rhesus macaques available to-date, [^{18}F]fluoro-hexa-PEG-IPQA exhibited a rapid redistribution after i.v. injection and a relatively fast blood clearance with half-times of 1.4 minutes (mono-exponential fitting) via both hepatobiliary and renal pathways. Data

indicated that [^{18}F]fluoro-hexa-PEG-IPQA degraded to radioactive metabolite with a $T_{1/2}$ ~ 4min post administration (Fig. 6). Inferior vena cava, heart, lung, liver, kidney, gall bladder, small intestine, upper large intestine, and urinary bladder were visually identified as organs with moderate to high tracer uptakes (Fig. 7). The critical organ was the gallbladder (0.470 mSv/MBq); other organs with higher radiation dose were the kidney (0.0999 mSv/MBq), small intestine (0.0694 mSv/MBq), upper large intestine wall (0.0495 mSv/MBq), and liver (0.0425 mSv/MBq). Lung tissue exhibited low uptake of 18F-PEG6-IPQA.

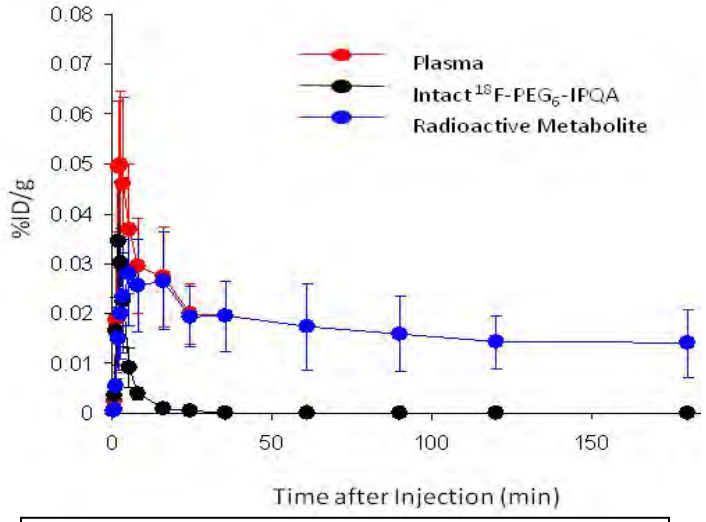

Figure 6: Plasma clearance curve for [^{18}F]fluoro-hexa-PEG-IPQA

The residence time of [^{18}F]fluoro-hexa-PEG-IPQA for each source organ was calculated from whole-body PET images. The persistent radioactivity accumulation in the gall bladder, liver, small intestine, and kidneys resulted in the highest residence organ time. There was no observable evidence of acute cardiac toxicity based on EKG, and no acute or delayed systemic toxicity based on blood hematological and chemical analyses was measured. The dose for the first cohort of humans in the phase I trial will be based on the dosimetry calculation from this non-human primate study. The radiation exposure to critical organs in humans will be administered at doses lower than the regulated limits.

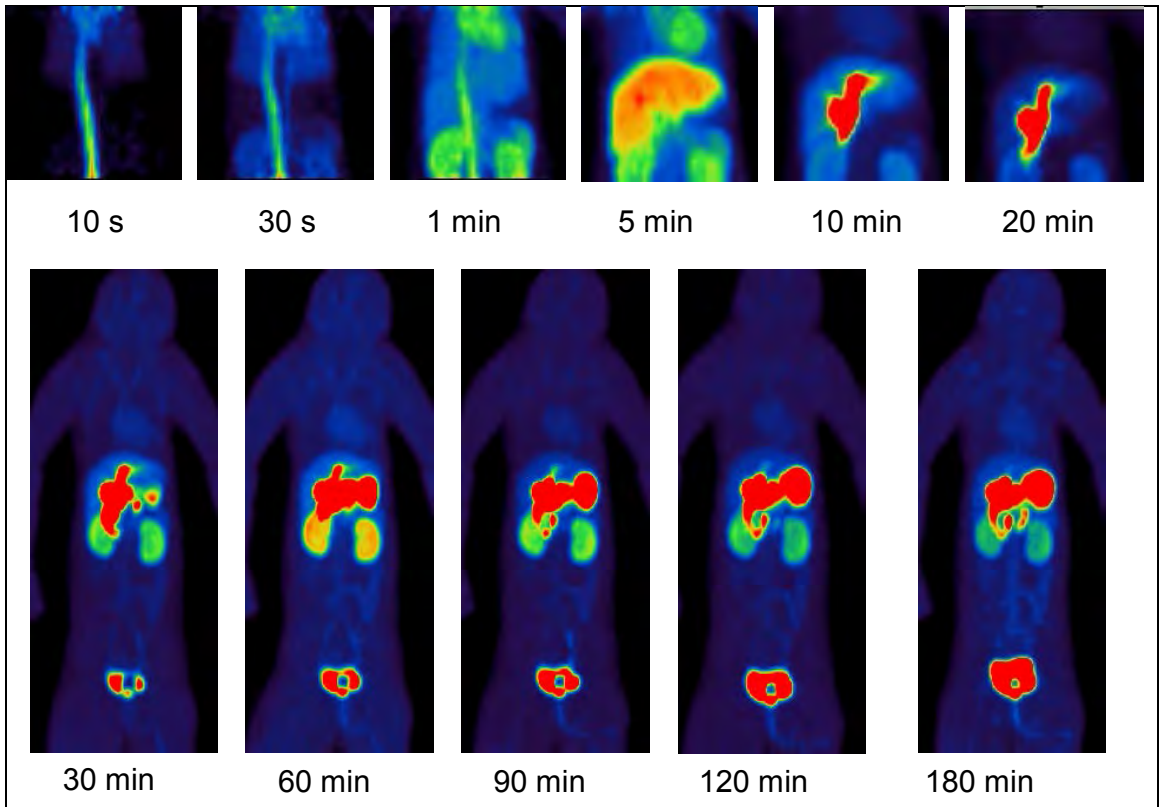

Figure 7: Time-activity distribution of [18F]fluoro-hexa-PEG-IPQA in a non-human primate.

Material manufacturing

We have initiated manufacturing the non-radio labeled (cold) fluoro-hexa-PEG-IPAQ and the precursor with Advanced Biomedical Compounds (ABX). The synthesis schemes of the cold compound were developed by our chemistry team (Fig. 8), and materials will be delivered to us in late March 2009 for use. The cold fluoro-hexa-PEG-IPQA (compound 1 from schemes 1&2) will be used in the IND-directed toxicology study at Charles River Laboratory (CRL). The precursor (compound 9 from scheme 3) will be used to manufacture ^{18}F-fluoro hexa PEG-IPQA clinical dose for phase I study.

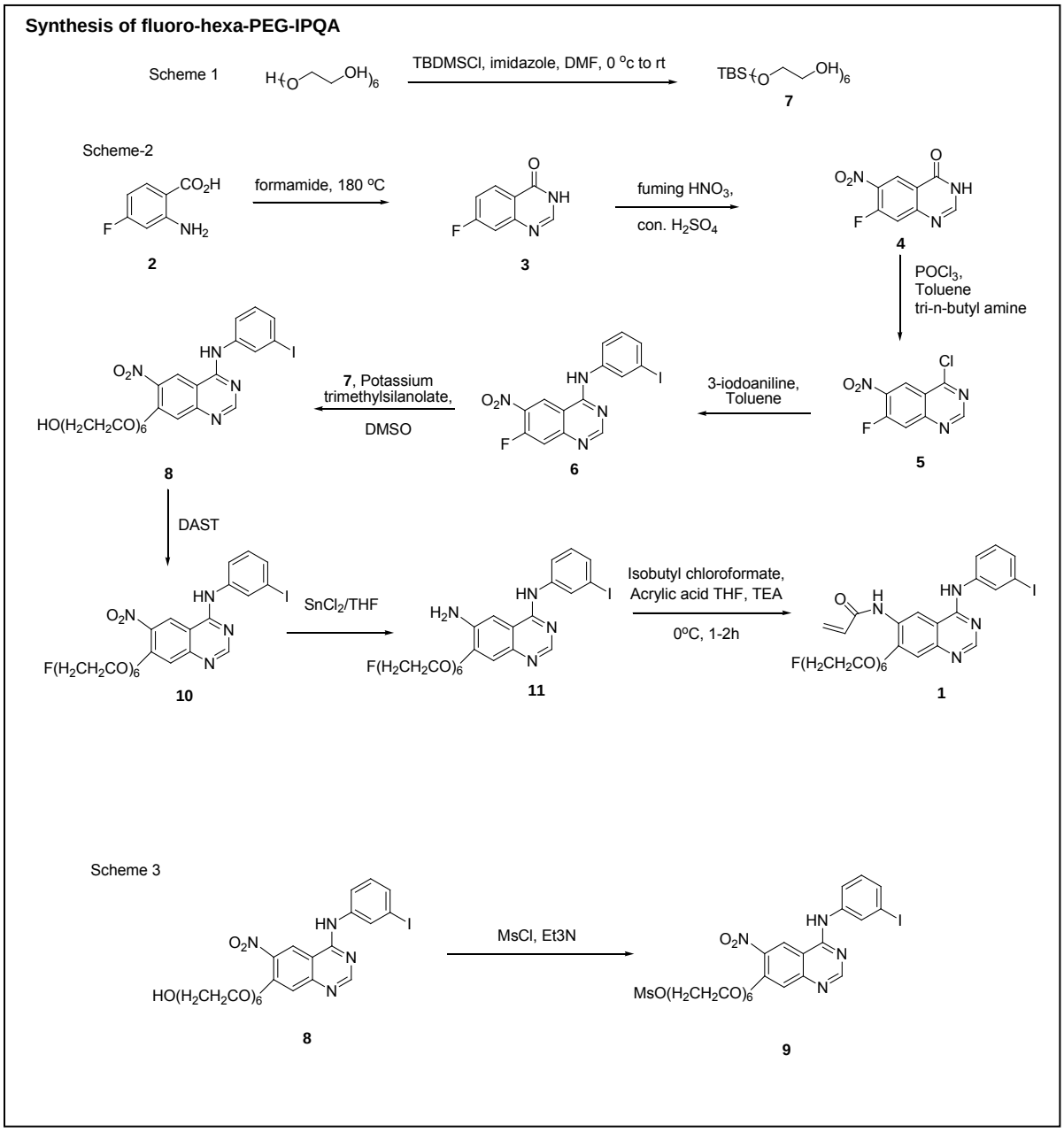

IND-directed Toxicology Study

We have finalized with CRL the toxicology protocol (Table 2) for the proposed rodent study. We incorporated the FDA's input resulting from a most current pre-IND conference we had with the FDA reviewers. To prepare the toxicology study for initiation as soon as the material is available from ABX, we have sent CRL our analytical method to begin study preparations based on the properties of our compound. Results from this study constitute part of the pharmacology and toxicology section of the IND in preparation.

Title:	A single-dose IV study of [^{18}F]flouro-hexa-PEG-IPQA in rats with a 14-day recovery period			
Study site:	Charles River facility, preclinical services Arkansas			
Compliance:	GLP			
Species/Strain:	Sprague-Dawley rats			
Dose Formulation Preparation:	Standard dose formulation prepared once. Standard sample collection for concentration verification once			
Dose Formulation Analysis:	Analysis on 1 occasion using validated HPLC methodology			
Dosing regimen:	Single dose on Study Day 1.			
Route of Administration:	Intravenous (bolus) dose administration			
Test system:	Group	Dose	Number of animals	
			Male	Female
	1	Control	10 M + 5 R	10 M + 5 R
	2	100 times	10 M + 5 R	10 M + 5 R
	M= main study animals sacrificed on Study Day 2. R= Recovery animals sacrificed on Study Day 15.			
Spares:	10 animals			
Total population:	70 animals			
Age:	Approximately 5 – 7 weeks at receipt			
Source:	Charles River			
Pretreatment period:	Approximately 10 days.			
Mortality observations:	Mortality/viability observations will be conducted twice daily on all animals.			
Detailed observations:	Daily on all animals.			
Body weight:	Daily on all animals			
Special Assessments:	General examination by veterinarian of all animals for study selection.			
Clinical Pathology parameters:	Coagulation, hematology, and clinical chemistry taken from all animals near termination.			
Toxicokinetics sample collection:	No bioanalytical samples obtained.			
Terminal procedures:	Full gross necropsy with organ weights and tissue collection on all main and recovery animals.			
Histopathology:	Standard histopathology on 65 tissue sections (including injection site) on 60 main and recovery animals.			
Audited draft report:	Audited draft report provided in approximately 12 weeks from the time of in-life completion.			

Table 2. IND-directed toxicology study protocol

cGMP manufacturing

We have continued improvements on lab-scale radiosynthesis (Fig. 9) so that it is readily scaled up and adopted by the cGMP manufacturing. We are working on an automated cGMP manufacturing process using GE Tracerlab with product specific hardware modifications. This automated process will be fully validated to meet cGMP requirements, and all QC methods for product release will also be validated. Results from this work constitute the chemistry, manufacturing, and control (CMC) section of the IND in preparation.

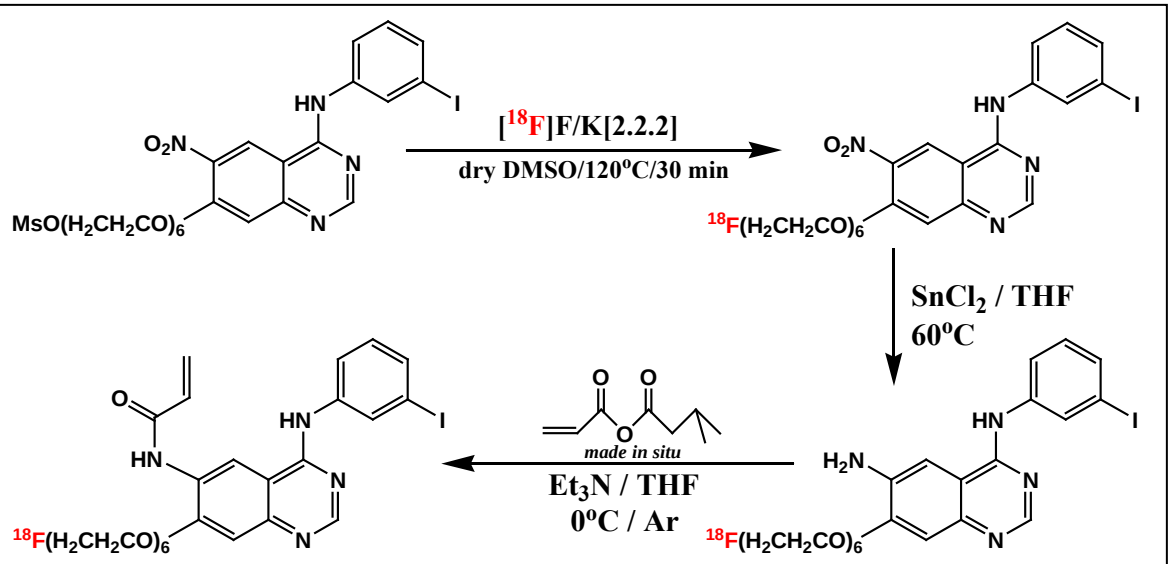

Figure 9 Radio labeling precursor to form [18F] fluoro-hexa-PEG-IPQA.

The development of a clinical trial protocol was led by Dr. David Stewart, M.D. (Deputy Chair, Thoracic/Head and Neck Medical Oncology). Our research team held a preliminary meeting with oncologists to discuss patient recruitment and study objectives. The primary and secondary objectives of the study are as follows:

Primary:

- To determine the optimum dosimetry of [^{18}F]fluoro-hexa-PEG-IPQA injection based on critical organ safety and detection sensitivity.
- To obtain data on [^{18}F]fluoro-hexa-PEG-IPQA distribution, pharmacokinetics, radiation dosimetry, and metabolites.
- To assess the safety of a single intravenous administration of [^{18}F]fluoro-hexa-PEG-IPQA in subjects with lung carcinoma.

Secondary:

- To obtain preliminary data on the feasibility of detection of both primary and metastatic tumor lesions in lung carcinoma using [^{18}F]fluoro-hexa-PEG-IPQA as compared to standard of care modalities.
- To correlate the magnitude of tumor [^{18}F]fluoro-hexa-PEG-IPQA uptake and retention with EGFR expression and/or treatment response.

Additional meetings will be held to discuss and refine inclusion and exclusion criteria, imaging procedures, safety monitoring, etc., to fully complete the protocol.

Aim 4 Perform pilot clinical PET imaging studies with the optimized ^{124}I or ^{18}F-labeled IPQA derivative under the RDRC guidelines in patients with NSCLC undergoing adjuvant therapy before tumor resection or biopsy. Compare PET image-based measures of EGFR activity with immunohistochemical measures of phospho-EGFR *in situ*.

Summary of Research Findings

Feb 2016 Report:

Conduct of Protocol

The patient population eligible for this trial included patients with stage IV adenocarcinomas of the lung harboring *EGFR* mutations.

Tumor tissue is routinely analyzed for *EGFR* mutations in all patients with stage IV adenocarcinoma of the lung seen in the clinic. We imaged five patients after administration of the IPQA-PET Scan imaging radiopharmaceutical. Three patients were treated in the first dose escalation cohort at 2mCi per patient, and two patients in the second dose escalation cohort were treated at 3.78 mCi per patient.

All the patients treated had stage IV disease with a classic EGFR mutation. The presence of measurable disease was documented by prior scans. They had been off active treatment for at least two weeks prior to dosing by the IPQA-PET radiopharmaceutical.
We successfully completed the enrollment and treatment of the first cohort of 3 patients to this study. Per protocol, a statistical analysis was then performed to determine the dose level for the next cohort of patients, which was determined to be 3.78 mCi per patient. All required regulatory approvals were obtained to initiate patient screening and accrual to the next cohort of 6 patients.

We now report on the treatment of the ***first two* patients** of the second cohort on protocol. The dose was delivered within 10% of the requested dose (on the high side) as per standard nuclear pharmacy regulations. Review of the clinical data for all 5 treated patients (Table 1) revealed that there was no tumor targeting with the radiopharmaceutical at the current dose level. Additionally, in the first 2 patients of the second cohort, the liver, GI and gall bladder were receiving the max doses of radiation at the current dose level, precluding further dose escalation (see Table 2 below). Given that tumor targeting was not observed and additional dose escalations prohibited by radiation levels of the target organs at the current level, the team declined to continue the trial, and will request closure of the protocol. Upon consultation with the DoD Program Director, the decision was made to terminate the study, complete the current grant year, and submit the final grant report in a timely manner.

A final statistical report of the clinical trial was completed as described below.

Statistical Methods and Results:
The primary goal of the study is to determine a safe and effective dose for using ^{18}F-PEG6-IPQA as a PET imaging agent. Up to 15 patients were to be enrolled and imaged in this study. The maximum allowed single absorbed radiation doses for sensitive organs (whole body, gonads and red marrow) and non-sensitive organs are 3 and 5 rems, respectively. Absorbed dose estimates for 25 organs were monitored. The study was designed with the intent to limit the probability that a patient exceeds the target dose (e.g., 3 or 5 rems depending on the organ) in any organ to be less than 0.10.

We proposed a three-stage design in which three female patients in the first stage and six patients (three females and three males) in each of the 2nd and 3rd stages were to be imaged, for a total of 15 patients. The initially planned dose level, determined based on primate experiments, was 70 MBq.

A total of 5 patients were enrolled in two cohorts (Table 1), including three female patients in the first cohort and 2 male patients in the second cohort. .

Table 1. Patients on the Study

Patient	Gender	Enrollment Date	Injection & Imaging Date	Cohort	Administered Dose (MBq)
1	Female	8/27/2014	8/28/14	1	73.6
2	Female	9/23/2014	9/23/14	1	46
3	Female	11/13/2014	11/18/14	1	53.9
4	Male	4/21/2015	4/21/15	2	126
5	Male	11/18/2015	11/19/15	2	109

Following the completion of the first cohort of three female patients (organ exposure data shown for Patient 1, Patient 2 and Patient 3 in the Table 2), the average and standard deviation were estimated. The 90th percentile for the distribution of equivalent dose per unit administered activity (1 rem/MBq = 10 mSv/MBq) for the highest radiation dose administered of the exposure for each organ (unit mSv/MBq) were estimated using the following formula,

$$UB_i = \bar{x}_i + t_{1-\alpha_i,\, n-1} \times SD_i,\ i = 1,2,\dots,\ 25, \qquad (1)$$

where *i* denotes organ, $\bar{x}_i$ is the observed mean exposure/dose (mSv/MBq) of the *i*th organ, SD_i is the observed standard deviation of the *i*th organ, *n* equals the number of patients treated, α_i is the one-sided type I error rate spent on the *i*th organ. The family-wise alpha level was maintained at 0.10 level,

$$\alpha = \sum_{i=1}^{25} \alpha_i = 0.10\,, \qquad (2)$$

but was distributed unevenly among organs based on how close the organ dose was to its limit. Based on these estimates, the acceptable administered dose levels for the next cohort was determined to be 140 MBq. Additional two patients (Patient 4 and Patient 5) have been enrolled into the study at the dose of 140 MBq.

The organ exposures per unit of administered dose for each patient are listed in Table 2. Figure 1 displays the organ exposure per unit of administered dose versus the administered dose for each patient. Figure 2 presents the total organ exposure (Rem) versus the administered dose for each patient. Also in Table 2, the average and standard deviation of organ exposures for each cohort and for all 5 patients, and the 90th percentile of each organ's exposure per unit (mSv/MBq) based on all 5 patients are estimated. The final alpha levels are the same as the ones that were used to determine the dose levels for the second cohort (Patient 4 and Patient 5).

Table 2. Organ Doses and 90th Percentile (UB) in mSv/MBq

Target Organ	Patient 1	Patient 2	Patient 3	Patient 4	Patient 5	Average Cohort 1	SD* Cohort 1	Average Cohort 2	SD* Cohort 2	Average All	SD* All	Alpha	90th percentile
Adrenals	0.0115	0.0119	0.0098	0.0099	0.0092	0.0111	0.0011	0.0095	0.0005	0.0105	0.0012	0.00027778	0.0223
Brain	0.0039	0.0040	0.0042	0.0039	0.0039	0.0040	0.0001	0.0039	0.0000	0.0040	0.0001	0.00027778	0.0051
Breasts	0.0048	0.0048	0.0046	0.0044	0.0043	0.0047	0.0001	0.0044	0.0001	0.0046	0.0002	0.00027778	0.0067
Gallbladder Wall	0.0946	0.2140	0.0232	0.2238	0.1450	0.1106	0.0964	0.1844	0.0558	0.1401	0.0840	0.065	0.2999
LLI Wall	0.0497	0.0337	0.0550	0.0322	0.0351	0.0461	0.0111	0.0337	0.0021	0.0412	0.0104	0.001	0.1161
Small Intestine	0.1360	0.0863	0.1500	0.0802	0.0873	0.1241	0.0335	0.0838	0.0051	0.1080	0.0325	0.01	0.2297
Stomach Wall	0.0129	0.0115	0.0127	0.0102	0.0103	0.0124	0.0008	0.0103	0.0000	0.0115	0.0013	0.00027778	0.0243
ULI Wall	0.1470	0.0941	0.1620	0.0913	0.0991	0.1344	0.0357	0.0952	0.0055	0.1187	0.0332	0.015	0.2283
Heart Wall	0.0078	0.0080	0.0070	0.0069	0.0066	0.0076	0.0005	0.0067	0.0002	0.0072	0.0006	0.00027778	0.0135
Kidneys	0.0275	0.0331	0.0241	0.0247	0.0235	0.0282	0.0045	0.0241	0.0008	0.0266	0.0040	0.00027778	0.0663
Liver	0.0474	0.0514	0.0260	0.0354	0.0276	0.0416	0.0137	0.0315	0.0055	0.0376	0.0115	0.001	0.1198
Lungs	0.0068	0.0070	0.0062	0.0059	0.0057	0.0067	0.0004	0.0058	0.0002	0.0063	0.0006	0.00027778	0.0120
Muscle	0.0083	0.0077	0.0084	0.0070	0.0070	0.0081	0.0004	0.0070	0.0000	0.0077	0.0007	0.00027778	0.0143
Ovaries	0.0291	0.0214	0.0317	0.0188	0.0200	0.0274	0.0054	0.0194	0.0008	0.0242	0.0058	0.001	0.0658
Pancreas	0.0131	0.0135	0.0114	0.0121	0.0112	0.0127	0.0011	0.0116	0.0006	0.0123	0.0010	0.00027778	0.0225
Red Marrow	0.0096	0.0083	0.0098	0.0078	0.0078	0.0092	0.0008	0.0078	0.0000	0.0087	0.0010	0.00027778	0.0183
Osteogenic Cells	0.0097	0.0093	0.0100	0.0084	0.0085	0.0097	0.0003	0.0084	0.0000	0.0092	0.0007	0.00027778	0.0162
Skin	0.0049	0.0047	0.0050	0.0044	0.0044	0.0049	0.0001	0.0044	0.0000	0.0047	0.0002	0.00027778	0.0072
Spleen	0.0166	0.0146	0.0135	0.0201	0.0261	0.0149	0.0016	0.0231	0.0043	0.0182	0.0051	0.00027778	0.0694
Testes				0.0057	0.0059			0.0058	0.0001	0.0058	0.0001	0.00027778	0.0097
Thymus	0.0054	0.0055	0.0054	0.0050	0.0050	0.0054	0.0001	0.0050	0.0000	0.0053	0.0002	0.00027778	0.0077
Thyroid	0.0043	0.0044	0.0045	0.0046	0.0046	0.0044	0.0001	0.0046	0.0000	0.0045	0.0001	0.00027778	0.0056
Urinary Bladder Wall	0.0674	0.0925	0.0682	0.0527	0.0548	0.0760	0.0143	0.0537	0.0015	0.0671	0.0159	0.002	0.1615
Uterus	0.0245	0.0200	0.0264	0.0171	0.0180	0.0236	0.0033	0.0175	0.0006	0.0212	0.0041	0.00027778	0.0622
Total Body	0.0110	0.0099	0.0108	0.0088	0.0087	0.0106	0.0006	0.0087	0.0001	0.0098	0.0011	0.00027778	0.0207

*SD – Standard Deviation

Figure 1. Organ Exposure (mSv/MBq) vs Administered Dose

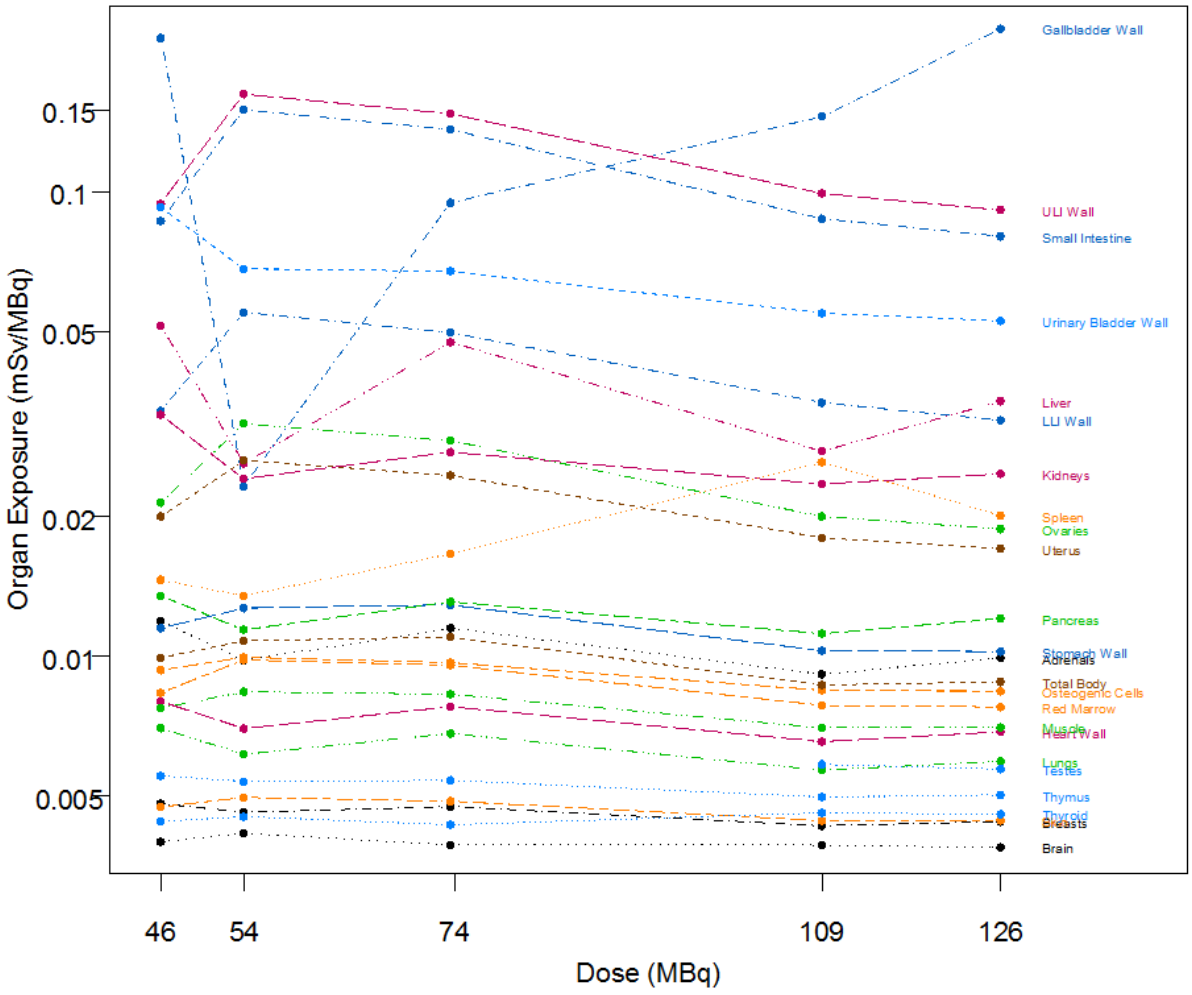

Figure 2. Organ Exposure (Rem) vs Administered Dose

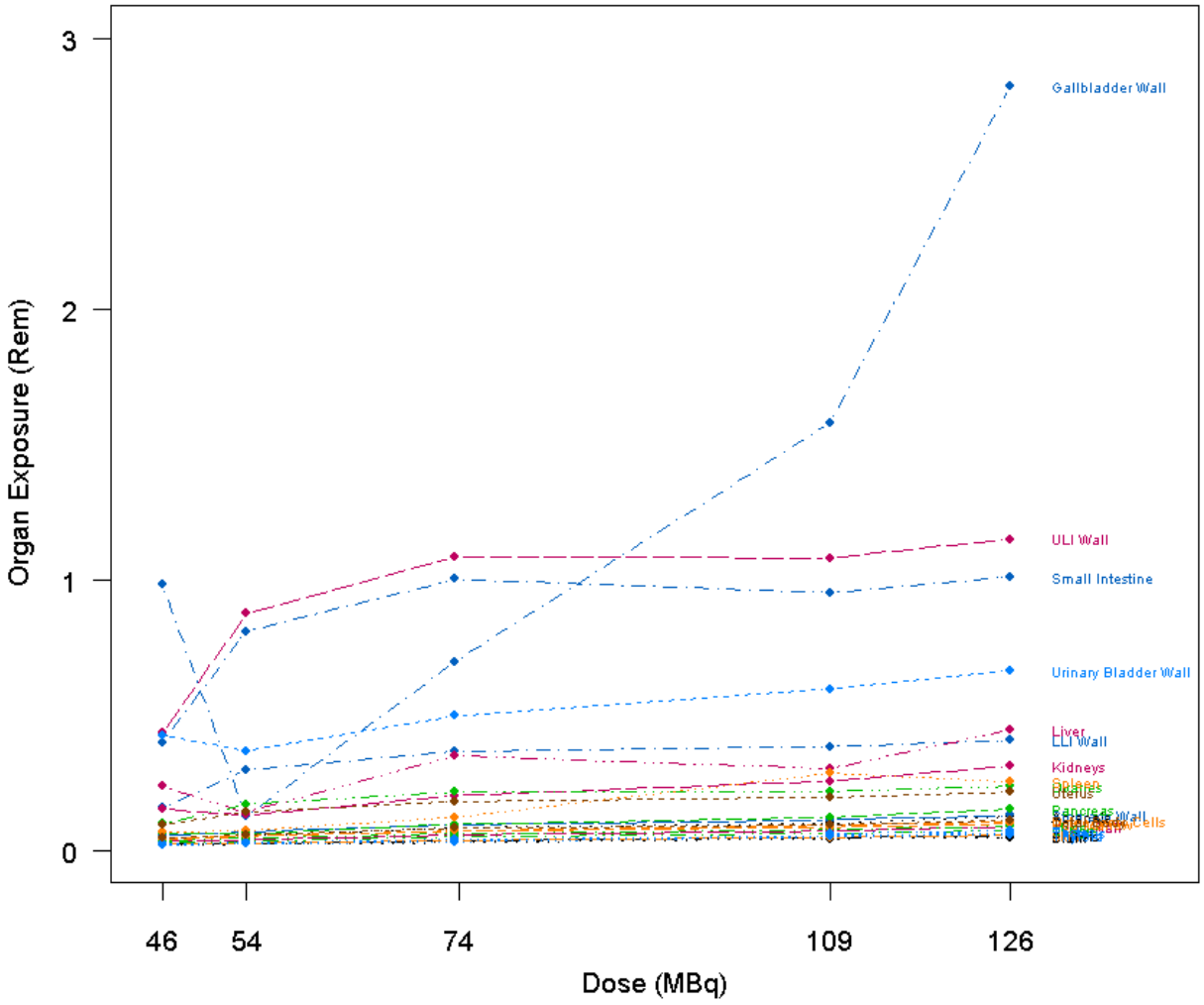

The study investigators reviewed the data of the five patients treated. There is no tumor targeting with the radiopharmaceutical at the current dose level. Additionally, the liver, GI and gall bladder is receiving the max doses of radiation at the current dose level precluding further dose escalation. Given that there is not tumor targeting up to this dose level and there we cannot dose escalate further, it was decided that the trial should be closed, essentially secondary to lack of activity. No clinically observable toxicities were reported. This study was subsequently closed to new patient accrual effective 2/22/2016.

Key Research Accomplishments:

- Completed accrual of the first cohort of patients (3 females), and the first 2 of the 6 patients required for the second cohort.
- All doses of the agent were delivered within 10% of the requested dose (on the high side) as per standard nuclear pharmacy regulations.
- Completed the required statistical analysis to determine the dose level for the second cohort of patients (3.78 mCi per patient), and completed the final statistical analysis for the trial.

We evaluated the results of the 5 patients treated and determined a lack of activity of the agent of the current dose level, and unacceptable levels of radiation in the liver, GI and gall bladder of the treated patients.

Conclusions:

The first cohort of three patients was completed and evaluated. Based on organ dosimetry, the appropriate dose escalation for the next cohort of 6 patients was determined to be no more than 3.78 (+,- 10%) mCi per patient. All required approvals (IRB, IND, HRPO) were obtained to initiate accrual to the second cohort, and 2 additional patients were consented and treated. Analysis of results on these two patients revealed the lack of tumor targeting as well as unacceptable levels of radiation in the liver, GI and gall bladder of the treated patients, leading to the programmatic decision to terminate the trial.

Reportable Outcomes:

None to date.

Project 3: Targeted Peptide-based Systemic Delivery of Therapeutic and Imaging Agents to Lung Cancer

(PI and co-PI: Renata Pasqualini, Ph.D., Wadih Arap, M.D., Ph.D.)

The studies outlined in this proposal focus on the use of peptide sequences with selective lung tumor-targeting properties. We will seek to validate these probes as delivery vehicles in drug and gene-targeting approaches. This approach directly selects *in vivo* for circulating probes capable of preferential homing into tumors. The strategy will be to combine homing peptides in the context of phage as gene therapy vectors. Given that many of our peptides also target angiogenic vasculature in addition to tumor cells, these studies are likely to enhance the effectiveness of therapeutic apoptosis induction and imaging technology.

Aim 1 To select peptides targeting primary and metastatic tumors in lung cancer patients.

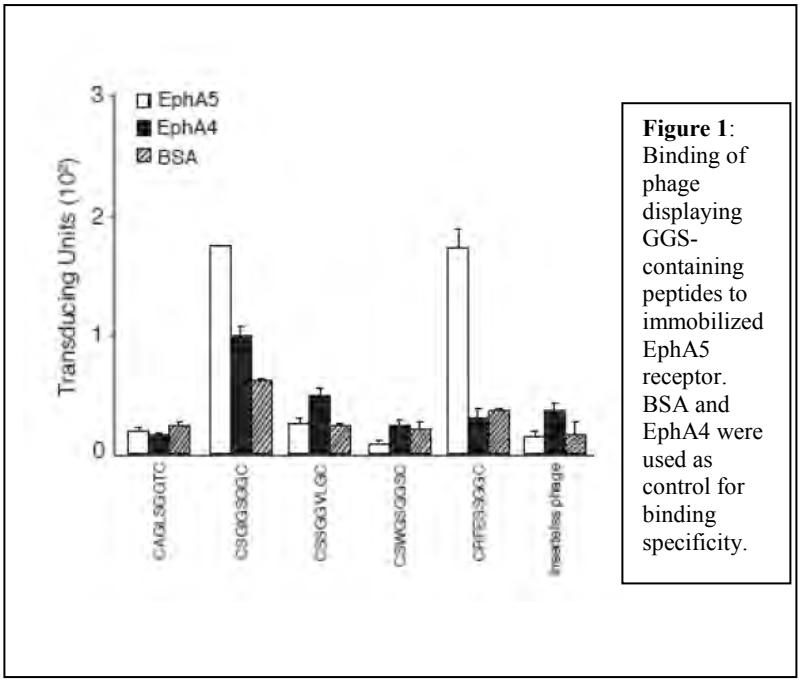

Figure 1: Binding of phage displaying GGS-containing peptides to immobilized EphA5 receptor. BSA and EphA4 were used as control for binding specificity.

Summary of Research Findings

Feb 2009 Report: Phage display screening on human cancer cells from the NCI-60 panel of cell lines suggested that the tripeptide motif GGS specifically targets human lung cancer cells.

Standard BLAST homology search and detailed protein sequence alignment of peptides displaying the motif GGS indicated members of the ephrin family of proteins as the proteins potentially mimicked by GGS-containing peptides. To validate this

hypothesis, we tested a series of phage displaying distinct peptides containing the GGS domain for its ability to bind to EphA5 receptor. EphA4 and BSA were used as controls (Fig.1). Phage displaying the peptide sequences CSGIGSGGC and CRFESSGGC showed specific binding to the candidate receptor and were selected for further characterization. Competition assays with synthetic peptide confirmed binding specificity (Fig. 2).

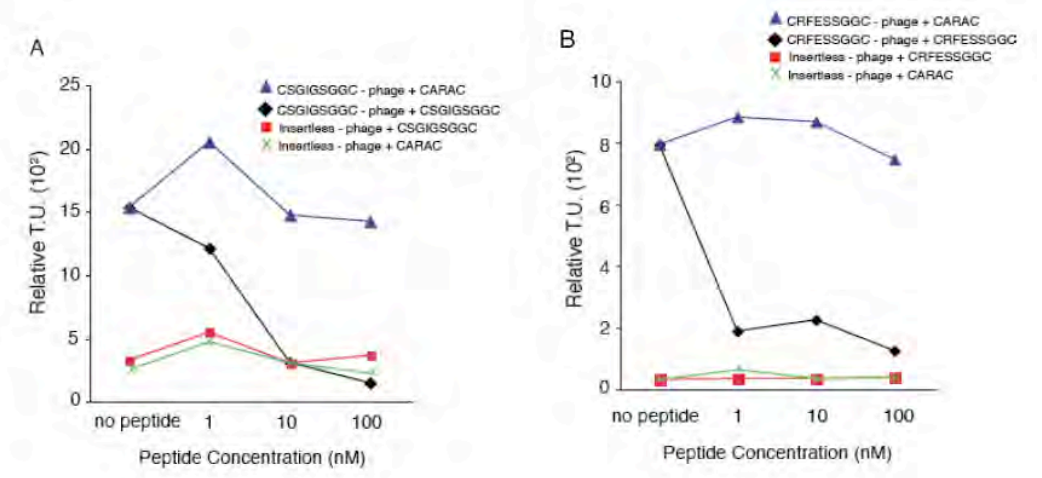

Figure 2: Binding of targeted phage is inhibited by synthetic peptides. Black line indicate specific inhibition. The unrelated peptide CARAC and insertless phage were used a s controls. A, CSGIGSGGC-phage. B, CRFESSGGC-phage.

We also tested binding of the selected phage to the endogenous receptor expressed on the surface of lung cancer cells. Receptor expression was first confirmed by immunofluorescence of two lung cancer cell lines: H460 and Hop92. The ovarian cancer cell line OVCAR-3 and EphA4 were used as negative controls. As shown in Figure 3A, lung cancer cell lines express high levels of EphA5 on their surface. Moreover, phage binding was specific to EphA5-expressing cell lines (Fig. 3B).

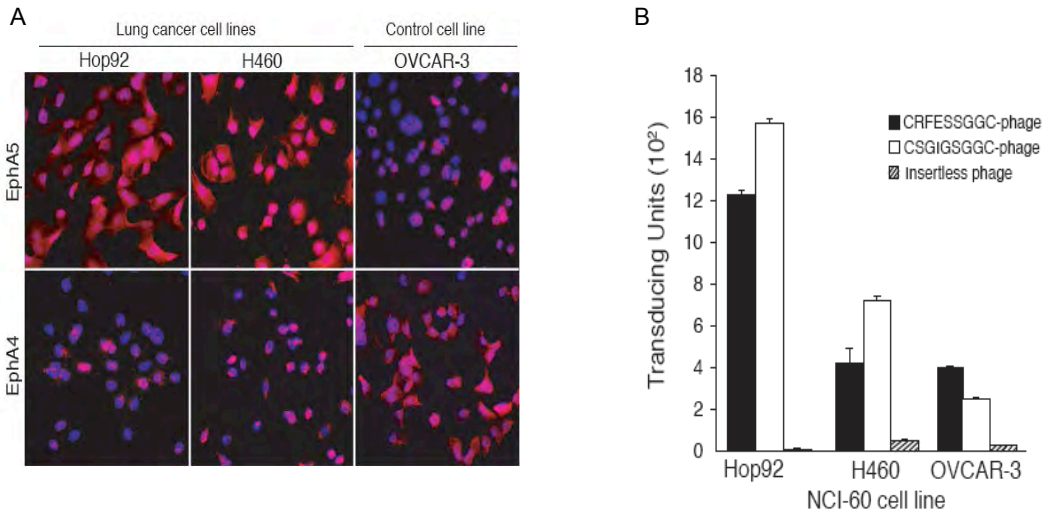

Figure 3: (A) immunofluorescence staining of lung cancer cells with anti-EphA5 receptor. The ovarian cancer cell line OVCAR-3 was used as negative control for EphA5 expression. (B) binding of EphA5-targeting phage to lung cancer cells.

In vitro functional properties of EphA5-targeting peptides

We established in vitro assays to study the biological effects of EphA5 targeting peptides on human lung cancer cells. Receptor phosphorylation was induced with the mimicked ligand in presence or absence of the competing peptide. We observed inhibition of EphA5 phosphorylation in the presence of both CRFESSGGC and CSGIGSGGC synthetic peptides (Fig. 4).

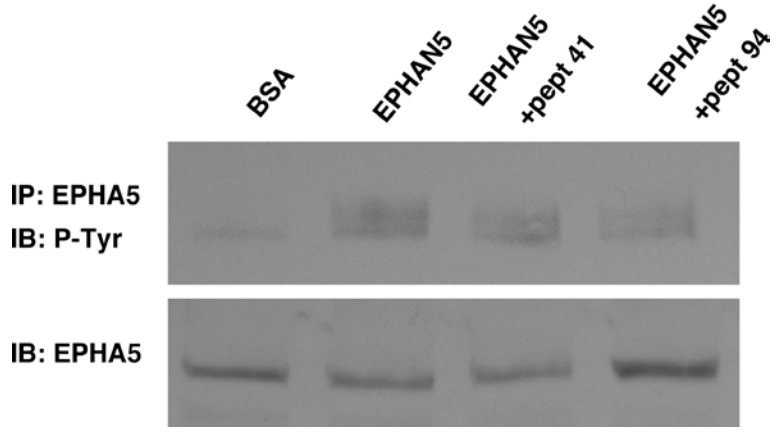

Figure 4: Phosphorylation of EphA5 receptor is inhibited by targeted peptides (peptide 41: CRFESSGGC; peptide 94: CSGIGSGGC). EPHAN5: ligand candidate. BSA was used as negative control.

Targeted peptides were able to inhibit phosphorylation of ERK1/2 (p44/p42) (Fig. 5), indicating suppression of the MAP kinase pathway and the involvement of EphA5 in the maintenance of lung cancer cells proliferation and survival. The same effect was observed in the phosphorylation of JNK, supporting the role of EphA5 in tumor cell proliferation/survival. Consistently, we did not observe alterations in the phosphorylation of pathways involved in cell migration (phosphorylation of p38).

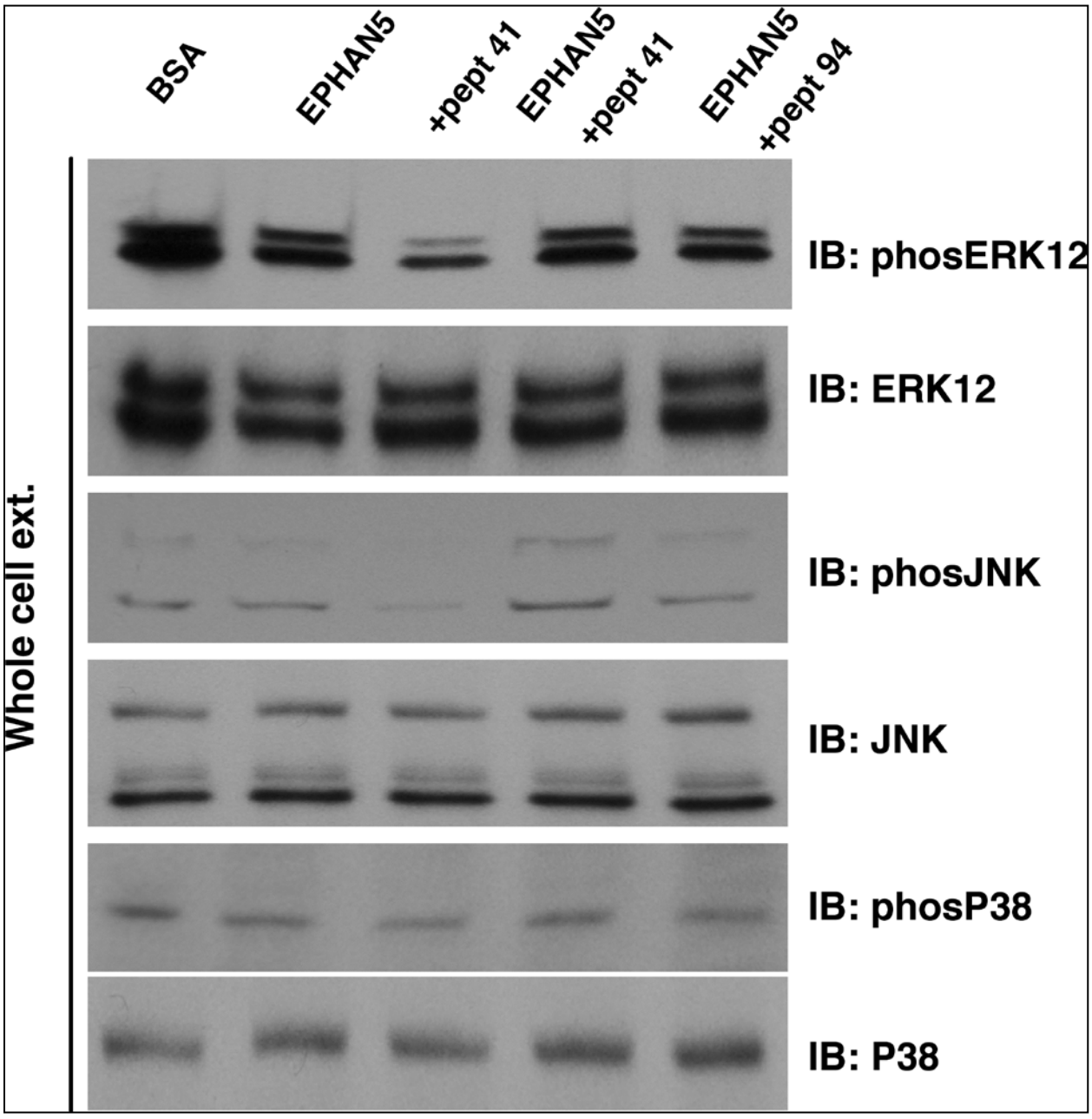

Figure 5: Activation of MAP kinase pathway was analyzed in presence or absence of targeted peptides. Arrows point to phosphorylated ERK1/2 and JNK. Inhibition of phosphorylation was observed in both cases. We did not detect alterations in the phosphorylation levels of P38.

As mentioned above, peptides selected from phage libraries have allowed the cloning of vascular receptors in non-proliferating and in angiogenic blood vessels. Although the biological basis for vascular heterogeneity is unknown, peptides selected by homing to blood vessels in mouse models have been used by several groups as carriers to guide the delivery of cytotoxic drugs, pro-apoptotic peptides, metalloprotease inhibitors, cytokines, fluorophores, and genes. Generally, coupling of a given entity to homing peptides yields targeted compounds that are more effective and less toxic than the parental entity. Moreover, vascular receptors

corresponding to the selected peptides have been identified in blood vessels of normal organs and tumors. These results show that it is possible to develop therapeutic strategies based on selective expression of vascular receptors.

Aim 2 To validate receptors for targeting human lung cancer.

Summary of Research Findings

Feb 2009 Report:

Homing of targeted phage to orthotopic human lung cancer model.

We examined the expression of EphA5 in samples of human lung cancer (Fig. 6). We observed over-expression of EphA5 in non-small lung adenocarcinoma epithelium (indicated by the arrows).

Second, to evaluate the targeting properties of the selected peptides in vivo, we administered targeted phage intravenously into human lung cancer-bearing mice. Lung and control organs were harvested and examined by IHC for presence of phage particles after 1h, 6h, and 24h of systemic circulation. We observed specific homing of phage to lung cancer colonies in all

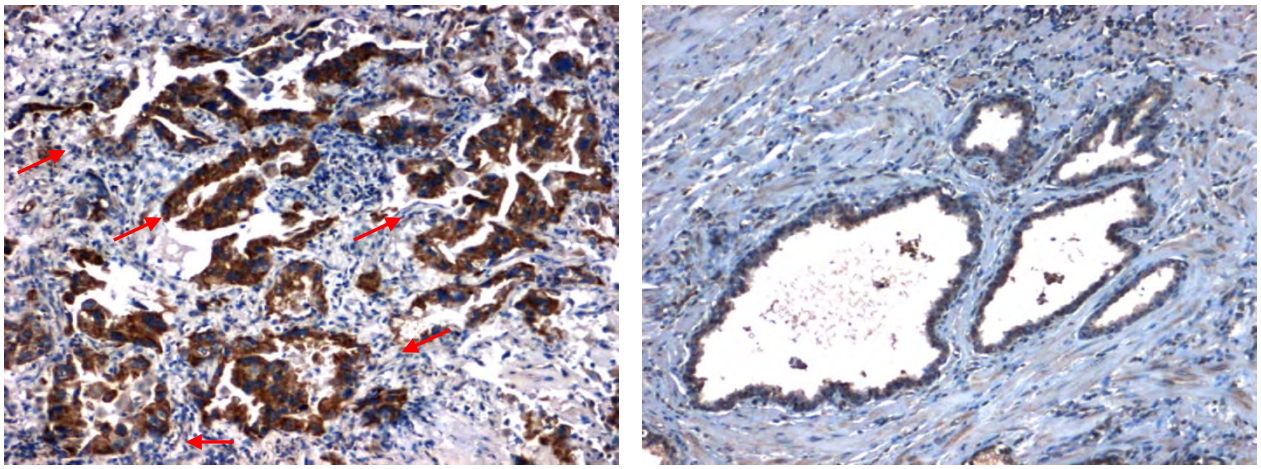

Figure 6: Human lung adenocarcinoma (pictured left) and control tissue (prostate, pictured right).

time points (Fig. 7, arrows). We did not detect phage in normal lung; uptake of phage was found to be restricted to lung cancer cells. Insertless phage was used as negative control and showed only background staining (Fig. 7).

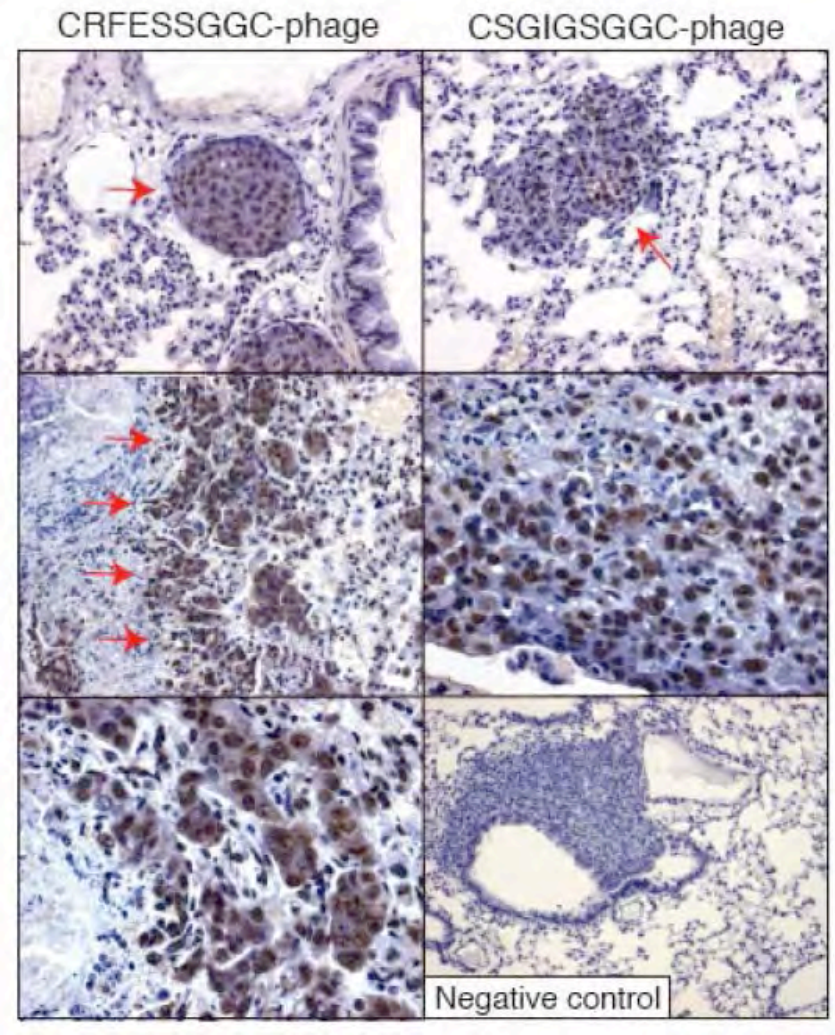

Figure 7: Homing of targeted phage to orthotopic model of human lung cancer. Arrows point to cancer cells targeted by phage. Insertless phage was used as negative control and showed only background staining.

Treatment of orthotopic human lung cancer with BMTP-11 and BMTP-78.

Here we analyzed the effect of BMTP-11 and BMTP-78 in human lung cancer-bearing mice. Animals (15 animals/group) were treated weekly with 10mg/kg of each compound (ip) for the period of 4 weeks. Control group did not receive any type of treatment. At the end of treatment, lungs and control organs were collected for (i) tumor colony count and (ii) tissue weight. We observed significant reduction of both tissue weight and tumor growth in animals treated with BMTP-11 and BMTP-78 (Fig. 8, $p<0.05$). Staining of apoptotic cells demonstrated specific killing of lung cancer cells in animals treated with both BMTP-11 and BMTP-78 (Fig. 9).

Targeted anti-cancer drug development program: BMTP-11 IND and BMTP-78 pre-IND

Our first MDACC-sponsored IND, based on BMTP-11, has received a “safe to proceed” status by the FDA in January 2009. The first-in-human clinical trial has a projected activation date of March 2009. Our second cancer IND filing with the FDA will focus on BMTP78. These peptidomimetics are targeted to the IL-11R and to GRP 78. Extensive studies have been performed and clearly established the relevance of these targets in human cancer tissue samples from nearly every type of tumor evaluated (including lung cancer). These studies indicate that these targets are suitable for delivery of therapies and imaging agents. Extensive toxicology work has been completed in mice and cynomolgus monkeys. Efficacy studies in lung cancer models have been extensively validated. We expect the upcoming clinical studies to be informative and establish a firm foundation for evolving these drugs into Phase II/III trials.

Merging tumor targeting and molecular-genetic imaging into an integrated platform is limited by a lack of strategies to enable systemic, ligand-directed delivery and imaging of specific transgenes. Many eukaryotic viruses subserve transgene delivery but require elimination of native tropism for mammalian cells; in contrast, prokaryotic viruses can be adapted to bind to mammalian receptors but are otherwise poor vehicles. We have introduced a system containing cis-elements from adeno-associated virus (AAV) and single-stranded bacteriophage. Our AAV/phage (AAVP) prototype targets ad integrin. We have shown that AAVP provides superior tumor transduction over phage and that incorporation of inverted terminal repeats is associated with an improved fate of the delivered transgene. Moreover, the temporal dynamics and spatial heterogeneity of gene expression mediated by targeted AAVP can be monitored by positron emission tomography. This new class of targeted hybrid viral particles will enable a wide range of applications in biology and medicine. Evaluation of this vector for therapeutic delivery of TNF to tumor-bearing dogs revealed positive results. A clinical trial is planned to bring this vector into the clinic.

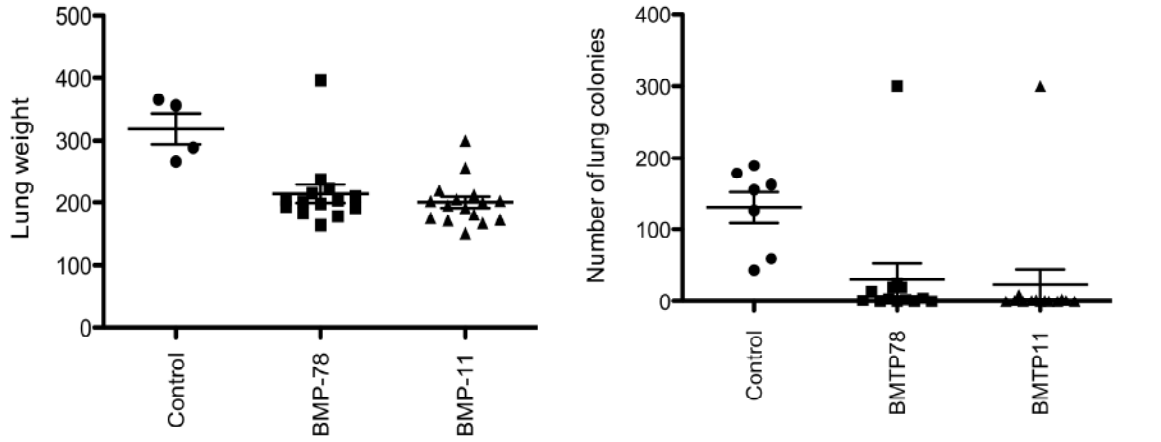

Figure 8: Treatment of tumor-bearing animals with BMTP-11 and BMTP-78. After 4 weeks of treatment, lungs of treated and untreated animals were collect and analyzed for the presence of lung cancer colonies. A significant reduction in lung weight and presence of lung cancer colonies was observed in animals treated with both compounds.

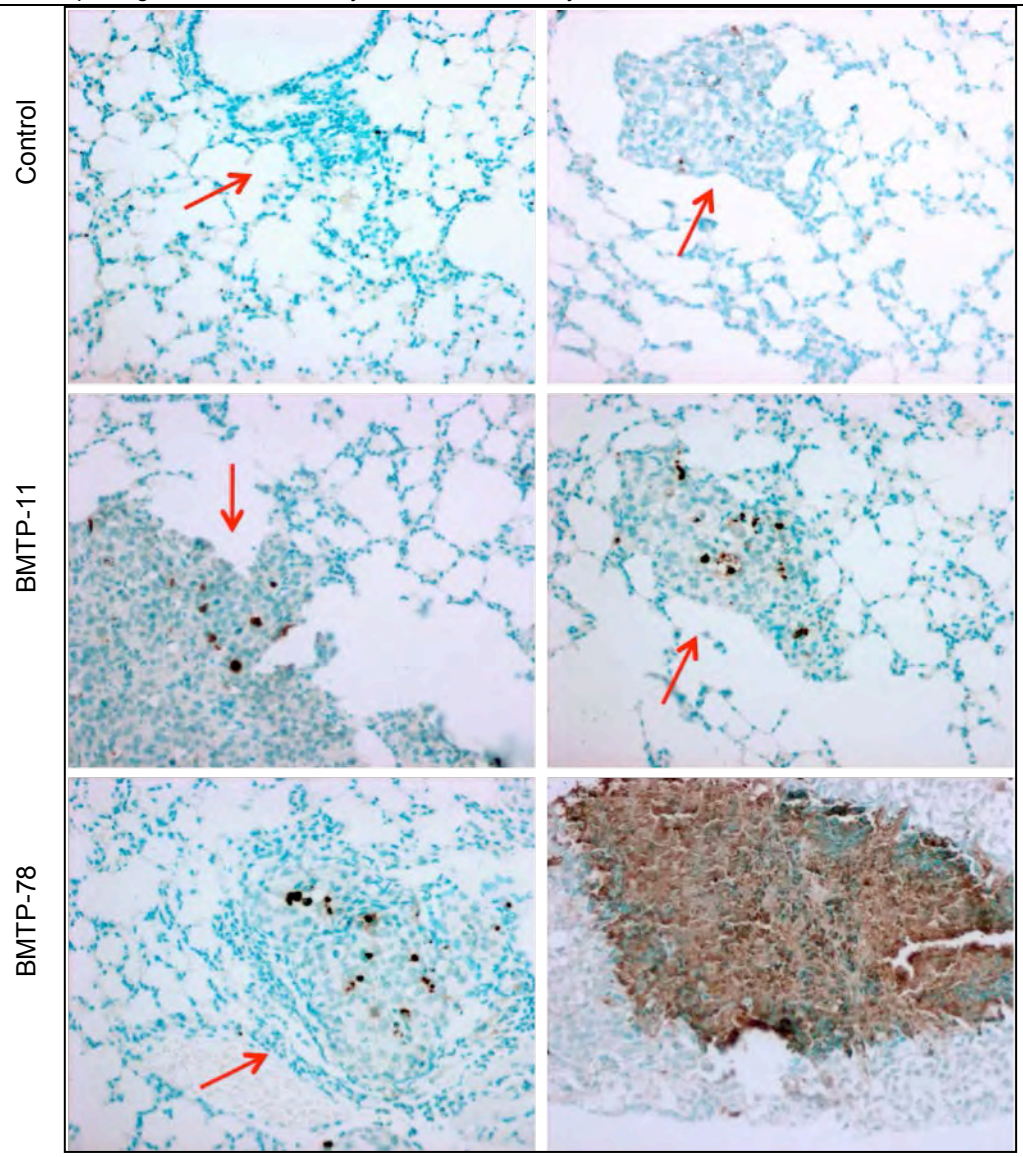

Figure 9: Lung of treated animals were analyzed for the presence of apoptotic cells after treatment with BMTP-11 and BMTP-78. Arrows point to lung cancer colonies containing apoptotic lung cancer cells (brown staining).

Phage-based direct assembly of gold nanoparticles and NIR applications

The integration of phage display-based combinatorial tissue targeting and nanotechnology has emerged from methodology we have established for the direct-assembly of gold (Au) nanoparticles onto phage. Given the challenges for reproducibly building at the nanometer scale, including the need for streamlined and "bottom-up" approaches for assembling nanoparticle architectures, the combination of phage and Au nanoparticles is an ideal system to gather the required expertise to control the fabrication and application of biological assisted nano-assemblies. This work was motivated from the premise that, in nature, the direct-assembly of molecules and particles is often directed by non-specific hydrophobic, van der Walls, and/or electrostatic interactions. We hypothesized that the assembly of phage and Au nanoparticles may also occur spontaneously through similar interactions. The outcome from testing this hypothesis was the design and validation of a method for Au-phage-based nano-assembly without genetic manipulation or complex conjugation chemistry. We have generated stable and biologically active networks of direct-assembled Au-phage scaffolds, in which we can tune the

chemical and physical properties of these biological structures. This tuning capability combined with the programmed tissue targeting property of the phage has proven most valuable, as it has allowed us to integrate multiple functions in a single nano-assembly, serving as a complementary and non-mutually exclusive tool among applications, i.e., near infrared (NIR) surface enhanced Raman scattering (SERS) detection, Au enhanced fluorescence in vitro imaging, MRI and CT scan in vivo imaging, and/or heat deposition for NIR photo-therapy. The identification of vascular markers targeted by circulating ligands continues to shed light on the complex cellular and molecular diversity of the human vasculature. In the near future, the integration of the molecular diversity of blood vessels with nanotechnology will be translated into clinical applications.

Aim 3 To design tools for molecular imaging of lung tumors.

Summary of Research Findings

Feb 2010 Report: In collaboration with Dr. Juri Gelovani, our group has previously reported the design, generation, and construction of AAV/phage (termed AAVP) particles (Hajitou et al. 2006, Hajitou et al. 2007, Soghomonyan et al. 2007) for targeted molecular-genetic imaging. These hybrid vectors containing prokaryotic and eukaryotic cis-genomic elements have the potential to integrate ligand-directed targeting and molecular-genetic imaging. In a related line of research, we have used labeled targeted peptide motifs themselves as imaging tools (Yao et al. 2005, Marchiò et al. 2004, Arap et al. 2004, Zurita et al. 2004, Cardó-Vila et al. 2003, Chen et al. 2003, Mintz et al. 2003). In pilot experiments, AAVP-based molecular-genetic imaging appears to be superior to FDG in side-by-side comparisons because it provides prediction of therapeutic response in addition to response monitoring (Hajitou et al., *PNAS*, 2008). Thus, we plan focus primarily on the development of AAVP-based molecular-genetic imaging. Finally, we have also designed and developed nanotechnology-based (i.e., bottom-up self-assembled) biocompatible networks of phage-gold as nanotechnology-based molecular sensors and reporters (Souza et al. 2006a, Souza et al. 2006b); this new methodology will be incorporated and it will likely prove to be quite synergistic with AAVP (Souza et al. Nature Nanotechnology, 2010).

Future Planned Research

There are several areas of research planned: (i) To use prototypes of this new class of targeted hybrid vectors for therapy and for molecular-genetic imaging; (ii) to develop AAVP-based library applications; (iii) to create other chimeric prokaryotic-eukaryotic vectors; and ultimately (iv) to generate an “imaging transcriptome” for lung cancer.

(i) We will use targeted prototypes of this class of hybrid vectors for molecular-genetic imaging/therapy, specifically for:
- Discovery of new ligand motifs that target human tumor endothelium (Staquicini et al., in progress)
- AAVP-based anti-vascular cancer therapy by targeted TNF in pet dogs with native tumors (Paoloni et al., in press)
- Integrate biocompatible networks to create a transducing matrix (Driessen et al., in preparation)

(ii) To develop AAVP-based combinatorial peptide libraries for use in directing patient selection, e.g., for patient settings such as pre-operative and with metastatic tumors. As such, the steps towards this goal are as follows:
- Design and production of targeted AAVP prototypes and libraries in GMP-facilities for patient applications.
- NIH RAC approval for long-term transduction in cancer patients.
- Proof-of-concept with a reporter/suicide gene (i.e., HSV-*tk*) or targeted TNF.

(iii) We will create other hybrid vectors with the biologic attributes of bacteriophage and animal viruses. Generation of a double-stranded DNA construct with elements of adenovirus and of lambda phage is ongoing (Sun et al., in progress)
(iv) The incorporation of transcriptional targeting (through tissue-specific or radiation-induced promoters) to ligand-directed AAVP-targeting may enable one to determine a gene's (or set of genes') status without tissue biopsy.

Mentoring, Past Outcomes, and Future Training
Several investigators have developed either into academic diagnostic radiologists (e.g., Bradley Restel, M.D.) or became independent laboratory-based Principal Investigators with an interest in molecular imaging (Amin Hajitou, Ph.D., Glauco Souza, Ph.D.). The current and next-generation of investigators in training include Suren Soghomonyan, Ph.D. and Michael Ozawa, M.D./Ph.D. student. We have requested a cross-appointment within the Department of Experimental Molecular Imaging (with Dr. Gelovani). We believe that a formal appointment within this department will mutually enhance the productivity of a Targeted Imaging Program (TIP) among other translational research initiatives. We also trust that reportable outcomes including improved cross-training of translational researchers in molecular imaging will be facilitated as a consequence of this faculty appointment, and so a series of meetings and standing related activities has been planned for mid- to late-2010.

Key Research Accomplishments

- Used labeled targeted peptide motifs themselves as imaging tools.
- Demonstrated that AAVP-based molecular-genetic imaging appears to be superior to FDG in side-by-side comparisons for predicting therapeutic response.
- Designed and developed nanotechnology-based (i.e., bottom-up, self-assembled) biocompatible networks of phage-gold as nanotechnology-based molecular sensors and reporters.

Conclusions
The central working hypothesis in our program is that differential protein expression in the human vascular endothelium associated with lung cancer offers the potential for developing novel diagnostic, imaging, and therapeutic strategies. In essence, combinatorial library selections (peptide- and antibody-based) are leveraged to discover, validate, and exploit the vascular biochemical diversity of endothelial cell surfaces towards a new vascular-targeted pharmacology. Such targeting technologies may lead to the development of ligand-directed agents for application in the treatment of cancer patients. Translational applications, such as first-in-human clinical trials, have now began within the institution, as the Food and Drug Administration (FDA) has recently granted a "safe-to-proceed" status for the first vascular-targeted Investigational New Drug, discovered, developed and being evaluated in patients at MDACC. Such trials will ultimately determine the value of this strategy. Two other drugs are in pre-IND stage and several others in pre-clinical laboratory phase. Long-term, the broader vision of the research is a large-scale mapping of receptors in human vasculature towards a new ligand-directed pharmacology.

Reportable Outcomes
Patent Application: Staquicini FI, Pasqualini R, Arap W, inventors; The Board of Regents of The University of Texas System, assignee. Compositions and methods related to DNA damage repair. United States Patent Application US 14/343,943. 2012 Sep 14.

Project 4: Inhibition of bFGF Signaling for Lung Cancer Therapy

(PI: Reuben Lotan, Ph.D.)

The survival of lung cancer patients is poor because this cancer is diagnosed at advanced stages. Therefore, improvements in early detection through the identification of molecular markers for diagnosis and for intervention combined with targeted chemoprevention are urgently needed. While the molecular events involved in lung cancer pathogenesis are being unraveled by ongoing large scale genomics, proteomics, and metabolomics studies, it is already well recognized that proliferation-, survival- and angiogenesis- promoting signaling pathways are amplified in lung cancer. Among the angiogenesis signaling pathways, the basic fibroblast growth factor (bFGF) and its transmembrane tyrosine kinase receptors (FGFRs) are playing important roles in addition to the well-studied vascular endothelial growth factor (VEGF) and its receptors (VEGFRs). Both types of angiogenesis signaling pathways, the VEGF/VEGFR and the bFGF/FGFR, have been detected in NSCLC and associated with lung cancer development. However, most efforts in preclinical and clinical trials have been directed to the VEGF/VEGFR pathway.

We hypothesize that bFGF triggers signaling pathways that contribute to malignant progression of lung cancers by stimulating tumor cell and endothelial cell proliferation and survival and augmenting angiogenesis. Therefore, agents that intervene in this pathway may be useful for lung cancer therapy either alone or in combination with agents that target the VEGF/VEGFR signaling pathways and/or with cytotoxic agents. We will address the following specific aims in order to understand the mechanism(s) underlying the *in vitro* and *in vivo* effects of bFGF on lung cancer and endothelial cells and the ability of bFGF inhibitors to suppress the growth of NSCLC *in vitro* and *in vivo.*

Aim 1 Determine the effects of bFGF on *in vitro* growth, survival, motility, invasion and angiogenesis of NSCLC cells and endothelial cells.

Summary of Research Findings

Feb 2008 Report: Previously, we analyzed the expression of bFGF by Western blotting and that of the FGF receptors 1 and 2 by RT-PCR in NSCLC cell lines. During the last year, we expanded these findings to include western blotting analyses of FGF receptors and RT-PCR expression of VEGF and its receptors 1 and 2 (Figure 12). The RT-PCR results (Figure 12A) show that two of the cell lines (1170-I and H441) express components that can mediate both FGF and VEGF signaling in that they expressed the ligands bFGF and VEGF and at last one type of receptor (FGFR and VEGFR). In contrast, the H1975 cell line does not express bFGF but does express the VEGF and both of its receptors. Still, even H1975 has the potential to respond to exogenous bFGF from the microenvironment *in vivo* because these cells express the FGF receptors 1 and 2. The Western blotting data (Figure 12B) show that 1170-I and H441 cells express several molecular forms of the bFGF protein (the lowest is the secreted form 18kDa and the two upper ones are >20 kDa and represent the intracellular higher molecular weight form that are not secreted but can translocate into the cell nucleus. H1975 cells express very low levels of the three species of bFGF proteins. All the cell lines expressed FGFR3, whereas FGFR2 was detected only in H441 cells. Analyses of medium and cell lysates by enzyme-linked immunosorbent assay (ELISA) for VEGF (Figure 12C) revealed that the majority of the factor was secreted into the medium and only a small amount was found in the cell lysates. In contrast, the majority of bFGF was found in the cell lysate and only a small amount was secreted into the medium (Figure 12D). It is noteworthy that there was a good agreement between the RT-PCR, Western blotting and ELISA assays. For example almost no bFGF was

detected by any of the methods in H1975 cells. In addition, the ELISA assay demonstrated that VEGF is the main secreted angiogenic factor among these three cell lines and that bFGF is primarily intracellular. Thus, VEGF may function as the major angiogenic factor, whereas bFGF may play a role as intracrine mitogenic factor for these cells. Additionally, the FGF receptors may mediate growth stimulation if normal cells in the tumor microenvironment produce bFGF. Of note, these analyses only represent the relative amounts of the factors and receptors not their function and it is important to analyze the function because it is possible that even small

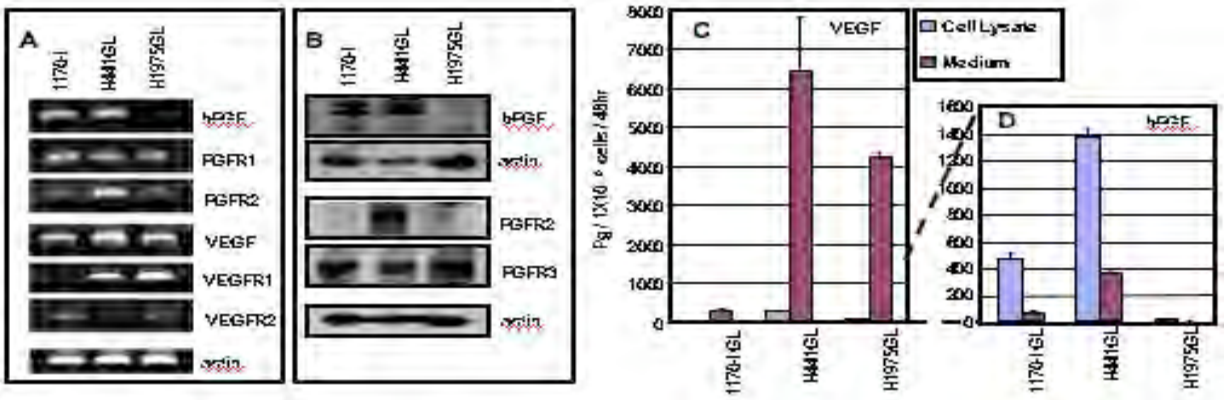

Figure 12. Expression of bFGF and VEGF and their receptors in NSCLC cells. A, B) The NSCLC cell lines indicated above each lane were harvested from nearly confluent cultures and used for extraction of total RNA (A) or total protein (B) and samples were analyzed by RT-PCR and western blotting, respectively for the expression of the factors and receptors indicated to the right of each row. C, D) cells were cultured in serum free medium for 48 hours and then the medium was collected and the cells were lysed and samples of both medium and cell lysate were analyzed using (ELISA) for the level of VEGF (C) or bFGF (D).

amounts of bFGF secreted into the medium will induce cell proliferation, motility and migration.

bFGF Signaling pathway in NSCLC cells. Previously, we reported that treatment of NSCLC cells with bFGF after serum starvation resulted in increased cell proliferation and a rapid and transient increase in phosphorylated ERK (p-p42/44) MAPK and Akt indicating that bFGF was mitogenic and enhanced survival pathway mediated by Akt.

During the last year, we expanded those initial observations to delineate the sequence of molecular events in bFGF signaling in NSCLC and found that: 1) Phosphorylation of FGFR1 was induced within 5 minutes of the addition of 10 ng/ml bFGF to NSCLC 1170-I cells (Figure 13A, top row). This effect was specific for FGFR1 as no increase in FGFR3 was observed after bFGF addition (Figure 13A, row 3). Interestingly, FGFR3 was phosphorylated constitutively, namely even without addition of bFGF. We suggest that endogenous bFGF, perhaps the secreted higher molecular weight variants of bFGF seen in Figure 12B (upper row) activated FGFR3. In other cells, bFGF has been shown to induce autophosphorylation of its receptor and this could lead to one or more of downstream effects by activation of MAPK (ERK1/2), phospholipase C gamma (PLCγ), or PI3K/Akt. We found that in 1170-I NSCLC cells, bFGF activated ERK1/2 and Akt but not the PLCγ pathways. Figure 10B shows that ERK was phosphorylated within 5 min of bFGF addition to the cells. ERK activation of was transient with a peak at 10 min. AKT was also activated by 10 min as indicated by the detection of phosphorylated Akt (Figure 10B, row 4). In contrast, PLCγ was phosphorylated at a low level before bFGF addition and no further or only a minor increase was observed after bFGF addition (Figure 13, row 6). It appears that although FGFR3 appeared to be constitutively activated, this

activation did not lead to phosphorylation of either ERK or Akt. However, it is possible that FGFR3 was responsible for the basal phosphorylation of PLCγ.

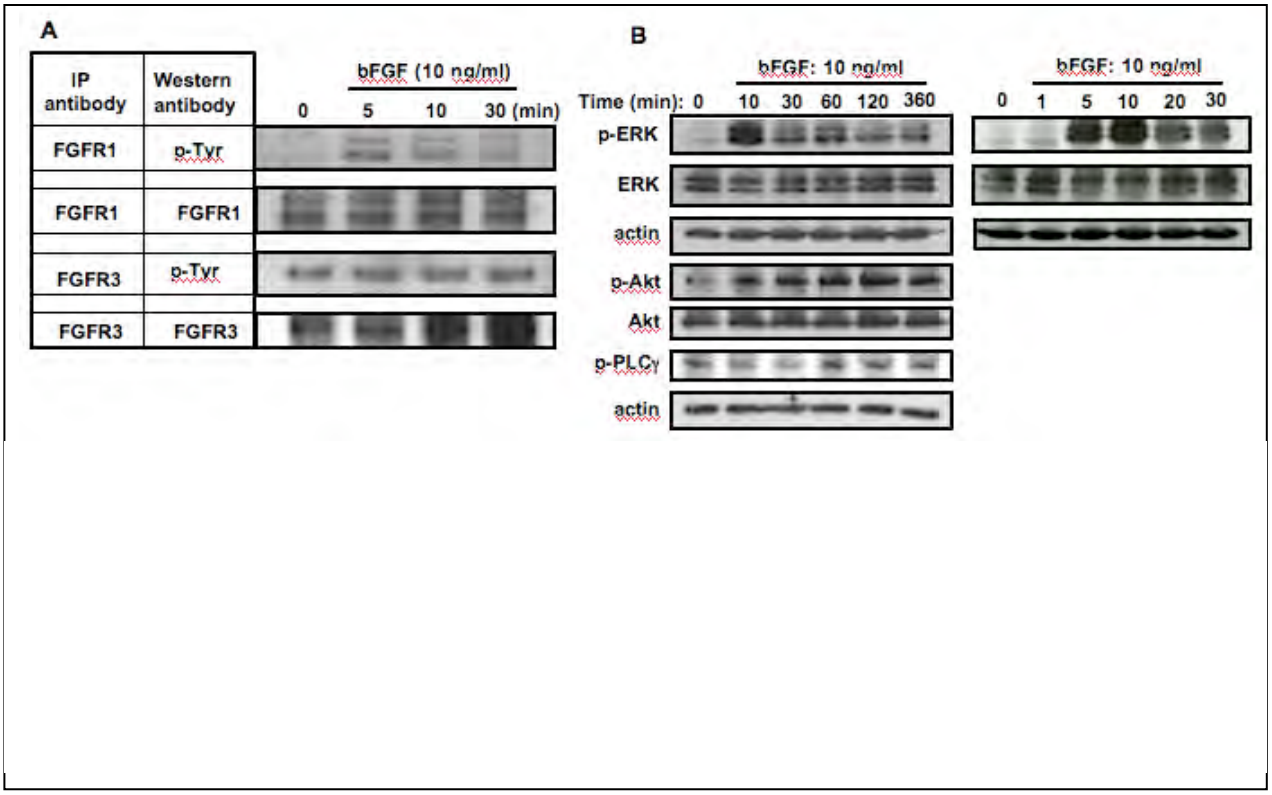

Effects of bFGF on cell growth. Previously, we have shown that bFGF was mitogenic to several NSCLC cell lines. We have now added data on the 1170-I tumorigenic bronchial

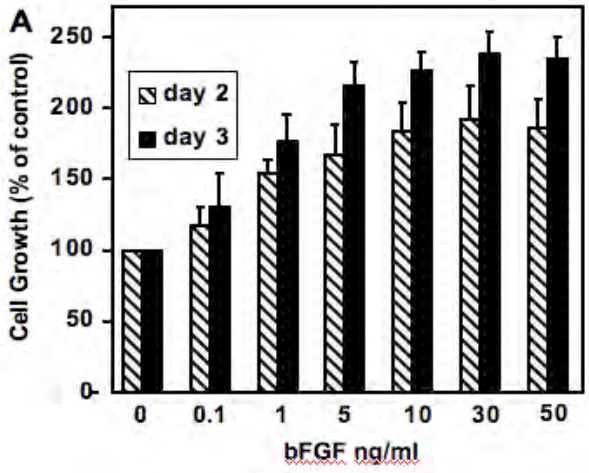

B

Cell cycle phase	control	bFGF (10 ng/ml)
G1	66.85	▼ 50.17
S	20.75	▲ 36.03
G2	11.9	12.24

Figure 14. A) 1170-I cells were seeded at a density of 2.0 X 10^3 / per well in 96 well plates with medium containing 10% serum and grown for 12 hr. The medium was then replaced with serum-free medium and the cells were incubated for 48 hr. Then the cells received a fresh serum-free medium with the indicated bFGF concentrations or no bFGF (control). After 48 hr and 72 hr, the cell numbers were estimated using the sulforhodamine B (SRB) assay. B) the same cells were cultured in 10-cm diameter dishes with the same medium changes as above and after 72 hr of treatment with bFGF or control medium, the cells were harvested and subjected to cell cycle analysis using flow cytometry.

epithelial cells. Figure 14 shows that the growth of these cells was stimulated by bFGF in a time- and dose-dependent fashion (Figure 14A) and cell cycle analysis indicated that bFGF decreased the percentage of cells in the G1 phase and increased the percentage of cells in the S phase (DNA synthesis).

Suppression of endogenous bFGF using SiRNA decreases the growth of 1170-I cells. Preliminary results presented in Figure 15 show that treatment of the 1170-I cells with siRNA that targets bFGF causes a decrease in the levels of the endogenous bFGF proteins (B) and this is accompanied by a decreased in cell growth (A)

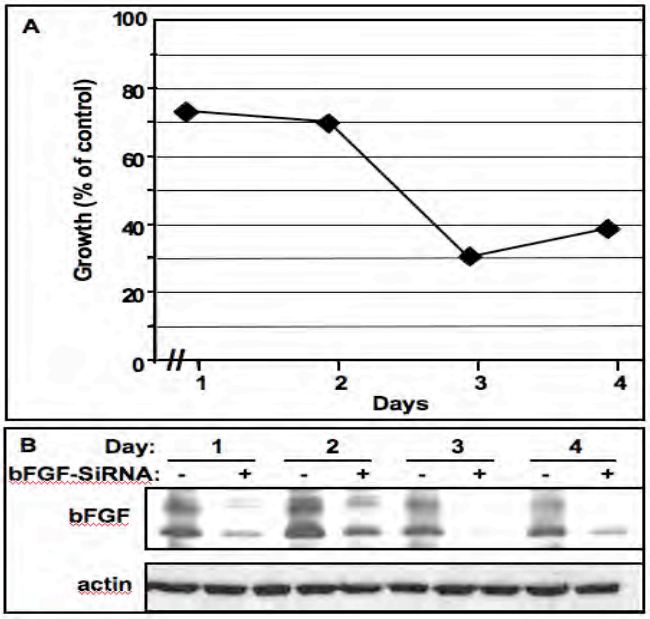

Figure 15. A) 1170-I cells were treated with small interfering RNA (siRNA) targeted against bFGF or control siRNA and the level of bFGF proteins was analyzed by western blotting after 1, 2, 3 and 4 days (B). Cell growth relative to untreated controls was also determined (A).

bFGF enhances the invasion of 1170-I cells. We used a standard invasion assay through a biological extracellular matrix coated on a polyporous membrane in a Boyden chamber to determine whether bFGF exerts invasive properties on the 1170-I cells. Figure 16 shows that

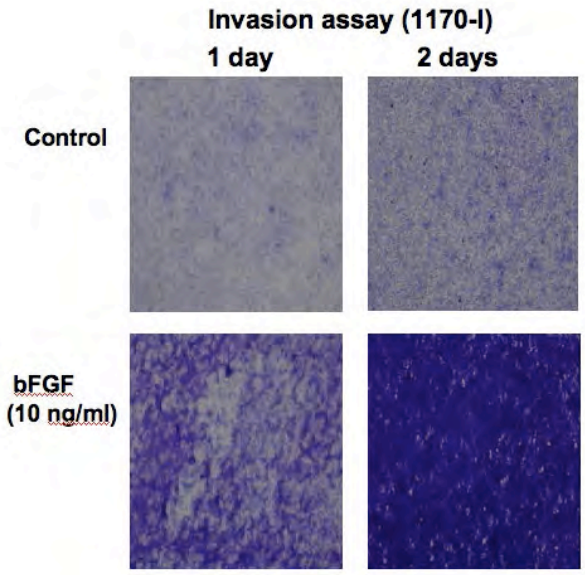

when bFGF is placed in the bottom chamber under the coated membrane 1170-I cells are induced to invade through the matrix and through the pores and migrate to the underside of the membrane.

Aim 2 Evaluate the relative potency of several inhibitors of bFGF binding to receptor (i.e., TMPP and analogs) in inhibiting effects of bFGF detected in Specific Aim 1 and evaluate the effects of these inhibitors in combination with paclitaxel on *in vitro* growth and survival of tumor cells.

Summary of Research Findings

Feb 2008 Report: We analyzed the effects of inhibitors of bFGF signaling on the growth of 1170-I cells. The inhibitors included the porphyrin analog, 5,10,15,20-tetrakis(methyl-4-pyridyl)-21*H*,23*H*-porphine-tetra*p*-tosylate salt (TMPP), which can inhibit bFGF and to a lesser extent VEGF binding to their cell surface receptors extracellular domain, the more specific bFGF inhibitor the pyrido-[2,3-d]pyrimidine, PD173074 that binds to the cytoplasmic tyrosine kinase domain of FGF receptor (FGFR1), and Ly294002, the inhibitor of the downstream phosphatidylinositol 3-kinase (PI3K). Figure 17 shows that the three inhibitors suppressed the growth of the 1170-I cells when the cells were cultured for 3 days in the absence of exogenous bFGF in a dose-dependent fashion. The TMPP and PD173074 also suppressed the mitogenic effect of exogenously added bFGF. LY294002 was the most potent inhibitor at the doses used in cells grown with or without bFGF. However, it is not a specific bFGF signaling inhibitor but rather an inhibitor that could also affect signaling by various other growth factors and receptors.

Aim 3 Evaluate anti-tumor activity (growth inhibition, apoptosis, suppression of angiogenesis) of the most effective inhibitor identified in Specific Aim 2 when used alone and in combination with paclitaxel in an orthotopic lung cancer model using luciferase-expressing NSCLC cells for *in vivo* bioluminescence imaging of tumor growth and response to treatment.

Summary of Research Findings

Feb 2009 Report: The most appropriate way to pursue our *in vivo* studies, as a prelude to potential clinical trials, is to secure a large source of the drug from our pharmaceutical counterparts. Therefore, from the beginning of this project, we tried to identify agents that target FGF receptor signaling and are under development in pharmaceutical companies. We had identified three companies and tested two of the compounds that they had agreed to provide. Initially, we examined the compound 5,10,15,20-tetrakis(methyl-4-pyridyl)-21H,23H-porphine-tetra-p-tosylate salt (TMPP), which showed inhibitory effects against lung tumor cells, as reported previously. However, the company (Prochon, Rehovot, Israel), which was the source of this agent, decided not to pursue the development of this compound. We contacted Sanofi-Aventis after learning that they had an FGFR inhibitor (SSR128129E). We found that this compound was ineffective in any of our cell lines at concentrations that were relevant for *in vivo* studies. Therefore, we stopped further experiments with this agent, and, as noted, Sanofi-Aventis has also stopped development of this agent due to toxicity.

We contacted Bristol-Mayer-Squibb, who had a dual vascular growth factor receptor (VEGFR) / Fibroblast growth factor receptor (FGFR) inhibitor in development, but we were not able to get this material for *in vitro* testing. Therefore, we were not able to carry out in vivo experiments with these small molecules. As an alternative, we examined two potential approaches that were described above under specific aim 3, namely the FGFR inhibitor 5'-(methylthio)adenosine and the adenoviral vector expressing dominant negative FGF receptor.

Aim 4 To investigate the expression of bFGF signaling components (bFGF, FGFR-1, FGFR-2, heparan sulfate, syndecan-1, and FGFR-3) by IHC staining of tissue microarrays (TMAs), and correlate the expression of bFGF/bFGFRs between tumor and non-malignant epithelial cells with angiogenesis.

Summary of Research Findings

Feb 2010 Report: Over the previous year, our research has focused on understanding the mechanism of the anti-tumor effects of agents that target FGFR1-mediated signaling, especially the adenoviral vector expressing the dominant-negative FGFR1 construct (AdV/DNFR1). We focused on this agent after demonstrating, as reported previously in last year's report, that it had a potent growth inhibitory effect on several lung cancer cell lines. We explored the potential role of the heat shock protein Hsp90 as downstream effectors of FGF signaling.

Differential growth inhibitory effects of adenoviral DNFR on normal and malignant lung cancer cells

We compared normal human bronchial epithelial cells (NHBE) to those of the malignant lung cell lines (1170-I, A549, and H1299) regarding their response to inhibition of FGFR1 signaling using an adenoviral vector containing the dominant-negative FGFR1 (AdV/DNFR1). We found that the malignant cells were more sensitive to growth inhibition than the normal cells (Table 2). NHBE and malignant lung cancer cells were treated with adenoviral vector containing only LacZ reporter or the dominant negative FGFR1 construct or without any treatment, and the cell numbers were determined 48 and 72 hours later using the colorimetric sulforhodamine B assay. Growth inhibition as a percentage of the untreated cells was calculated and the inhibition by the LacZ vector was subtracted from that of the AdV/DNFR1.

Table 2. Effects of AdV/DNFR1 on cell growth

Cells	Growth inhibition by AdV/DNFR1	
	48 hours	72 hours
Normal NHBE	10.0	16.2
1170-I	23.1	32.5
A549	21.3	42.0
H1299	20.8	39.8

Table 3. Effects of AdV/DNFR1 on cell cycle and apoptosis in H1299 cells

Cell cycle phase	Control	AdV/DNFR1
G1	38.7	26.0
S	38.1	20.5
G2/M	23.2	53.5
Apoptosis	3.22	14.7

The growth inhibition was primarily the result of induction of a cell cycle arrest in the G2/M phase and, to a much lesser degree, via induction of apoptosis (Table 3). The malignant lung cancer cells H1299 were treated with adenoviral AdV/DNFR1 or control vector and, after 48 hours, they were harvested and their DNA was stained with propidium iodide or with the apoptosis TUNEL reagents; cell cycle and apoptosis were then analyzed by flow cytometry.

Mechanisms of cell cycle arrest in G2/M by AdV/DNFR1 infection

To understand the mechanism by which suppression of FGFR1 signaling using the AdV/DNFR1 inhibits growth by G2/M cell cycle block, we analyzed various proteins that regulated cell cycle in 1170-I cells treated with AdV/GFP control vector or AdVDNFR1. Cdc2, a cyclin- dependent kinase (also called CDK1), determines the onset of mitosis in all eukaryotic cells. In its unphosphorylated state, CDK1 forms a complex with cyclin B1 to trigger entry into mitosis.

The function of cdc2 is inhibited by phosphorylation on tyrosine 15, which causes dissociation from cyclin B1. This phosphoryation can be caused by the kinase Wee1 while the phosphatase cdc25 can dephosphorylate cdc2. Thus, increase in Wee1 and decrease in cdc25 can each induce a G2 arrest. Chk1 kinase can activate Wee1 and inactivate Cdc25 phosphatase and these effects can lead to G2 arrest as well. P21 can inhibit cdc2-cyclin B complex and block cell

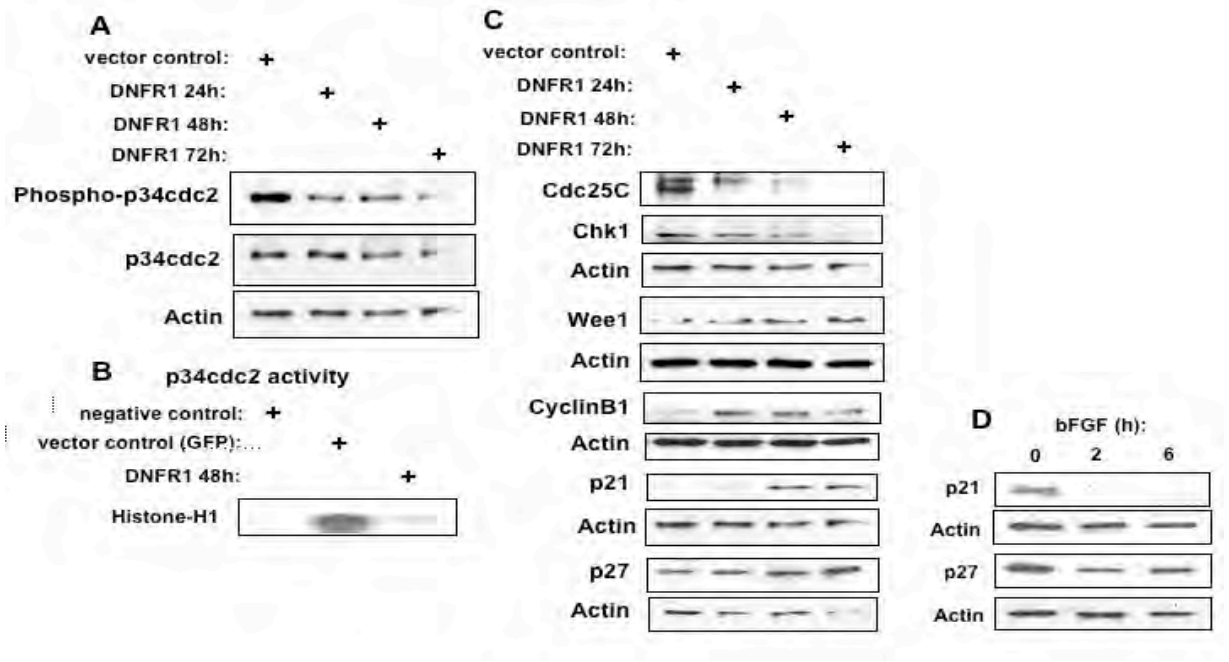

Figure 11. ***A***: Analysis of cell cycle related proteins in AdV / DNFR1 infected 1170-I cells. The cells were infected with vector control (GFP) or the dominant negative vector and after 24, 48 and 72 hours, the cells were harvested and lysates were prepared. ***A and C***: The lysates were separated by 10% SDS-PAGE and analyzed for levels of the indicated proteins by Western blotting. ***B***: The lysates were subjected to *in vitro* kinase assay by immunoprecipitating p34cdc2 followed by analysis of its kinase activity using histone H1 as a substrate and of [^{32}P] adenosine triphosphate (ATP) as phosphate donor followed by gel electrophoresis and autoradiography of the dried gel. ***D:*** The 1170-I cells were treated with vehicle or 20 ng/ml bFGF for 2 or 6 hours in KGM medium (without supplement). The cells were lysed and analyzed by Western blotting for levels of p21, p27 and actin.

cycle in G2. As shown in Figure 1, we found that AdVDNFR1 decreased the expression of p34cdc2 mainly after 48 and 72 hours, but more rapidly decreased the level of cdc2 phosphorylation, after only 24 hr (Figure 11A). Furthermore, the kinase activity of cdc2 was suppressed in the DNFR1 infected cells (Figure 11B). In addition, the expression of DNFR1 decreased the levels of cdc25 and Chk1 and increased Wee1, and the cyclin–dependent kinase inhibitors (CKI) p21 (inhibits cdk2 and cdk4) and p27 (CDKN1B) (Figure 11C). These changes can explain the G2 arrest. The increase in cyclin B1 is not clear but, with a low level of cdc2, cyclin B1 would not be able to function in triggering mitosis. Interestingly, the effect of the DNFR1 was opposite to the effect of bFGF, which suppressed the levels of the cell cycle kinase inhibitors (CKI) p21 and p27 (Figure 11D). The opposite effects of DNFR1 and bFGF lend further support to the conclusion that DNFR1 blocks the FGFR1 signaling. These results indicated that the adenoviral vector containing a dominant negative FGFR1 receptor construct could potentially be useful for treatment of lung cancer *in vivo*. Studies targeting lung cancer could benefit from an aerosolized delivery by inhalation.

Induction of Hsp90 by bFGF and effects of Hsp90 inhibition on lung cancer cell growth

Other reported that the mitogenic effects of bFGF in breast cancer cells require the presence of the heat shock protein Hsp90. Hsp90 is ubiquitous but its expression is elevated in many cancer cells, including lung cancer compared to normal cells. It regulates cellular stress responses by acting as a chaperon protein; namely, it preserves the function of proteins by maintaining their conformation and stability. These client proteins play important functions such as growth, differentiation, and survival. Initially, we determined whether Hsp90 and other Hsps are expressed in lung normal and malignant cells. We found that only Hsp90 showed a consistent increased level between normal and malignant cells, and its level increased gradually from normal through immortalized and transformed cells to malignant cells (Figure 12).

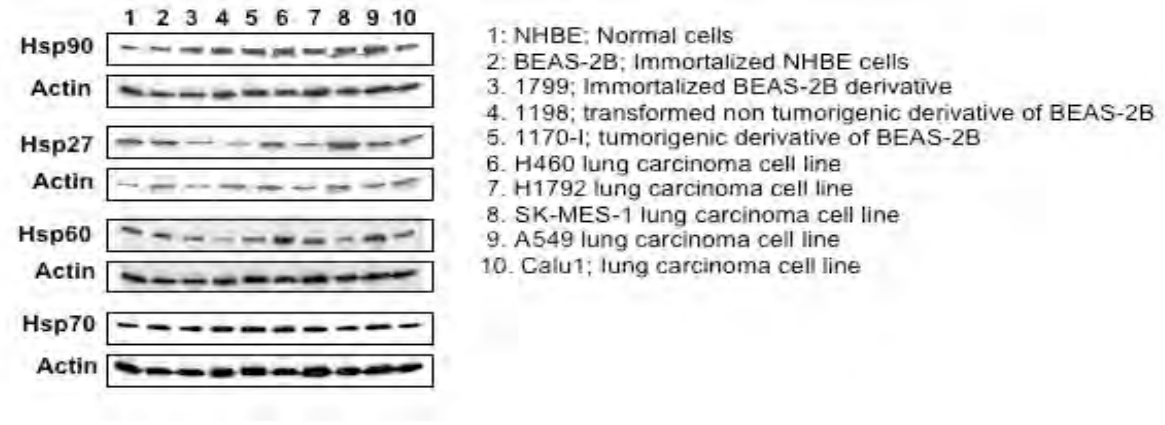

Figure 12. Expression of Heat shock proteins in normal, immortalized, transformed and tumorigenic/malignant lung cells. The indicated 10 cell lines were cultured in their optimal growth media and harvested and lysed then analyzed by Western blotting for the expression of Hsp90, Hsp27, Hsp60, and Hsp70. Actin was used as an internal control to compare protein loading in the different lanes.

To determine whether Hsp90 is important for the growth of lung cancer cells and whether its expression is related to the effects of bFGF and to FGFR signaling in lung cancer cells, we analyzed the effects of the Hsp90 inhibitor Geldanamycin on the lung cancer cells in the absence and presence of bFGF. We found that treatment of lung cancer cells with Geldanamycin inhibited cells growth by blocking cells in the G2 phase of the cell cycle and by inducing apoptosis (Figure 13A). Treatment with a low dose of 50 nM Geldanamycin was able to decrease the percentage of cells in the S phase and double the cells in the G2/M phase. However, the overall effect on apoptosis was rather small (<10%). Treatment with a high dose of 1 μM Geldanamycin induced a more substantial decrease in S phase, an increase in G2/M (Figure 13A, lower panels), and a particularly impressive increase in apoptosis up to 76.8% (Figure 13B, lower panels).

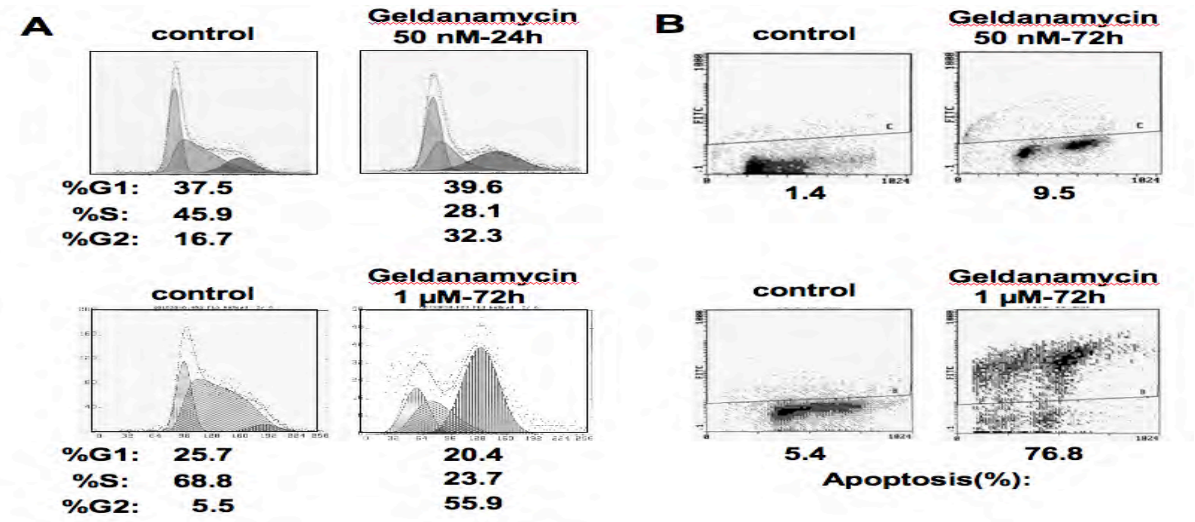

Figure 13. Effects of Geldanamycin on cell cycle and apoptosis in 1170-I lung cells. The cells were grown in control medium or in medium with either 50 nM or 1 μM Geldanamycin. After 24 hours, cells were harvested for cell cycle analysis after propidium iodide staining of their DNA followed by flow cytometry. Other cultures of the same experiments were harvested after 72 hours and analyzed for apoptosis by the TUNEL assay. The numbers below the flow cytometry data represent either % cells in different phases of the cells cycle (**A**) or % apoptosis (**B**).

To explore the mechanism of the effects of Geldanamycin, we analyzed the level of proteins related to cell cycle regulation and apoptosis and found that Geldanamaycin increased the level of cyclin B1 and p21 and decreased the level of Wee1 (Figure 14). Importantly, Geldanamycin decreased the level of cdc2 (Figure 14B) and suppressed the kinase activity (Figure 14C). The

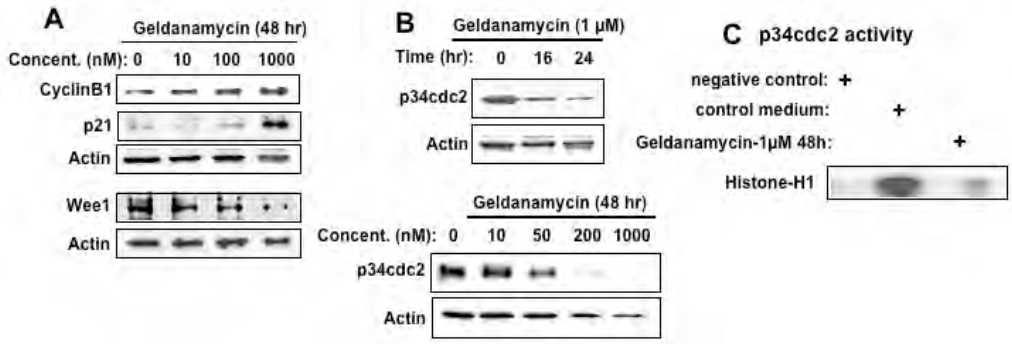

Figure 14. Effects of Geldanamycin on the levels of cell cycle related proteins in 1170-I cells. The cells were grown in control medium or medium with the indicated concentrations of Geldanamycin for 48 hours (**A**, lower panel in **B**, and **C**) or for 16 or 24 hours (**B**). The cells were harvested at those times and subjected to Western blotting analysis (**A** and **B**) or to cdc2 kinase activity using Histone H1 as a substrate (**C**).

latter effects were reminiscent of the effects of the dominant-negative FGFR1 infection (Figure 11).

To explore the possible cross talk between Hsp90 and FGF signaling, we analyzed the effect of bFGF treatment on Hsp90 level and found that treatment of lung cancer cells with bFGF induces the heat shock protein Hsp90 without affecting the levels of other Hsp protein like Hsp27 and Hsp70 (Figure 15).

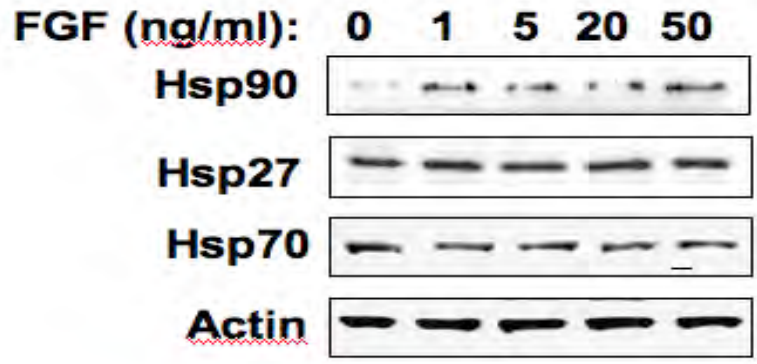

Figure 15. Induction of heat shock protein Hsp90 by bFGF in 1170-I cells. The cells were treated for 2 hours with the indicated concentrations of bFGF then harvested and analyzed by western blotting for the expression of Hsp27, 70 and 90. The same membrane was probed with actin as a control for protein loading.

To assess the possible role of Hsp90 in the growth stimulatory effects of bFGF on the lung cells, we examined the ability of Geldanamycin to affect the growth stimulation of the lung cells by bFGF. We found that Geldanamycin inhibited, in a dose-dependent fashion, the growth

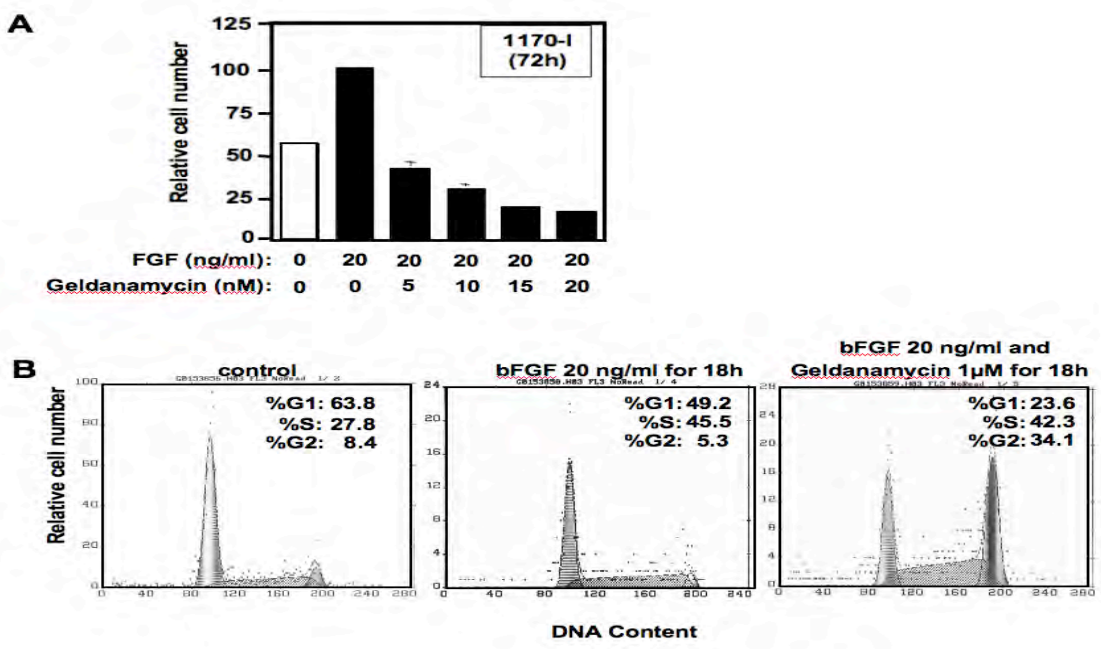

Figure 16. Effects of Geldanamycin on the mutagenic effect of bFGF. 1170-I cells were grown in control medium or medium with 20 ng/ml bFGF without and with the indicated concentrations of Geldanamycin for 72 hours (**A**) or 18 hr (**B**). The cells were harvested at those times and subjected to cell counting by a colorimetric assay (**A**) or to cell cycle analysis by propidium iodide DNA staining followed by flow cytometry (**B**).

stimulatory effect of bFGF in 1170-I cells (Figure 16). These results suggest that Hsp90 function is important for the mitogenic effects of bFGF in the lung cells.

Reportable Outcomes

Publications Not Previously Reported: Pierre Saintigny, Erminia Massarelli, Steven Lin, Young-Ho Ahn, Yulong Chen, Sangeeta Goswami, Baruch Erez et al. "CXCR2 expression in tumor cells is a poor prognostic factor and promotes invasion and metastasis in lung adenocarcinoma." *Cancer Research* 2013 73(2): 571-582. PMID: 23204236. PMCID:PMC3548940

Conclusions

Feb 2010 Report: Our results indicate that the adenoviral vector containing a dominant negative FGFR1 receptor construct, which inhibits FGFR signaling, could potentially be useful for treatment of lung cancer *in vivo.* Studies targeting lung cancer with this adenoviral construct are warranted. Such studies could focus on adenovirus delivery by inhalation using an aerosolized preparation. In terms of understanding FGFR signaling, our studies highlighted an important role for Hsp90 as a downstream mediator of FGF effects. This suggests that combined targeting of FGFR signaling (e.g., by AdVDNFR1) and Hsp90 function (e.g., by Geldanamycin or other Hsp90 inhibitors) could provide additive or synergistic efficacy.

Project 5: Targeting mTOR and Ras signaling pathways for lung cancer therapy

(Project Co-leaders: Shi-Yong Sun, Ph.D., Suresh Ramalingam, M.D.)

Aim 1 To determine whether an mTOR inhibitor inhibits the growth of human NSCLC cells via G1 growth arrest or induction of apoptosis, and to identify the molecular determinants of mTOR inhibitor sensitivity.

Summary of Research Findings

Feb 2007 Report*:* We have concluded that both mTOR inhibitor rapamycin and RAD001 inhibit the growth of human NSCLC cells, but have minimal effects on cell cycle and apoptosis.

Using findings generated from this aim, an NIH R01 research grant proposal entitled “Enhancing mTOR-targeted Cancer Therapy” was prepared and successfully granted the 5-year award starting on August 15, 2006. One major objective of this proposal is to understand the mechanism by which mTOR inhibitors induce Akt activation in human NSCLC cells as well as other types of cancer cells.

Aim 2 To determine whether the effect of mTOR inhibitors on the growth of human NSCLC cells is enhanced in the presence of a PI3K inhibitor or a MAPK inhibitor.

Summary of Research Findings

Feb 2007 Report: In the 2006 progress report, we summarized the findings of the enhanced growth-inhibitory effects of the combination of the mTOR inhibitor rapamycin and the PI3K inhibitor LY294002, and of rapid Akt activation after mTOR inhibition. The work has been published in *Cancer Research* (Sun et al., Cancer Res, 2005). These results were also confirmed by other laboratories in different cancer cell lines and in RAD001-treated cancer specimens.

Recent studies also show that prolonged treatment (24 h) with mTOR inhibitors disrupts mTOR-rictor complex (mTORC2), leading to inhibition of Akt in a few cancer cell lines (Sarbassov et al.,

2006). Therefore, we studied the effects of long-term treatment with the mTOR inhibitor rapamycin on Akt activation in human NSCLC cells. In our cell systems, we found that prolonged treatment with mTOR inhibitors still increased Akt phosphorylation, albeit with inhibition of mTORC2 (Figure 1).

Furthermore, we established a rapamycin-resistant A549 NSCLC cell line, named A549-RR, by chronically exposing the cells to gradually increased concentrations of rapamycin over 6 months. This cell line is resistant to RAD001 as well. We found that the rapamycin-resistant cell line A549-RR, which was maintained in culture medium containing 1 μM rapamycin, exhibited decreased levels of rictor in the mTORC2 and high levels of activated Akt compared with parental A549 cells (Figure 2).

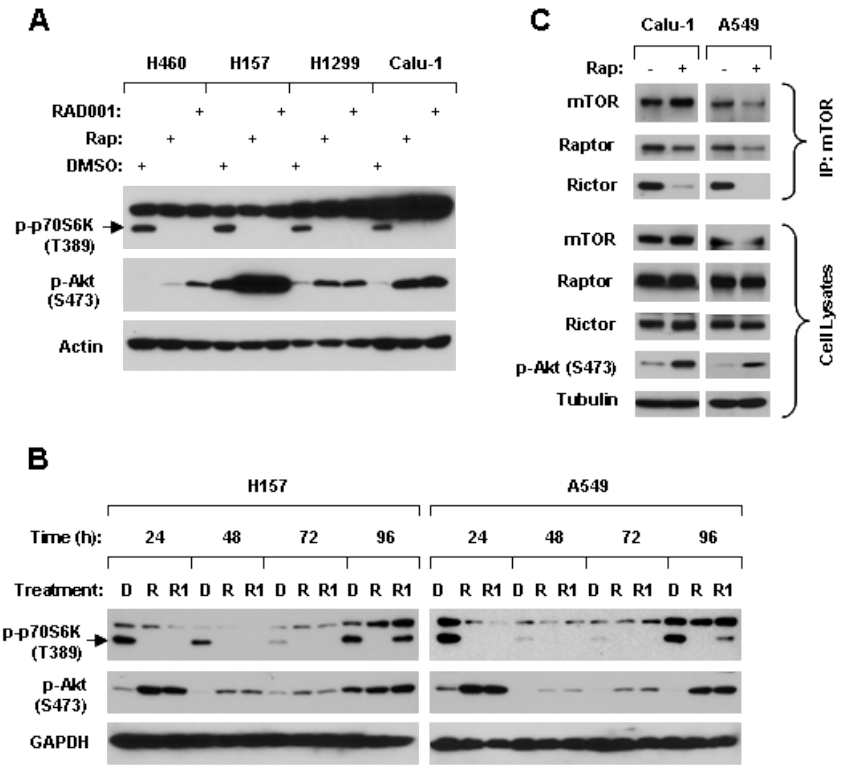

Figure 1. Effects of prolonged treatment with mTOR inhibitors on Akt phosphorylation (*A* and *B*) and mTORC2 assembly (C) in human lung cancer cells. ***A*** and ***B***, The indicated cell lines were seeded in 10-cm diameter cell culture dishes and treated on the second day with DMSO (D), 10 nM rapamycin (R) or RAD001 (R1) for 24 h (***A***) or 1 nM rapamycin for the indicated times (***B***). The cells were then harvested for preparation of whole-cell protein lysates and subsequent Western blot analysis. ***C***, Calu-1 and A549 cells were treated with 10 nM rapamycin for 24 h. The whole-cell protein lysates were then prepared and subjected to IP using mTOR antibody. Cell lysates and mTOR immunoprecitates were analyzed by Western blotting.

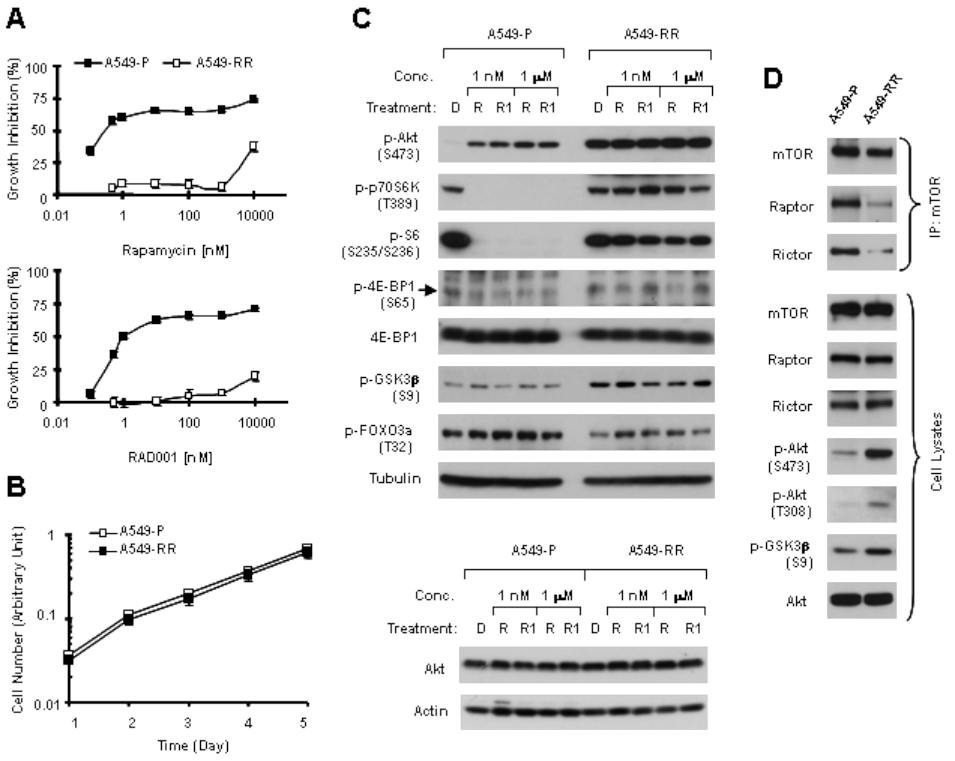

Figure 2. Comparison of cell sensitivities to mTOR inhibitors (*A*), growth rates (*B*), phosphorylation of p-Akt, p-p70S6K and p-S6 (*C*), and the levels of mTORC1 and mTORC2 (*D*) between A549 parental (A549-P) and rapamycin-resistant A549 cells (A549-RR). ***A***, The indicated cell lines were plated in 96-well plates and then treated with different concentrations of rapamycin or RAD001 as indicated on the second day. After 3 days, the cell numbers were estimated using the SRB assay. Each point represents a mean ± SD of four replicate determinations. ***B***, The similar number of A549-P and A549-RR cells were seeded in 96-well plates. At the indicated times, one plate was fixed for estimation of cell number using the SRB assay. Each point represents a mean ± SD of four replicate determinations. ***C***, The indicated cell lines were plated in 10-cm diameter cell culture dishes and treated on the second day with DMSO (D), the given concentrations of rapamycin (R) or RAD001 (R1) for 1 h. The cells were then harvested for preparation of whole-cell protein lysates and subsequent Western blot analysis. Rapamycin was removed from the culture medium for at least 24 h before A549-RR cells were used in the experiments. ***D*,** The whole-cell protein lysates were prepared from A549-P and A549-RR cells and then subjected to IP using mTOR antibody. Cell lysates and mTOR immunoprecitates were analyzed by Western blotting.

These compelling results indicate that long-term treatment with the mTOR inhibitor rapamycin in human NSCLC cells still induces Akt activation, which should be independent of mTORC2. Importantly, we found that when the rapamycin sensitivity of A549-RR cells was gradually restored upon withdrawal of rapamycin, a corresponding decline of phosphorylated Akt was observed, suggesting that Akt activation by the mTOR inhibitor rapamycin is associated with acquired rapamycin resistance (Figure 3).

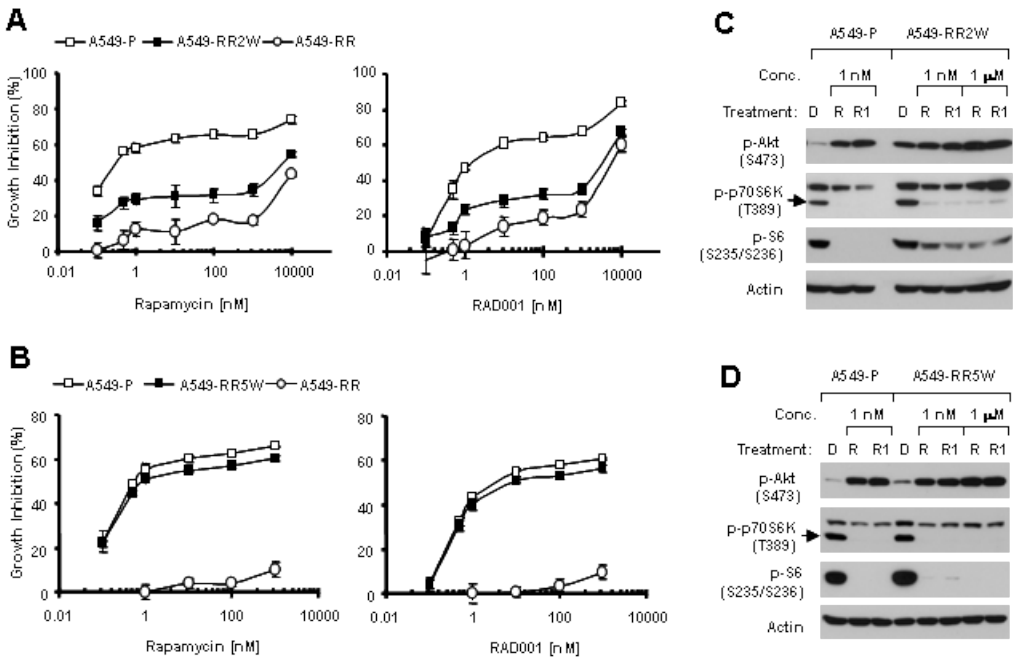

Figure 3. Impact of removal of the selective pressure rapamycin on rapamycin resistance (*A* and *B*) and phosphorylation of p-Akt, p-p70S6K and p-S6 (C and *D*). ***A*** and ***B***, A549-RR cells were cultured in complete medium without rapamycin for two months and 5 months to generate A549-RR2W and A549-RR5W cell lines, respectively. A549-RR2W and A549-RR5W cell lines were then used for the experiments. *A* and *B*, The indicated cell lines were plated in 96-well plates and then treated with different concentrations of rapamycin or RAD001 as indicated on the second day. After 3 days, the cell numbers were estimated using the SRB assay. Each point represents a mean ± SD of four replicate determinations. ***C*** and ***D***, The indicated cell lines were plated in 10-cm diameter cell culture dishes and treated on the second day with DMSO (D), the given concentrations of rapamycin (R) or RAD001 (R1) for 1 h. The cells were then harvested for preparation of whole-cell protein lysates and subsequent Western blot analysis.

This finding thus provides a strong rationale for combining an mTOR inhibitor with a PI3K inhibitor or an Akt inhibitor in the clinical treatment of lung cancer. Moreover, we found that A549-RR cells were fully sensitive to PI3K inhibitors (i.e., LY294002 and wortmannin), further refining our recommended clinical treatment strategy targeting the mTOR signaling pathway through intermittent utilization of an mTOR inhibitor and a PI3K inhibitor to avoid the development of rapamycin resistance. A manuscript detailing the results is in review by *Clinical Cancer Research* (Wang et al., 2007).

We have also studied mTOR-inhibitor-induced ERK activation and enhancement of mTOR inhibitor-induced growth inhibition by the MEK inhibitor U0126. We found that prolonged treatment (> 12 h) with the mTOR inhibitor rapamycin increased ERK phosphorylation, in addition to rapidly increasing Akt phosphorylation, in some NSCLC cell lines (Figure 4A-4C). Interestingly, we detected increased levels of p-ERK (p-p42/44) in the rapamycin-resistant cell line A549-RR compared to those in the parental A549-P cells (Figure 4D), suggesting that ERK activation is involved in rapamycin resistance. These findings provide a scientific rationale for combination of an mTOR inhibitor, such as rapamycin, with a MEK/ERK inhibitor, such as U0126.

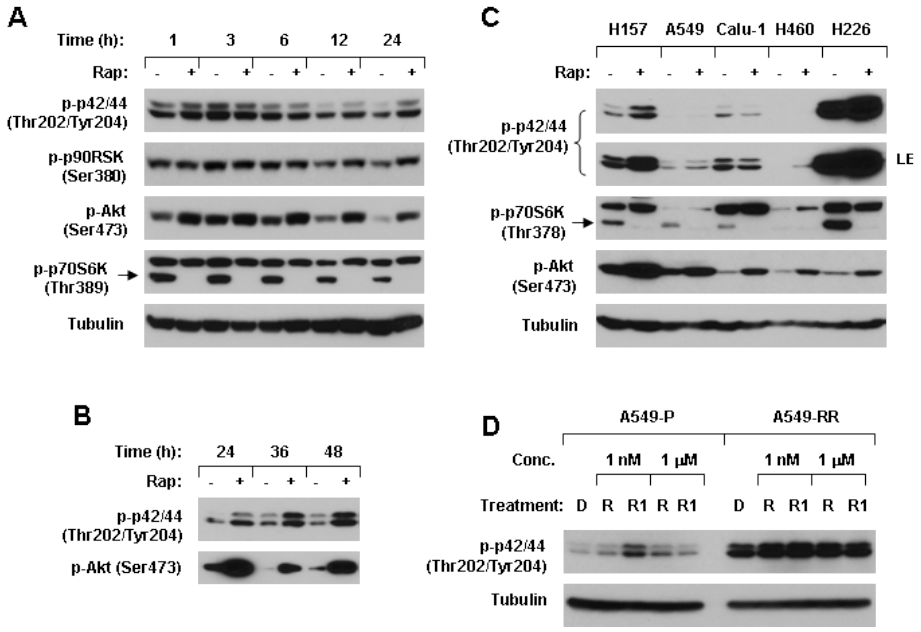

Figure 4. Prolonged treatment with rapamycin increases ERK (p42/44) phosphorylation in human NSCLC cells. ***A*** and ***B***, H157 cells were treated with 10 nM rapamycin (Rap) for the indicated times. ***C***, The indicated cell lines were treated with 10 nM rapamycin for 24 h. ***D***, the parental A549 (A549-P) cells and rapamycin-resistant A549 (A549-RR) cells were treated with rapamycin (R) or RAD001 (R1) at 1 nM or 1 μM for 1 h. Whole-cell protein lysates were prepared from the aforementioned treatments for detection of the given proteins with tubulin serving as a loading control by Western blot analysis.

We also studied the effects of rapamycin combined with U0126 on the growth of human NSCLC cells in both short- (3 d) and long-term (10 d) treatments. With both 3-day (Figure 5A) and 10-day (Figure 5B) treatments, the combination of rapamycin and U0126 had better growth-inhibitory effects than each single agent alone in both H460 and H157 cells. Collectively, these results indicate that co-targeting mTOR and MEK/ERK signaling pathways augments the inhibition of the growth of human NSCLC cells.

Aim 3 To evaluate the efficacies of the combinations of rapamycin with LY294002 or U0126 in nude mice models of lung cancer xenografts *in vivo*.

Summary of Research Findings

Feb 2009 Report: Results from the previous reporting period showed that mTOR inhibitors increase eIF4E phosphorylation in cultured lung cancer cells. Moreover, we determined whether mTOR inhibitors increased p-eIF4E levels *in vivo*. We further detected p-eIF4E levels in lung xenografts in mice exposed to RAD001 for 14 days using both Western blotting and immunohistochemistry (IHC). As presented in Figure 1A, p-eIF4E levels in both A549 and H460 xenografts treated with RAD001 detected by the Western blotting were significantly higher than those treated with vehicle control ($p < 0.001$). By IHC, we found that five out of six A549 xenograft tumors did not or expressed very low levels of p-eIF4E. However, six tumors exposed to RAD001 for 14 days exhibited increased levels of p-eIF4E (with various degrees) that were significantly higher than vehicle control tumors (Fig. 1B; $P < 0.01$). Collectively, these results indicate that RAD001 increases eIF4E phosphorylation *in vivo* in lung xenografts.

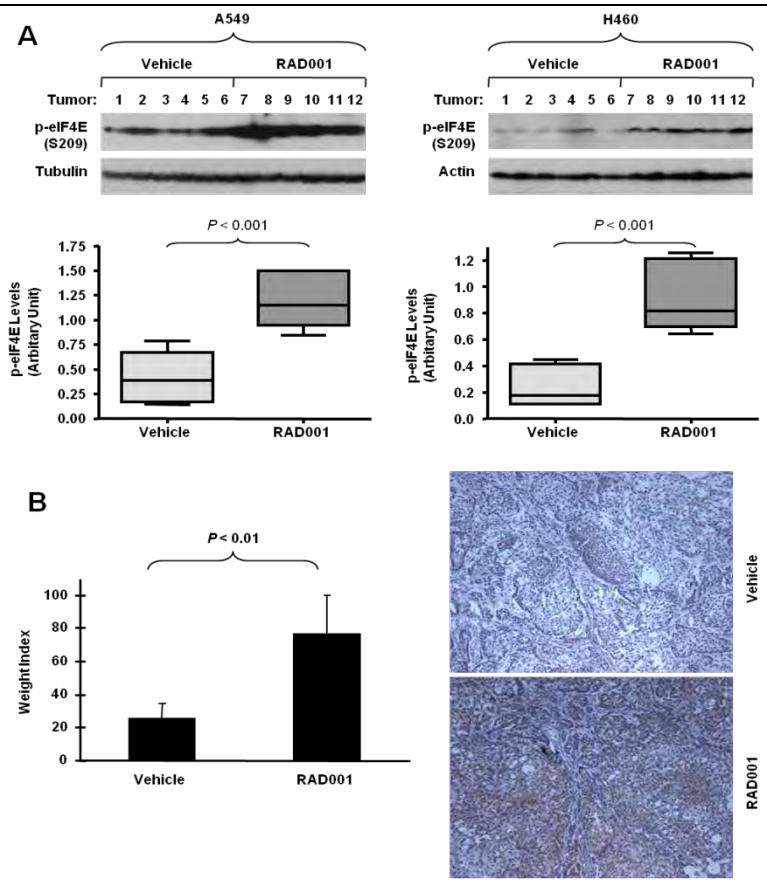

Figure 1: RAD001 increases p-eIF4E levels in lung cancer xenografts evaluated with either Western Blot analysis (*A*) or IHC (*B*). A549 cells at 5 x 10^6 in serum-free medium were injected s.c. into the flank region of nude mice. When tumors reached certain size ranges (~100 mm^3), the mice were randomized into two groups (n = 6/group) for the following treatments: vehicle control and formulated RAD001 (4 mg/kg/day, oral gavage). After 14 days, the mice were sacrificed and the tumors were removed, frozen (*A*) or fixed (*B*). ***A***, p-eIF4E was evaluated with Western blot analysis (upper panels) and the data was scanned and quantitated using NHI Image J software (lower panels). ***B***, p-eIF4E levels were detected using IHC and scored as a weight index (percentage × intensity) (left panel). Representative pictures of p-eIF4E expression (100X) were presented (right panels). The difference between vehicle and RAD001 treatments was analyzed by unpaired student *t* test with or without Welch correction.

In addition to induction of Akt phosphorylation by mTOR inhibitors, we found that mTOR inhibition also induced activations of the MEK/ERK signaling pathway in some cancer cell lines after a prolonged treatment. The combination of rapamycin with the MEK inhibitor U0126 significantly enhanced growth inhibitory effects of cancer cells, suggesting that MEK/ERK activation may counteract mTOR inhibitors' anticancer efficacy. Similarly, the combination of an mTOR inhibitor with the EGF receptor inhibitor erlotinib synergistically inhibited the growth of both human cancer cells in cell cultures and xenografts in nude mice (Fig. 2). Moreover, the presence of erlotinib suppressed rapamycin-induced phosphorylation of Akt, ERK and eIF4E as well, implying that erlotinib can suppress mTOR inhibition-induced feedback activation of several survival signaling pathways including Akt, ERK and eIF4E. Thus, we suggest a therapeutic strategy for enhancing mTOR-targeted cancer therapy by preventing mTOR inhibition-induced feedback activation of several survival mechanisms. These reportable outcomes were published in *Cancer Biology and Therapy* (Wang et al. 2008).

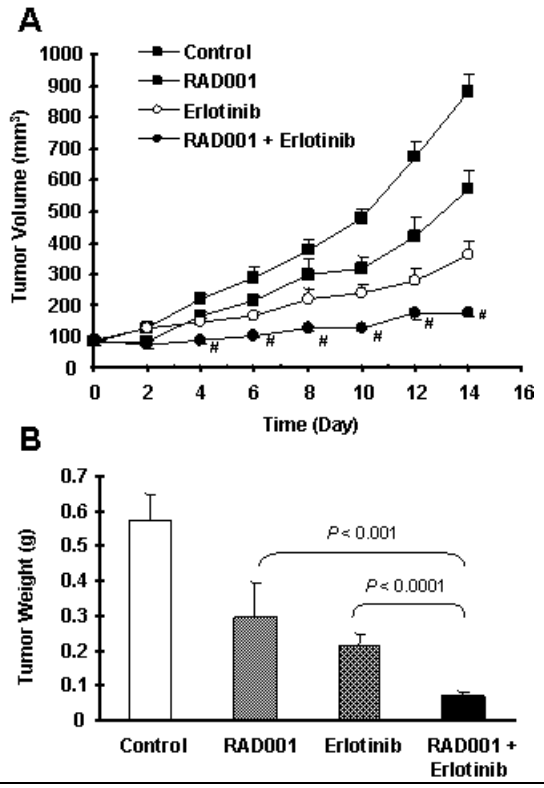

Figure 2: The combination of mTOR inhibition and EGFR inhibition exhibits enhanced anticancer efficacy ***in vivo*.** Four groups of mice with either A549 xenografts were treated with vehicle control, RAD001 (3 mg/kg/day) alone, erlotinib (80 mg/kg/day) alone, and RAD001 plus erlotinib on the same day after grouping. After 14 days, the mice were sacrificed. The tumors were then removed and weighed (*B*). During the treatments, tumor sizes were measured once every two days (*A*). Tumor sizes treated with erlotinib alone and RAD001 plus erlotinib were significantly smaller than vehicle control treatment at all measurement times ($p < 0.01$). Tumor sizes treated with RAD001 alone were significantly smaller than vehicle control treatment at days 10, 12, and 14 ($p < 0.01$). # $p < 0.05$ compared to either RAD001 or erlotinib alone treatment. The data are means ± SE of 6 tumors from 6 mice.

As noted above, the mTOR inhibitor RAD001 increase p-eIF4E levels in vivo (Fig. 1). In xenografts treated with the combination of RAD001 and erlotinib, eIF4E phosphorylation was not increased compared with RAD001-treated tumors. Accordingly, the combination of RAD001 and erlotinib was more potent than each agent alone in inhibiting the growth of lung cancer xenografts. Additionally, we noted that the expression of Mcl-1, which is regulated by cap-dependent translation mechanism and important for eIF4E-mediated oncogenesis, was slightly higher in RAD001-treated tumors, but significantly inhibited in lung tumors treated with the combination of RAD001 and erlotinib. We suggested that erlotinib enhances RAD001's anticancer activity *in vivo* involving abrogation of mTOR inhibition-induced eIF4E phosphorylation. Modulation of eIF4E phosphorylation may serve as a predictive biomarker for RAD001/erlotinib-based cancer therapy. This part of the data will be presented in the upcoming 2009 AACR meeting. The *in vivo* results on the combination of RAD001 and LY294002 in lung cancer xenografts, which were summarized in the last year's report, have been published in Cancer Res (Wang et al. 2008).

Aim 4 To conduct a pilot clinical biochemical induction trial to investigate the effect of RAD001 in operable NSCLC patients and identify molecular determinants ofRAD001 sensitivity and prognosis.

Summary of Research Findings

Feb 2013 Report: We conducted this 'window- of-opportunity' study to characterize the biologic activity of everolimus, an allosteric inhibitor of mTOR pathway, in patients with surgically resectable NSCLC. Patients with Stage I-III NSCLC underwent baseline tumor biopsy and FDG PET/CT scan followed by treatment with everolimus 5mg daily (Arm A) or 10mg daily (Arm B) for up to 28 days. A repeat PET/CT scan was obtained 24 hours prior to surgery. Blood samples for pharmacokinetic (PK) assay for drug levels were collected at 0.5, 1, 2, 5, 8 and 24 hours

post-drug ingestion on Days 1, 8 and 21. Control patients not treated with everolimus (Arm C) also had paired FDG PET/CT scans prior to surgery. Target modulation by everolimus was assessed in vivo by PET and ex vivo by immunohistochemical detection of total and phosphorylated mTOR, Akt, S6, p70S6, eIF4e and 4EBP1 in pretreatment and post-treatment tissue samples. We enrolled 32 patients (Arm A - 12; Arm B - 11; Arm C - 9); median age: 63 yrs (range 35-77); gender: 14 males, 18 females; stage: I - 14; II - 12; IIIA - 6; histology: adenocarcinoma - 21; squamous - 7; others - 4. Treatment was tolerated well with mostly grade 1/2 toxicities (hyperglycemia, hypertriglyceridemia, anemia and fatigue) and 31 of 32 patients proceeded with surgery on schedule. Paired PET/CT scan in everolimus-treated patients showed a significant reduction in median SUVmax (-21.74%, -23.23% vs. 8.63%; p=0.027 for Arms A, B and C respectively) and anatomic tumor growth arrest as measured by blinded independent CT scan review (-3.13%, 0% vs. 10%; p=0.039 for Arms A, B and C respectively). Comparison of baseline and resected tumor specimens following 3-4 weeks of treatment with everolimus showed effective pathway modulation with a significant difference in mean baseline and post-treatment pS6 immunoscore from 119 to 59, 257 to 115 vs. 181 to 169 for Arms A, B & C respectively; p=0.01 for comparison by dose of everolimus.

Key Research Accomplishments

1. This completed study demonstrates that modulation of downstream targets of mTOR were accomplished with the 10 mg dose of everolimus, but only to a lesser extent with the 5 mg dose. Based on this finding, the 10 mg dose of everolimus should be considered the biologically optimal dose for solid organ tumors. Our findings have significant implications for further development of mTOR inhibitors in NSCLC.
2. We have now developed a novel combination of everolimus with BKM120, a PI3K inhibitor, that is currently being studied in a phase I clinical trial at our institution. This study is based on promising pre-clinical data that showed synergistic inhibitor effects on the growth of human NSCLC cells, both in vitro and in vivo.
3. The above-mentioned combination approach is included as a full project in our pending NCI application for a P01 award in lung cancer.

Reportable Outcomes

Taofeek Kunle Owonikoko, Daniel L. Miller, Seth Force, Gabriel Sica, Scott Arthur Kono, Nabil F. Saba, Madhusmita Behera, Zhengjia Chen, Allan Pickens, Jennifer Mendel, Robert Fu, William F Auffermann, Jaqueline Willemann Rogerio, William E Torres, Haian Fu, John A. Hohneker, Shi-Yong Sun, Anthony A Gal, Suresh S. Ramalingam, Fadlo Raja Khuri. A phase IB window-of-opportunity study of everolimus in patients with resectable non-small cell lung cancer (NSCLC). Submitted as an abstract to the annual ASCO meeting, 2013.

Owonikoko TK, Ramalingam SS, Miller DL, Force SD, Sica GL, Mendel J, Chen Z, Rogatko A, Tighiouart M, Harvey RD, Kim S. A Translational, Pharmacodynamic, and Pharmacokinetic Phase IB Clinical Study of Everolimus in Resectable Non–Small Cell Lung Cancer. Clinical Cancer Research. 2015 Apr 15;21(8):1859-68.

Conclusions

Everolimus exerts a measurable, dose-dependent biologic activity in NSCLC tumors. 'Window of opportunity' studies in early stage NSCLC provide strong mechanistic insights and may guide development of novel targeted agents.

Project 6: Identification and Evaluation of Molecular Markers in Non-Small Cell Lung Cancer (NSCLC)

(PI and co-PI: Ralf Krahe, Ph.D., Li Mao, M.D)

A better understanding of the lung cancer biology and an identification of genes involved in tumor initiation, progression and metastasis are an important first step leading to the development of new prognostic markers and targets for therapy. In the same context, identification of reliable predictive markers for response or resistance to therapy in NSCLC patients is also desperately desired for optimal delivery of targeted therapy and/or standard chemotherapy. The proposed studies aim to identify the two types of markers that would eventually help develop smarter clinical trials, which will selectively recruit patients who are more likely to respond to one regimen over another and lead to improvement of overall therapeutic outcomes.

Aim 1 To expression profile by DNA microarray technology aerodigestive cancers - with primary focus on adenocarcinoma and squamous cell carcinoma (SCC) of the lung, and head and neck squamous cell carcinoma (HNSCC), including primary tumors and normal adjacent tissue, and (where available) metastatic lesions.

Summary of Research Findings

Feb 2009 Report: We completed the expression profiling on 8 matched tumor/normal adjacent tissue (T/N) pairs of lung cancers, 5 adenocarcinomas, and 3 squamous cell carcinomas (SCC) from an initial total of 22 NSCLC T/N pairs. However, due to the limited number of samples and limited expression profiling obtained, statistically meaningful conclusions for the lung cancer part of the study and, therefore, meaningful comparisons with the HNSCC part of the study were not possible. We therefore decided to focus our efforts on Aims 2 and 3.

Aim 2 To DNA profile the same samples by complementing DNA approaches to stratify RNA expression profiles on the basis of their corresponding DNA profiles.

Summary of Research Findings

Feb 2009 Report: Originally, we proposed to correlate DNA and RNA profiles from the 21 NSCLCs gathered in Aim 1. Due to the issues related to sample procurement, it was not feasible to acquire the necessary number of matching RNA/DNA samples that would result in a significant statistical power. We decided to gather DNA samples without matching RNA samples from 108 NSCLC patients with complete clinical and follow-up data (56 adenocarcinomas, 48 SCC, and 25 other lung cancers) for a total of 129 primary tumor (PT) and 45 matching normal adjacent tissue (NAT/PT) pairs, which we used for genomic profiling.

We performed genomic profiling of the same HNSCC samples on which we performed transcriptomic profiling (see above Aim 1) using the Affymetrix 10K *Xba*I array. Using 24 genetically matched NAT and PT pairs and 12 matching metastatic lymph nodes (MLN), we genotyped a total of 8,430 tag SNPs. Analysis of the genotype data with GeneSpring GTv2 (Agilent) for allelic imbalance (AI), indicative of loss-of-heterozygosity (LOH), showed that the majority of AI events occurred from normal to primary tumor, while the transition from primary tumor to metastasis was marked by few little additional events (0-2%). In the NAT/PT comparison, we identified five regions with significant AI: 9p24.1-p23 (38%), 5q33.3 (25%), 3q25.32-q26.1, 13q14 and 17p13 (all 21%), and 3p23-p22.3 (13%). Our overall objective was to

investigate regions of frequent AI in HNSCCs that are shared with NSCLC to identify candidate tumor suppressor genes as well as to assess whether additional "hits" at these loci were present or likely.

Due to limited resolution, we hypothesized that the 10K SNP array probably underestimates LOH, resulting in missed LOH over short genomic segments and poorly defined regional boundaries. To identify additional tumors with smaller losses and to pinpoint the most frequently lost genes within the six most frequently lost regions (9p, 3p, 3q, 5q, 11q, and 17p), we performed LOH analysis in 27 N/P and 14 N/M pairs using a total of 35 microsatellite (MS) markers. In all cases, the MS LOH data confirmed the LOH identified by the SNP array. For all frequently lost regions, the MS data identified loss in additional tumors that were not detected on the SNP array. This was particularly striking for three regions, namely 3p26.1-p25.2, 17p13 and 11q23.2-q23.3. Although SNP LOH at 3p26 and 11q23 was most frequently observed in the NAT/MLN comparison, MS revealed that LOH was much more frequent in N/P. The most frequently lost genes are shown in the table below; all are genes previously reported to be associated with tumorigenesis.

Cytoband	Tumor Suppressor Candidate	Comment
3p26.1-25.2	*VHL*	Involved in tumor angiogenesis
3q25.31	*RARRES1*	Down-regulated by methylation in prostate cancer,
5q33.3	*CCNJL*	Cyclin J-like, cell cycle regulation
9p24.1-p23	*PTPRD*	Regulates cell growth and transformation
17p13	*TP53*	Classic tumor suppressor, cell cycle, repair
11q23.2	*TAGLN*	Transgelin, early marker for transformation

Table 1: Frequently lost gene regions in SNP arrays

The 9p24.1-p23 region was identified in the SNP analysis as the most frequently lost region in this sample set. This region contained only a single gene, *PTPRD*, and we focused on this gene as a candidate tumor suppressor. We compared LOH at *PTPRD* with LOH at *TP53* and *CDKN2A*, both genes reported as being frequently lost early in tumorigenesis. We found that LOH at *PTPRD* in both primary tumors and metastasis (17/26 P=65%, 9/13 M=69%) was as frequent as LOH at *TP53* in primary tumors and even more frequent in metastases (16/26 N/P=62%, 4/13 N/M=31%).

To address the question of whether *PTPRD* was also frequently lost in other tumor types, we compared microsatellite LOH at both *PTPRD* and *TP53* in HNSCC to a set of matched T/N samples from lung and colorectal (CRC) cancers. LOH at *PTPRD* in CRC (3/9=33%) was similar to LOH at *TP53* (4/10=40%). LOH at *PTPRD* in lung cancer (8/20=40%) was even more frequent than at *TP53* (5/20=25%). Thus LOH at *PTPRD*, while not quite as frequent in lung cancer and CRC as in HNSCC, was nevertheless frequently seen. Therefore, *PTPRD* may be a non-specific marker of early tumorigenesis in many epithelial tumors.

As both *PTPRD* and *RARRES1* have CpG islands in their 5' promoter regions that may be subject to epigenetic inactivation by promoter hypermethylation, we investigated hypermethylation as a "hit" that is functionally equivalent to loss (reported in Aim 3).

The genes *TCF21* and *CHD5* had been identified in other studies as possible early markers of tumorigenesis. We also investigated LOH at these two genes in HNSCC and lung cancer samples using MS markers. At *CHD5,* we found little LOH in HNSCC samples (12% in PT and 10% in MLN) and only slightly more in lung cancer (33% of 22 PT). At *TCF21,* LOH in HNSCC was striking (59% of PT and 50% of MLN); lung cancers have somewhat less LOH at this locus (43% of 37 PT).

Aim 3 To evaluate the contribution of promoter hypermethylation and transcriptional inactivation of known cancer genes subject to epigenetic silencing to cancer phenotype.

Summary of Research Findings

Feb 2009 Report: Last year, we reported that the transcription factor *TCF21* was the most often hypermethylated (≥30% methylation) gene in both HNSCC (96%, n=24) and NSCLC (95%, n=21). This finding was confirmed when we investigated a second larger validation sample set of 108 NSCLC patients with complete clinical and follow-up data (56 adenocarcinomas, 48 SCC, and 25 other lung cancers) for a total of 129 PT and 45 matching NAT/PT pairs. Overall, 73% of lung cancers showed *TCF21* hypermethylation (n=129). Adenocarcinomas and SCCs together showed hypermethylation in 78% (n=100) of tumors, while other lung cancers showed hypermethylation in 64% of cases (n=25). Adenocarcinomas compared to SCCs showed slightly higher levels of (40%±2.5 vs. 37%±2.7) and more frequent (90% vs. 70%) methylation, respectively.

To determine the effect of *TCF21* promoter hypermethylation on gene expression, we collaborated with Dr. Ignacio Wistuba (Pathology Core) to perform TCF21 protein immunohistochemical (IHC) analysis on a TMA of 300 lung cancer cases. Similar to our DNA-based methylation data, 253 of 300 cases [85%; 166/191 (87%) adenocarcinoma and 87/109 (80%) squamous cell carcinoma] resulted in no or significantly decreased TCF21 expression. Correlation of methylation status with available clinical factors (Biostatistics Core) showed a significant correlation with histology (adenocarcinoma, p = 0.0026), sex (females, p = 0.0209), and smoking status (never smokers, p = 0.0476). However, race, TNM stage, and prognosis were not significantly associated. Given the interesting association of histology, sex, and smoking-status (adenocarcinoma in female never-smokers), which is reminiscent of recent findings for *EGFR* mutations in lung cancer patients, we investigated the possibility that EGFR mutation status might predict TCF21 expression. Multivariate analysis showed that histology, but not gender or smoking status, was associated with low TCF21 expression. However, when adenocarcinoma cases (n=172) were considered alone by both univariate and multivariate analysis, no significant correlation was observed.

A high percentage (85%) of the lung cancers were hypermethylated at *TCF21*. Approximately 35% of samples showed both LOH and hypermethylation. We sequenced the remaining tumors to determine whether mutation might furnish a second hit, but results showed no *TCF21* coding mutations identified. Based on our results, the primary mode of inactivation of *TCF2*1 would appear to be methylation (>85%) followed by deletion (43-59% depending on the tumor type, NSCLC vs. HNSCC). Some tumors have 2 hits (35%), but most tumors would appear to have a single hit (more frequently methylation and less frequently LOH), suggesting that this may be another case of a haploinsufficient tumor suppressor gene. TCF21 is an important basic helix-loop-helix transcription factor that plays an important role in the epithelial-mesenchymal transition (EMT), and haploinsufficiency may be sufficient to be tumorigenic. Based on our methylation profiling, we conclude that *TCF21* promoter hypermethylation and TCF21

expression are good biomarkers of both early lung and head and neck cancer (manuscript in preparation).

We completed the evaluation of methylatable TSG [*PTPRD* and *RARRES1*]. According to Knudson's "two-hit" hypothesis, second hits at tumor suppressor genes are needed for tumorigenesis. In our expression analysis of these same samples, *PTPRD* mRNA was seen to be reduced approximately 2-fold in primary tumors when compared to adjacent normal tissue (T=-2.1527). In order to determine whether the reduced expression of *PTPRD* was due to haploinsufficiency or hyper-methylation, we used PyroMethA to investigate methylation at both *PTPRD* promoters. The maximum percent methylation seen in any primary tumor for island 1 was 27.8% and for island 2 it was 29.7%. These percentages were not significantly different from maximum levels seen in the matching normal samples (28% for island 1 and 23% for island 2). The largest positive change seen between normal and tumor was 22.7% in primary tumors for island 1 and 21.8% for island 2. However, the mean change was less than 4% and probably within our range of experimental error. Overall, it does not appear that hyper-methylation plays an important role in *PTPRD* loss of function. The observed reduced expression may be entirely due to LOH, and *PTPRD* may therefore be a haplo-insufficient tumor suppressor.

Since *RARRES1* had previously been reported to be hypermethylated in prostate cancer and squamous cell carcinoma of the esophagus, we also investigated promoter hypermethylation at this locus. Approximately 24% of lung cancer and 10% of HNSCC tumors showed significant hypermethylation, as did a number of cancer cell lines.

We also performed global hypomethylation of tumors. Loss of genome-wide methylation is a common feature of cancer, and the degree of hypomethylation has been correlated with genomic instability. Global methylation of repetitive elements possibly arose as a defense mechanism against parasitic DNA elements, including retrotransposons and viral pathogens. Given the alterations of global methylation in both viral infections and cancer, we examined genome-wide methylation levels in HNSCC, in which a specific set of cancers (oropharyngeal) has been causally associated with human papilloma virus (HPV). LINE hypomethylation was more pronounced in HPV-negative than in HPV-positive tumors. Moreover, genomic instability, measured by genome-wide LOH and SNP analysis, was greater in HNSCC samples with more pronounced LINE hypomethylation. Global hypomethylation was variable in HNSCC. Its correlation with both HPV status and degree of LOH as a surrogate for genomic instability may reflect alternative oncogenic pathways in HPV-positive versus HPV-negative tumors.

Aim 4 To determine protein signatures of treatments of erlotinib and other therapeutic agents, alone or in combination, in NSCLC and identify molecular predictors of response.

Summary of Research Findings

Feb 2009 Report: During the last project period, we used adenocarcinoma and squamous cell carcinomas to test the expression levels when treated with SAHA (HDAC inhibitor) and 5-Aza-citidine (DNMT inhibitor). Results of these tests suggested that we could use the same tumor models to develop biomarkers able to predict further responses to similar treatment regimens.

In our current study, we used the adenocarcinoma and squamous cell carcinoma models to test a neurotrophic receptor kinase (Trk) inhibitor for similar expression profiles noted in earlier results. Although expression of Trk can be detected in primary tumors, most of the cancer cell lines lost the expression profile needed for validation of anti-Trk agents. We screened eight of

our heterotransplant lung cancer models for expression of Trks (Trk-A, Trk-B, and Trk-C) and their corresponding growth factors (NGF, BDNF, and NT3) using real-time RT-PCR (Table 1).

Model No.	Histology	TrkA/NGF (2 power - ΔCT x 1E6)	TrkB/BDNF (2 power - ΔCT x 1E6)	TrkC/NT3 (2 power - ΔCT x 1E6)	Response To Trk inhibitor
MDACC1	Adeno	0.1/0.2	1.0/0.3	0/0	No growth inhibitory effect
MDACC2	Poorly dif	0/0	0.2/0.1	0.4/3.9	No growth inhibitory effect
MDACC3	Squamous	0/0	0/0.2	0/0.7	
MDACC4	Squamous	0/0	2.4/0.1	0/1.0	
MDACC5	Adeno	1.9/0.5	0/7.8	0/1.1	
MDACC6	Adeno	0/0	0/0.1	0/0.5	Inhibitory
MDACC7	Adeno	0/0	0.2/3.0	0/0	Inhibitory (78%)
MDACC8	Adeno	0.4/3.0	0/32.8	0/0	Inhibitory
MDACC9	Sqamous	Not tested	Not tested	Not tested	

Table 1: Heterotransplant lung cancer models

We detected modest expression of certain Trks and their ligands in the tumors.

We then conducted *in vivo* testing using the Trk inhibitor as a single agent to determine a potential anti-tumor effect in the heterotransplant lung cancer models. Five different tumor models were used in the initial testing, using only one animal per treatment group per model to serve for screening purposes. In 100mg/kg dose, the tumor inhibitory effect was observed in 3 of the 5 models, particularly in one of the adenocarcinoma tumor models (model 7) where tumor growth was inhibited by 78% compared to the vehicle-treated control. This model expressed only Trk-B and its ligand, BDNF, but not other Trks and their ligands. We then conducted second stage experiment by focusing on the two models (models 7 and 8) showing signs of tumor inhibition. Five animals were assigned to each treatment group for each model. Although the tumor growth inhibition was minimal for model 8, a similar inhibitory effect (71% inhibition) was observed in model 7 as compared with vehicle treated controls.

In previous studies, it has been shown that early passages of heterotransplant tumors contain infiltrating inflammation cells that disappear in later passages of the tumors. This observation is reasonable because most of the infiltrating inflammation cells are terminally differentiated and are not renewable. However, it is poorly understood whether other tumor stroma cells that may have stem-cell features in the tumors remain of human origin in the tumor models. The presence of tumor-stroma may help evaluate agents that target the tumor microenvironment as part of their mechanisms of action. Our preliminary data from three passages of the tumors suggests the presence of human-origin tumor stroma (Fig. 1). The stroma DNA derived from the tumors showed predominantly human origin whereas DNA from the tumor cells contained no murine component (Fig. 1). Although additional experiments are needed, the result is encouraging.

Aim 5 To determine a clinical utility of the molecular predictors.

Summary of Research Findings

Feb 2008 Report: Any biomarker developed must be tested in clinical trials to determine its sensitivity and specificity and to validate its utility in the clinic. Additionally, the assay should be tested for its ability to use small amounts of tissues or body fluids obtainable in clinical practice. The most sensitive and reliable clinical tests currently available are antibody-based assays.

Overexpression of EGFR is common in head and neck squamous cell carcinoma (HNSCC). To correlate with research by my Co-PI, Dr. Krahe, in Aims 1-3, we analyzed the genetic nature of *EGFR* gene including mutations and gene copy numbers in HNSCC and its clinical correlations in 134 HNSCC tumors. Aberrant *EGFR* copy numbers were found in 32 (24%) of 134 tumors, including 22 (17%) with increased copy number and 10 (7%) with decreased copy number. Patients whose tumors had *EGFR* copy number alterations (particularly patients with increased copy numbers) had significantly poorer overall, cancer-specific, and disease-free survivals compared with patients with normal copy numbers ($p < 0.0001$). At 5 years after initial diagnosis, 20 of the 22 (91%) patients with increased copy number died of disease compared with 30 of the 102 (29%) patients with normal copy number. No mutations on *EGFR* exons 18, 19, and 21 were detected in any of the tumors. We conclude that a subset of HNSCC manifests *EGFR* copy number alterations, and this is associated with a poor clinical outcome, suggesting a biologic role of the alterations. (Temam, J Clin Oncol 25:2164-2170, 2007)

In another study, we analyzed potential biologic roles of ΔDNMT3B, a newly identified DNMT3B subfamily in promoter-specific DNA methylation regulation in human lung cancer. We have previously shown a strong correlation between the promoter methylation of *RASSF1A* gene but not *p16* gene and expression of *ΔDNMT3B4* in primary lung cancer, suggesting a role of ΔDNMT3B in regulating promoter-specific methylation of common tumor suppressor genes in tumorigenesis. We now provide the first experimental evidence showing a direct involvement of ΔDNMT3B4 in regulating *RASSF1A* promoter methylation in human lung cancer cells. Knockdown of *ΔDNMT3B4* expression by small interfering RNA resulted in a rapid demethylation of *RASSF1A* promoter and re-expression of *RASSF1A* mRNA but had no effect on p16 promoter in the lung cancer cells. Conversely, normal bronchial epithelial cells with stably transfected *ΔDNMT3B4* gained an increased DNA methylation in *RASSF1A* promoter but not *p16* promoter. We conclude that promoter DNA methylation can be differentially regulated and ΔDNMT3Bs are involved in regulation of such promoter-specific *de novo* DNA methylation. (Wang et al, Cancer Res 67:10647–52, 2007)

Key Research Accomplishments

- DNA profiling of 28 HNSCC matched T/N pairs and 14 matching lymph node metastases identified regions of LOH and allelic imbalance in HNSCC that are shared with adenocarcinomas.
- Genotyping of 8,430 tag SNPs from 24 genetically matched NAT and PT pairs and 12 matching lymph node metastases.
- Completed gene-specific hypermethylation analysis of 10 genes in HNSCC and NSCLC samples.
- Confirmed *TCF21* promoter hypermethylation and TCF21 expression as good biomarker of both early lung and head and neck cancer.
- Established 14 heterotransplant primary NSCLC tumor models, which will allow us to evaluate target therapeutic agents and to initiate biomarker discovery experiments.
- Identified ΔDNMT3B4 as regulator of RASSF1A promoter in human lung cancer cells.

Resources

Additional 7 heterotransplant primary NSCLC tumor models have been established which allowed us to initiate evaluation of target therapeutic agents and biomarker discovery experiments. Three peer-reviewed publications were partially supported by this project.

Manuscripts Published in Peer-reviewed Journals

1. Colella S, Richards KL, Bachinski LL, Baggerly KA, Tsavachidis S, Lang JC, Schuller DE, and Krahe R. Molecular Signatures of Metastasis in Head and Neck Cancer (provisionally accepted, *Head Neck*).
2. Temam S, Kawaguchi H, El-Naggar AK, Jelinek J, Tang H, Liu D, Lang W, Issa JP, Lee JJ, Mao L. Epidermal growth factor receptor copy number alterations correlate with poor clinical outcome in patients with head and neck squamous cancer. J Clin Oncol 25(16):2152-5, 2007.
3. Wang J, Bhutan M, Pathak AK, Lang W, Ren H, Jelinek J, He R, Shen L, Issa JP, and Mao L. *ΔDNMT3B* variants regulate DNA methylation in a promoter-specific manner. Cancer Res, 67(22): 10647-10652, 2007.

Conclusions

We performed RNA and DNA profiling on available samples to identify genes and genomic regions that are altered in NSCLC and interrogated additional candidate methylatable genes as potential tumor suppressor genes in NSCLC, to identify their potential as biomarkers. These experiments have generated a list of molecular candidate biomarkers for further investigation in larger sample sets.

Core B: Biostatistics & Data Management Core

(Core Director: J. Jack Lee, Ph.D.)

Feb 2016 Report: The Biostatistics and Data Management Core has supported all the IMPACT Projects in their research efforts, especially in the area of biostatistical support in clinical trial design, implementation, and analysis of experimental results. We also developed statistical methods to enhance the design and analysis pertinent to the lung cancer research.

Specific Aims:

1. To ensure that the results of all projects are based on well-designed experiments and are appropriately interpreted by providing experimental design; sample size estimates; power calculations; and integrated, comprehensive analysis for each basic science, pre-clinical, and clinical study.
2. To develop a data management system that integrates clinical, pathological, and basic science data while providing data integrity through process tracking and quality control.
3. To provide statistical and data management support for genomic and imaging studies including microarray, proteomics, and molecular targeted imaging.
4. To develop and adapt innovative statistical methods pertinent to biomarker-integrated translational lung cancer studies.
5. To produce statistical reports for all projects.
6. To collaborate and assist all project investigators with the publication of scientific results.

Summary of Research Findings and Key Accomplishments

For the remaining active project of this grant, Project 2, "Molecular Imaging of EGFR Expression and Activity in Targeting Therapy of Lung Cancer," Core B worked with study investigators in the previously described revisions of the protocol "A phase I study of 18F-Fluoro-PEG6-IPQA as a PET Imaging Agent for Active/Mutant EGFR Expression in Tumors (2009-0832)." Core B also completed the required statistical analysis of the first cohort accrued to the trial to determine the recommended dose, and the analysis of the results of the first 2 patients from the second cohort.

Statistical Design: Up to 15 patients were planned to be imaged in this study using ^{18}F-PEG6-IPQA as a PET imaging agent. The maximum allowed single absorbed radiation doses for sensitive organs (whole body, gonads and red marrow) and non-sensitive organs are 3 and 5 rems, respectively. Absorbed dose estimates for 25 organs must be monitored. The study is designed with the intent to limit the probability that a patient exceeds the target dose (e.g., 3 or 5 rems depending on the organ) in any organ to be less than 0.10.

We proposed a three-stage design in which three female patients in the first stage and six patients (three females and three males) in each of the 2nd and 3rd stages are imaged, for a total of 15 patients. Since imaging quality is usually better in smaller patients, we stipulated that the first three patients were to be female and small in size, to maximize the likelihood of achieving useful data with the starting level of administered dose/activity.

Following the completion of each stage, the 90th percentile for the distribution of equivalent dose per unit administered activity (1 rem/MBq = 10 mSv/MBq) for the highest radiation dose administered will be estimated and used to determine the acceptable administered dose levels (or activities) for the next cohort. The initial administered dose level, determined as described below based on primate experiments, will be 70 MBq. Radiation absorbed dose will be estimated and monitored after each patient study and the administered dose will be recomputed if any patient exceeds the allowed single-dose limit in any organ

The 90th percentile of each organ's exposure per unit (mSv/MBq) and its standard deviation will be updated after observing data from each stage using the following formula:

$$UB_{ij} = \overline{x}_{ij} + t_{1-\alpha_i, n-1}.s_{ij}, i = 1,2,...,25, j = 1,2 \quad (1)$$

Where *i* denotes organ, *j* denotes dose level, $\overline{x}_{ij}$ is the observed mean exposure/dose (mSv/MBq) of the i^{th} organ at j^{th} dose, S_{ij} is the observed standard deviation of the i^{th} organ at j^{th} dose, *n* equals the number of patients treated at each dose level, α_i is the one-sided type I error rate spent on the i^{th} organ. The family-wise alpha level will be maintained at 0.10 level,

$$\alpha = \sum_{i=1}^{25} \alpha_i = 0.10, \quad (2)$$

but will be distributed unevenly among organs based on how close the organ dose is to its limit.

The 90th percentile of each organ's dose (rems) is calculated as UB_{ij} x Dose$_j$ /10 (Dose$_1$=70 MBq). If for any organ, the 90th percentile of dose exceeds its limit, then dose escalation will not occur and the trial will stop. If the 90th percentile of dose in each organ does not exceed its dose limit, then the next cohort of patients can be administered the same or a higher activity. The next administered dose will be determined such that the upper bound of absorbed dose to any given organ will not exceed its limit, i.e.,

$$Dose_{j+1} = \min\{Limit_i/UB_{ij}*10,\ MAX\},\ i = 1,2,\ldots,25,\ j = 1,2 \quad (3)$$

where $Limit_i$ is the exposure limit (3 or 5 rems) for the i^{th} organ and MAX is the pre-specified maximum administered dose level, 370MBq.

The study conduct and the analysis results were reported in the Project 2 section.

Conclusions

Core B provided statistical support for Project 2, including the development of relevant statistical methodologies and final analysis of the clinical trial.

Reportable Outcomes

Publications Not Previously Reported:

1. Ma Y, Yin G. Cure rate model with mismeasured covariates under transformation. Journal of the American Statistical Association. 2012.
2. Yin G, Li H, Zeng D. Partially linear additive hazards regression with varying coefficients. Journal of the American Statistical Association. 2012.

Core C: Pathology Core

(Director: Ignacio Wistuba, M.D.)

The IMPACT interdisciplinary research proposal for studying targeted therapy of lung cancers has required extensive histopathologic, IHC, and molecular studies of cell and tissues specimens, which have been assisted, coordinated or performed by the Pathology Core. One of the most important roles of the Pathology Core has been to provide professional technical services for proper procurement, storage and use of human and animal tissues, as well as technical assistance for IHC analysis. In addition, the Pathology Core has provided assistance for collection and evaluation of tissue specimens in IMPACT clinical trials in lung cancer patients.

Aim 1 Develop and maintain repository of tissue, cell and serum specimens from patients with lung neoplasia, as requested by the various component projects.

Summary of Research Findings

Feb 2011 Report: For the IMPACT clinical trial using erlotinib (Tarceva), chemotherapy, and radiotherapy in advanced NSCLC patients (Protocol 2005-1023; Principal Investigator: R. Komaki), the Pathology Core assisted in the evaluation of tumor tissue specimens of 35 NSCLC cases with adequate tissue for biomarker analysis. *EGFR* mutation (exons 18-21) was detected in 4 tumors and *KRAS* (codons 12-13) mutation in 2 tumors with adenocarcinoma histology. *EGFR* copy number increase by FISH (high polysomy and gene amplification, FISH+) was detected in 10 (30%) out of 34 tumors successfully tested, including 9 tumors with high polysomy and 1 with gene amplification. Additionally, the expression of EGFR and phosphorylated-EGFR were examined by immunohistochemistry (IHC) using a semi-quantitative score (range 0-400) addressing intensity and extension of the membrane and cytoplasmic expression in malignant cells. EGFR and p-EGFR expression positive cells (score ≥200) were detected in 11 (31%) and 10 (29%) out of the 35 cases examined, respectively. Recently, the protein expression of epithelial-mesenchymal transition (EMT) IHC markers were

optimized and are currently being tested in 25 tumor specimens with histology sections available for analysis.

Aim 2 Develop innovative tissue and cell reagents from lung cancer patients for the investigation and validation of the molecular endpoints relevant to each component project.

Summary of Research Findings

Feb 2011 Report: The development of new tissue and cell reagents from lung cancer patients was completed in 2008. These reagents and data are available for future analysis of molecular abnormalities of lung cancer, including tissue microarrays (TMA), lung cancer cell lines repository, lung cancer heterotransplants (in collaboration with L. Mao), and pleural fluid specimens from lung cancer patients (in collaboration with C. Jimenez). In particular, the repository of pleural fluid specimens from 120 patients have been fully characterized from the cytology standpoint and the clinical information has been annotated.

Aim 3 Process human and animal cell and tissues for histopathological, immunohistochemical (IHC) and molecular analyses, including tissue microdissection, as required by each component project.

Summary of Research Findings

Feb 2010 Report: As indicated in the other Aims, most of the collaborations with the IMPACT research projects have been completed as reported previously. The preparation and processing of tissue specimens for research projects are described in Aim 4 and includes mostly histopathological, IHC, and molecular analysis.

Aim 4 Perform and evaluate IHC analysis in human and animal cell and tissue specimens, as required by the various component projects.

Summary of Research Findings

Feb 2010 Report: Most of our collaborations with the other IMPACT projects were completed in 2007 and 2008. During the current project period we have collaborated with the IMPACT investigators to finalize the preparation of manuscripts for publications (see below, *a* to *c*). In addition, we have finalized most of our own research activities (see below, *d* to *f*).

Completed or published projects during the current project period in collaboration with IMPACT research projects.

a) Analysis of GRP78, IL-11R and Eph5A markers in human NSCLC tissue specimens (Collaboration with Project 3, R. Pasqualini). From this work, two manuscripts are in preparation**.**

b) Molecular abnormalities (protein expression and methylation) analysis of *TCF21* gene in NSCLC (Collaboration with Project 6, R. Krahe)**.** From this work, one manuscript is in preparation.

c) Analysis of the IHC expression of angiogenesis-related markers HIF-1α and carbonic anhydrase IX (CA IX) in tumor specimens from 330 NSCLC patients using TMAs (Collaboration with Project 1, R. Herbst)**.** These data have been shared with Dr. J. Heymach's lab (M.D. Anderson Thoracic/Head and Neck Medical Oncology Department) and have been

used to expand their *in vitro* mechanistic work on the role of HIF-1α pathway in lung cancer progression and response to therapy. This work was reported last year.

d) Association of *EGFR* gene abnormalities with estrogen and progesterone receptors expression. A paper by G. Raso et al. was published in 2009 in *Clinical Cancer Research*. The submission of this paper was reported last year.

e) Characterization of HER family receptors markers and *EGFR* gene abnormalities in NSCLC primary tumors and brain metastasis. A paper by M. Sun et al. was published in 2009 in *Clinical Cancer Research*. The resubmission of this paper was reported last year.

f) Analysis of VEGFA and VEGFR-2 copy number and mutation in NSCLC. In collaboration with Dr. R. Herbst (Project 1), we previously showed that VEGFR and EGFR pathways are positively correlated in early stage NSCLC and IHC expression of p-VEGF-R2 is an indicator of worse overall survival in stage I-IIIA NSCLC. Recently, we extended our study to characterize the frequency of VEGFR2 gene (*KDR*) variations and *KDR* and VEGF copy number gains in NSCLC tumor tissue and correlated with patients' clinicopathologic features, including outcome. We extracted DNA from microdissected tissues obtained from 200 surgically resected NSCLCs. KDR single nucleotide polymorphisms (SNP) 889G/A (rs2305948), 1416A/T (rs1870377), and -37A/G (rs2219471) were genotyped by PCR-based sequencing. *KDR* and *VEGF* gene copy numbers were examined by real-time quantitative PCR. Tumor sections were immunohistochemically stained and analyzed for protein expression of VEGFR2, VEGF, and CD34 for microvascular density (MVD). NSCLC patients with *KDR* 1416 AT/TT variant genotypes had significantly better overall survival (OS; hazard ratio [HR] = 0.56; P = 0.035) than did patients with the wild-type *KDR* 1416 AA genotype. NSCLC patients who were treated with adjuvant chemotherapy and who had the *KDR* 1416 AT/TT (P = 0.015) or -37 AG/GG (P = 0.029) variant genotypes showed significantly better OS than did the rest of the patients in the study population. *KDR* and *VEGF* gene copy gains were detected in 34 (37%) and 2 (2%) of 91 NSCLC tumors, respectively. *KDR* gene copy gain was associated with a worse OS in NSCLC patients (HR= 2.96; P = 0.004). Furthermore, tumors with *KDR* gene copy gain had significantly higher VEGFR2 expression, lower VEGF expression, higher MVD, and larger vessel areas than did tumors lacking *KDR* gene copy gain. Our findings suggest an association between *KDR* SNP genotypes and survival in NSCLC patients, including those patients receiving adjuvant chemotherapy. *KDR* copy number gain was frequently identified in NSCLC and was associated with a worse survival in these patients, and with tumors' increased angiogenesis. From this work, an abstract was presented as poster in the 13th World Lung Cancer Conference (IASLC), San Diego, CA (July 31-August 4, 2009).

g) Role of *NKX2-1* (*TITF-1*) gene amplification and protein overexpression in lung cancer and its association with *EGFR* abnormalities. Following our data indicating that *NKX2-1* amplification by FISH correlated with outcome in patients with NSCLC, including both adenocarcinoma and squamous cell carcinoma histology, we have expanded our initial observation to a larger set of NSCLC cases and established a DNA q-PCR methodology for analysis of *NKX2-1* copy number analysis. This work was presented as a platform presentation in the 100 Annual AACR Meeting, Denver, CO (April 18-22, 2009). We have also investigated the role of *NKX2-1* methylation in the silencing of expression in squamous cell carcinomas of the lung (presented as a poster in the IASLC in 2009). A manuscript with all these data is in the final stages of preparation and it will be submitted in March 2010 by X. Tang and H. Kadara et al.

h) *EGFR* and *HER2* copy analysis by FISH in tumor specimens from NSCLC patients, and correlation with *EGFR* and *KRAS* mutations and patients' clinicopathologic features. During the last year we performed the statistical analysis of the gene copy number by FISH of these two genes in a large series of NSCLC (n=330) tumors. Data from the preliminary analysis were presented as a poster discussion at the IASLC in 2009, and a manuscript is in preparation by Sun et al.

Key Research Accomplishments

- Maintained a large repository of lung cancer tissue, cytology, and cell lines specimens with annotated clinical data, to be utilized for research projects and clinical trials.
- Maintained a series of lung cancer heterotransplants in mice in collaboration with Project 6.
- Characterized the molecular abnormalities of *VEGF* and *KDR* (VEGFR2) genes in NSCLC, including the identification of high frequency of *KDR* copy number gain (~30%) in tumors.
- Published 2 papers in a prestigious peer-reviewed journal (*Clinical Cancer Research*) on the characterization of EGFR-related abnormalities in NSCLC brain metastasis and on the expression of ER expression in *EGFR*-mutant and wild-type tumors.
- Presented 4 abstracts at scientific meetings: one at the 2009 AACR annual meeting, three at the 13th IASLC World Lung Cancer Conference (IASLC), and with an additional abstract to be presented at the 2010 AACR annual meeting.

Conclusions

The Pathology Core has assisted and collaborated actively with several research projects to perform multiple histopathological, immunohistochemical, and genetic studies in a large series of lung cancer tissue, including the collection and processing of prospectively collected samples from two ongoing clinical trials. In addition, the Pathology Core has managed to complete and publish several research activities, which fully integrate with some of the IMPACT research projects. The Pathology Core has successfully fulfilled the goals proposed for the fifth year of the IMPACT program.

DRP-1: Treatment of Malignant Pleural Effusion with ZD6474, a Novel VEGFR and EGFR TK Inhibitor

(PI and co-PI: Roy Herbst, M.D., Ph.D., Carlos Jimenez, M.D.)

Recurrent malignant pleural effusion is a debilitating clinical problem that requires palliation with repeated therapeutic thoracentesis or pleurodesis (Putnam, J Surg Clin North Am 2002). Malignant pleural effusions have been associated with high levels of VEGF. Treatment with a VEGFR tyrosine kinase inhibitor resulted in a decrease in the amount of pleural effusion in an animal model (Yano, CCR 2000). We hypothesize that malignant pleural effusion formation in cancer patients can be decreased with ZD6474 (AstraZeneca), a VEGFR and EGFR tyrosine kinase inhibitor.

Aim 1 To determine clinical effect of ZD6474.

Aim 2 To investigate biological correlates.

Aim 3 To investigate radiographic correlates.

Aim 4 To assess quality of life.

Summary of Research Findings

Feb 2011 Report: The amended single arm, open-label study to evaluate the efficacy of ZD6474 on the management of pleural effusion in NSCLC patients was activated in June of 2007.

The study was closed early, on July 19, 2010, with 28 patients enrolled. Early closure was due to the company's decision not to continue development of this agent in this setting. Eight patients are excluded from the ongoing clinical analysis based on the following factors:

- Seven patients did not receive medication:
    - Non-compliance (1)
    - Benign pleural effusion (2)
    - Non-amenable for intrapleural catheter (IPC) placement (3)
    - Renal dysfunction (1)

One patient was not evaluable due to placement of a defective intrapleural catheter.

Best response:

- Eleven patients had stable disease
- Two patients had partial response
- Seven patients had disease progression

Days with intrapleural catheter in place: Median time to intrapleural catheter removal was 35 days. IPC catheters were removed for the following reasons:

- Achievement of pleurodesis (16 patients)
- Pleurodesis failure (3 patients)
- Death (1 patient)

Related adverse events:

- 5 patients with grade 3 QTc prolongation
- 1 patient with drug-related erthema mutiforme and rash/desquamation
- 1 patient with grade 3 weight loss and anorexia

One patient stopped the medication at week 6 after developing neurological symptoms and hyponatremia. One patient with a defective intrapleural catheter was excluded from the study at week 6. One patient stopped the medication at week 7 due to recurrence of QTc prolongation after dose reduction. One patient has the IPC dislodged on day 15, and the IPC was later removed on day 23 due to emphysema.

Systematic examination of pretreatment and changes in the plasma and pleural effusion angiogenic profiles consisting of a panel of proangiogenic cytokines and chemokines, soluble receptors, and potential biomarkers of endothelial damage. We collected samples of pleural effusion and plasma from patients consenting to an optional specimen collection (see Table 1) and, in collaboration with Drs. John Heymach and Hai Tran, performed a cytokine and angiogenesis factor (CAF) analysis (Table 2) in the baseline and 2-week specimens, as described below.

Table 1: Acquired samples

Sample Type	*Timepoint*	*Frequency*	*Percent*
Plasma	*2-Weeks*	9	15.25
Plasma	*Baseline*	12	20.34
Pleural	*2-Weeks*	18	30.51
Pleural	*Baseline*	20	33.90

Methodology:

Multiplex bead-based technology enables the simultaneous quantitation of up to 100 analytes. This technology uses polystyrene beads internally dyed with differing ratios of two spectrally distinct fluorophores. Each fluorophore can have any of 10 possible levels of fluorescent intensity; thereby creating a family of 100 spectrally addressed bead sets. These assays contain dyed beads conjugated with monoclonal antibodies specific for a target protein or peptide such as a cytokine or a phosphoprotein. Each of the 100 spectrally addressed bead sets can contain a capture antibody specific for a unique target protein. The antibody-conjugated beads are allowed to react with sample and a secondary, or detection, antibody in a microplate well to form a capture sandwich immunoassay. Multiplex assays can be created by mixing bead sets with different conjugated antibodies to simultaneously test for many analytes in a single sample. The use of this technique has been well documented in the literature and results are comparable to that of ELISA [1-3]. Analysis of these factors have been completed up to 23/27 proteins (Bio-Rad) from a single specimen have been completed from various matrices including: human serum and plasma and cell media from human cancer cell lines using Bio-Plex 200 system (Bio-Rad Laboratories, Hercules, CA) with the Bio-Plex Manager software. Currently, up to 50 human cytokines can be analyzed from 2 separate kits (2-plex, 21-plex & 27-plex). We also incorporated newly available markers of the EGFR axis including Amphiregulin, Betacellulin, EGF, EGFR, Epiregulin, FGF-basic, HB-EGF, PDGF-BB, PlGF, Tenascin C, and TGF-α (Table 3).

Table 2: Cytokines and Angiogenic Factors Profiling (CAF)

pro/antiangiogenic factors	EGF axis	chemokines	interleukins
VEGF, FGF-basic	EGF, EGFR, TGF-α	MCP-1, -3	IL-1α, -1β, -1RA
HGF, PDGF-bb	Amphiregulin, Betacellulin	MIP-1α, β	IL-2, -2Ra
MMP-9, PlGF	HB-EGF	RANTES (CCL5)	IL3 - IL10
	hypoxia	MIP-2	IL-12 – IL18
endothelial function/damage	Osteopontin*	MIG (CXCL-9)	
sVEGFR-2	CA-9*	Eotaxin (CCL11)	**growth factors**
sE-selectin	**IGF axis**	IP-10 (CXCL10)	GM-CSF
VCAM-1	IGF-I*, -II*	SDF-1a (CXCR4)	G-CSF
	IGF-BP3*	KC (CXCL1)	M-CSF
inflammation/ adhesion		GRO-α	SCGF-β
sICAM-1		CTACK (CCL27)	SCF
IFN- α, γ			Beta-NGF
TNF-α, β			
MIF, LIF	*ELISA assays (Various)		

Depending on target protein, a typical calibration curve was generated covering the dynamic range from 2 to 32,000 pg/mL. Typical sample volume required for each sample well ranged from 50 – 100 μL. Human CVD Biomarker Panel 1 (3-plex includes MMP-9, sICAM-1, and sE-Selectin) from Millipore (Catalog # HCVD1-67AK). The remaining analytes were determined by using validated, enzyme-linked immunosorbent assays (ELISA) assays. Soluble VEGFR1 and sVGFR2 was analyzed by EIA (Invitrogen, Carlsbad, CA). For each plate, the standard curves were assessed to ensure that the expected assay range was achieved. For each individual sample, the mean concentration was calculated for duplicate samples, and the coefficient of variance % (CV%) calculated for each of the analytes. If the median CV% was greater than 25%, analysis of the sample was repeated. In the rare case that the repeat CV% is greater than 25%, one of the two analyses will be selected based on lower CV% and consistency with prior values.

Preliminary Results:

Data was sent to send to Biostatistics Core for analysis and a preliminary report was generated with the following results.

Several CAFs were observed to significantly change in specimens obtained at baseline compared to specimens obtained at 2-weeks after initiation of therapy from both pleural effusion and plasma samples from paired sets (Tables 3a and 3b).

Table 3a: Pleural Effusion CAF changes over 2 weeks (baseline to 2 weeks)

CAF	*n*	*mean ± std, median(min, max)*	*pValue*
PIGF	18	0.86 ± 0.61, 0.77 (-0.36, 2.18)	0
MCP-1	18	1.71 ± 1.66, 1.48 (-0.35, 4.97)	0.0005
MCP-3	18	1.83 ± 2.23, 1.41 (-2.48, 7.24)	0.0008
IL-8	18	1.57 ± 1.79, 1.66 (-1.84, 4.66)	0.0023
IL-18	18	0.22 ± 0.29, 0.15 (-0.38, 0.8)	0.0028
HGF	18	0.69 ± 0.88, 0.77 (-1.42, 2.42)	0.0047
M-CSF	18	0.71 ± 1.05, 0.79 (-1.19, 3.2)	0.009
Eotaxin	18	1.26 ± 1.61, 1.31 (-0.94, 4.95)	0.012
SCGF-b	18	0.21 ± 0.33, 0.12 (-0.3, 1.06)	0.0139
IGF-I	18	0.37 ± 0.55, 0.41 (-1.03, 1.22)	0.0139
b-NGF	18	0.61 ± 0.94, 0.74 (-1.48, 2.04)	0.0208
G-CSF	18	0.27 ± 0.83, 0.29 (-2.17, 1.79)	0.0268
IL-5	18	1.35 ± 2.64, 0.8 (-2.95, 7.56)	0.0268
IFN-a2	18	0.15 ± 0.34, 0.23 (-0.58, 0.65)	0.0304
HB-EGF	18	0.19 ± 0.34, 0.18 (-0.36, 0.93)	0.0395
IL-1Ra	18	-0.61 ± 0.44, -0.57 (-1.91, 0.13)	.0000
sEGFR	18	-0.3 ± 0.3, -0.28 (-1.05, 0.28)	.0003
CTACK	18	-0.33 ± 0.35, -0.23 (-1, 0.36)	.0016
Amphiregulin	18	-0.55 ± 0.79, -0.59 (-2.04, 1.2)	.0104

Table 3b: Plasma CAF changes over 2 weeks (baseline to 2 weeks)

CAF	*n*	*mean ± std, median(min, max)*	*pValue*
Eotaxin	9	0.46 ± 0.32, 0.44 (0.12, 0.89)	0.0039
PIGF	9	0.56 ± 0.44, 0.46 (0.07, 1.35)	0.0039
MCP-1	9	0.56 ± 0.57, 0.52 (-0.07, 1.51)	0.0117
IL-18	9	0.48 ± 0.53, 0.35 (-0.2, 1.54)	0.0195
IFN-a2	9	1.57 ± 2.64, 0.55 (-0.41, 7.64)	0.0273
sVEGFR2	9	-0.29 ± 0.21, -0.27 (-0.63, 0)	.0078
sEGFR	9	-0.24 ± 0.28, -0.18 (-0.83, 0.04)	.0117

Interestingly, the 5 factors that were increased in plasma, including Eotaxin, PlGF, MCP-1, IL-18 and IFN-α2, were also present and increased in the pleural effusion samples; only sEGFR was shown to be decreased from both sample types.

From our prior experience with vandetanib (ZD6474) in the front-line therapy with or without chemotherapy doublet for patients with NSCLC, a distinct pattern of plasma CAF correlated with either chemotherapy-based or vandetinib alone (1). It was reported that in the vandetanib

treatment alone arm, plasma concentrations of VEGF increased at 3 week post and sVEGFR-2 was shown to be decreased at 8 days post initiation of therapy and progressively continue to declined, results that were associated with PFS. With our limited number of samples (n=9) in this trial, changes in VEGF were not significant but sVEGFR-2 significantly decreased over the first 2 weeks after starting vandetanib therapy (p=0.0078).

We then correlated baseline pleural effusion CAFs with both best therapeutic and best radiographic responses. Two factors, HB-EGF (p=0.073) and Eotaxin (p=0.053), from pleural effusions were associated with best therapeutic responses. For best radiographic responses, only GROa (p=0.035) was statistically significant, with other CAFs trending towards significance including Eotaxin (p=0.059), TNFa (p=0.097) and IGF-I (p=0.097).

For baseline plasma CAF, only IL-15 (p=0.040) was statistically significant, while IFN-g (p=0.070) and IL1ra (p=0.070) were trending in correlation with best therapeutic responses. There were no associations noted with plasma CAF and best radiological responses. Additionally, there were no CAF levels significantly modulated (over the 2-week period from baseline) with either therapeutic or radiographic responses.

We have shown that the relative changes of CAFs over short period (up to 2 weeks) is very minimal, less than 10% (unpublished), in a small group of NSCLC cancer patients. Certainly, due to the small sample size in this study, some of these changes may be due to chance; however, modulation with similar factors have been reported for two VEGFR tyrosine kinase inhibitors, vandetanib and pazopanib (1, 2).

Key Research Accomplishments

- Completed patient enrollment to the clinical trial.
- Measured and analyzed all collected plasma and pleural effusion samples using magnetic multiplex bead-based and ELISA assays.
- Completed the preliminary biostatistics analysis.

Reportable Outcomes

Publications Not Previously Reported: Massarelli E, Onn A, Marom EM, Alden CM, Liu DD, Tran HT, Mino B, Wistuba II, Faiz SA, Bashoura L, Eapen GA. Vandetanib and Indwelling Pleural Catheter for Non–Small-Cell Lung Cancer With Recurrent Malignant Pleural Effusion. Clinical Lung Cancer. 2014 Sep 30;15(5):379-86.

Conclusions

The amended single arm, open-label study to evaluate the efficacy of ZD6474 on the management of pleural effusion in NSCLC patients was closed on July 19, 2010, with 28 patients enrolled. Using the pleural effusion specimens collected from the 20 evaluable patients, we performed ELISA assays to determine that several CAFs from plasma and pleural effusions were associated with best responses (therapeutic and radiographic).

DRP-2: TALK - Teens and Young Adults Acquiring Lung Cancer Knowledge

(PI: Alexander V. Prokhorov, M. D., Ph.D.)

Ninety percent of lung cancer cases in adults are direct results of smoking. In children and young adults, tobacco use remains a major public health problem in spite of the recent declines

in smoking prevalence among children and adolescents. Over the past 2-3 decades, numerous factors of smoking initiation among adolescents have been thoroughly investigated. A considerable volume of literature is currently available providing important clues with respect to designing tobacco prevention and cessation among youth.

Focusing on this major public health problem – tobacco use among young individuals and lack of in-depth knowledge of lung cancer issues – Project TALK (Teens and Young Adults Acquiring Lung Cancer Knowledge) was conceived and funded as a smoking cessation/prevention pilot project for culturally diverse high-risk young populations that include school drop-outs, economically disadvantaged, and underserved. Using modern technologies, the Departments of Behavioral Science and Thoracic/Head & Neck Medical Oncology have joined their efforts to conduct this developmental project under the leadership of Dr. Alexander V. Prokhorov. The project will assist in making major advances in lung cancer education and prevention among youth. Project TALK will produce a CD-ROM-based education/behavior change for teenagers and young adults (15-24 years of age).

Aim 1 **Develop intervention program.** Focus groups will be held with adolescents and young adults to ensure we are capturing the essence of the program, using the right messages, and employing the appealing video and animated characters. (Years 1-2)

Aim 2 **Develop and beta-test CD-ROM.** This includes the design of the animation, illustrations, scripts and accompanying videos. (Years 1-2)

Aim 3 **Implement program in agreed upon locations and recruit young adults to participate in the study.** (Years 3-4)

Aim 4 **Collect and analyze data.** (Years 3-4)

Summary of Research Findings

Feb 2009 Report:

Participant Recruitment: A total of 239 high-risk alternative school students were recruited from the Houston area. Mean age of the participants was 16.2 years (SD=1.0), 79% were male. Thirty-six percent were Hispanic and 49% were African-American. Sixty-eight percent were in high school and 32% in middle school. The majority (70%) was not employed and 30% were employed part-time or full-time. Approximately 25% were current smokers and 29% former smokers.

The recruitment process at Fifth Ward Enrichment Center was assisted by the program's Executive Director; a school counselor at M.R. Wood assisted in recruiting the participants for the study. At M.R. Wood, the students were notified of the project by the school counselor and incoming students were given orientation packages that included the informed consent to be completed and turned in to the teaching staff or counselor. Other students were recruited by Project TALK staff through informal interactions with students who had heard about the game and were interested in participating.

Description of Educational Videogame: The educational videogame, available in both CD-ROM and kiosk form, uses a hospital metaphor in which participants "travel" to different "rooms" to learn about the dangers of tobacco use. The game allows users to personalize the experience by indicating their age, gender, race/ethnicity, smoking status, level of addiction and readiness to quit. Depending on the user's smoking status, the user enters a "nonsmoker" or "smoker" educational track. Each track has a different set of hospital rooms to explore, from which users

pick up necessary items required to "escape" from the hospital successfully. The various rooms educate users on the causes of lung cancer, role of smoking in lung cancer development and tobacco cessation/prevention.

Testing: The on-site program testing was completed in May 2008.

Survey: The evaluation instruments of the program have been designed and consist of a baseline survey, 7-day follow-up survey, and 6-month follow-up survey. Both the baseline survey and 7-day follow-up survey were used at the target sites. The 6-month follow-up survey was administered over the phone. Participants are then given the option to leave comments or suggestions with regard to their perception of the program and how it can be improved. The 6-month follow-up survey contains all the same questions as the 7-day follow-up survey, but was conducted by phone rather than in person.

Seven Day Feasibility Analysis: The primary outcomes for the 7-day feasibility evaluations included: (1) Ease of use and enjoyment of various features of the game; (2) The quality of the interactive multi-media presentations and the environment and their ability to generate interest in smoking and lung cancer prevention; (3) Motivational appeal, educational value and behavior modification post- completion of game; and (4) Post-completion knowledge of modules in the game. Comparisons of these outcomes by smoking status were done using analysis of variance, chi-square tests and nonparametric methods as appropriate.

Results: The 7-day feasibility survey was completed by 213 participants. The demographic profile of these participants was similar to the demographic profile of the 239 participants at baseline. Mean age of the 213 participants was 16.1 years (SD=1.0), 78% were male. Thirty-six percent were Hispanic and 51% were African-American. Over 50% reported playing the game two or more times. The top three highly rated rooms were surgery/operating theater, patient records and TV/theater rooms. Over 87% of participants reported ease of use with all aspects of the game and the majority of participants enjoyed most features in the game. After playing the game, 94% reported that the materials increased their knowledge about smoking effects and 77% reported that they were inspired never to start or to quit and 70% planned to share the game with family or friends. Post-completion knowledge of modules was assessed. The participants were tested on their knowledge about specific modules and the majority of participants reported that smoking and secondhand smoke is harmful to health, harmful to the unborn child and expensive. However, knowledge regarding nicotine addiction and the more severe consequences of smoking on mortality compared to other addictions was low.

Six-Month Feasibility Analysis: The 6-month survey has been completed by 146 participants. All participants played the game at least once and 40% played twice or more times. Over 85% of participants reported ease of use of this educational tool and the majority of participants enjoyed the experience. After playing the game, 94% reported increased knowledge about the tobacco effects, 82% were inspired never to start or to quit, and 82% planned to share the game with family or friends.

Mediating Variables of Smoking at 6-month Follow-up: The primary outcomes of interest in this study were the mediating determinants of smoking initiation and cessation including the pros and cons of tobacco use, decisional balance and temptations to smoke. These outcomes were analyzed using mixed model regression with time and baseline smoking status and their interaction as fixed effects. There was a significant interaction effect for cons of smoking ($F = 5.3$; $p<.05$), decisional balance ($F = 8.0$; $p<.01$), and temptations to smoke ($F = 7.6$; $p<.01$). For baseline smokers, 6-month temptations to smoke were significantly lower than baseline, and 6-

month cons of smoking were significantly higher than baseline. For nonsmokers, these variables did not change significantly.

Smoking Initiation and Cessation: Overall rates of self-reported smoking cessation and initiation at 6-month follow-up were not verified by cotinine or CO validation. Out of 146 participants who responded at 6 months, 34 were baseline smokers (23%) and 112 were non-smokers (77%). At 6 months, 18 (53%) out of 34 baseline smokers reported that they were abstinent and 7 (6%) out of 112 baseline non-smokers reported that they had initiated smoking. When stratified by gender and ethnicity, the results showed that more males and Hispanics quit smoking compared to females and non-Hispanics, although the results were not statistically significant due to small numbers. Those who quit also had significantly lower scores on the pros of smoking, decisional balance, and temptations to smoke compared to those who remained smokers ($p<.05$).

Key Research Accomplishments

- Performed testing at two sites with a total of 239 participants.
- Completed 7-day follow-up survey with a total of 213 participants.
- Completed 6-month follow-up survey with a total of 146 participants.

Conclusions

Project TALK was successfully developed according to the timeline. It produced an innovative, highly informative, and easy to navigate videogame that was enthusiastically accepted by young individuals at high risk of initiating tobacco use. More than half the smokers who participated had quit smoking at the 6-month follow-up. Overall, results have shown an increased level of awareness regarding the dangers of smoking across the participants enrolled. We aim to place our informational materials in other strategic areas across the community to duplicate results seen in this project.

Career Developmental Project (CDP1): Identification of Membrane Proteins in Bronchial Epithelia Cells as Biomarkers of Early Detection for Lung Cancer

(PI: Ja Seok Peter Koo, Ph.D.)

Lung cancer is the leading cause of cancer deaths. Early detection of the malignant lesion leads to an improved 5-year survival rate after surgical resection. Therefore, advanced screening tools are needed urgently to detect lung cancer at an early stage to improve control of such deadly lung cancer.

Aim 1 To isolate membrane proteins uniquely expressed on the surface of squamous metaplasia using organotypically cultured bronchial epithelial cells.

Summary of Research Findings

Feb 2009 Report: Membrane proteins were isolated from *in vitro* models of squamous metaplastic bronchial epithelial cells and compared with that of normal mucocilliary bronchial epithelial cells by 2-dimensional polyacrylamide gel electrophoresis. Normal human tracheobronchial epithelial (NHTBE) cells from passage 3 originated from samples collected from smokers and non-smokers; samples were cultured with or without retinoic acid for the formation of in vitro model of squamous metaplasia by air-liquid interface method. Cells were harvested at 12 days after air-liquid formation. Non-small-cell lung cancer cell lines (H226, H2170) were grown on plastic plate in RPMI 1640 containing 10% fetal bovine serum. H226 and

H2170 cells were harvested at 80% confluence. Membrane proteins were extracted using ReadyPrep™ Protein Extraction Kit (Membrane I) (Bio-Rad) according to the manufacturer's instruction. To analyze the differentially expressed proteins, 20 µg of membrane protein extracted was subjected to two-dimensional PAGE analysis. The samples were loaded onto 7-cm immobilized pH gradient strips (pH 3-10, nonlinear), which were passively rehydrated for 15 hours. Isoelectric focusing was conducted using a Protein isoelectric focusing cell system for 40,000V/h. After equilibration process, the strips were applied to 10% nongradient SDS-PAGE gel, and the gels were stained using Silver Stain Plus kit (Bio-Rad).

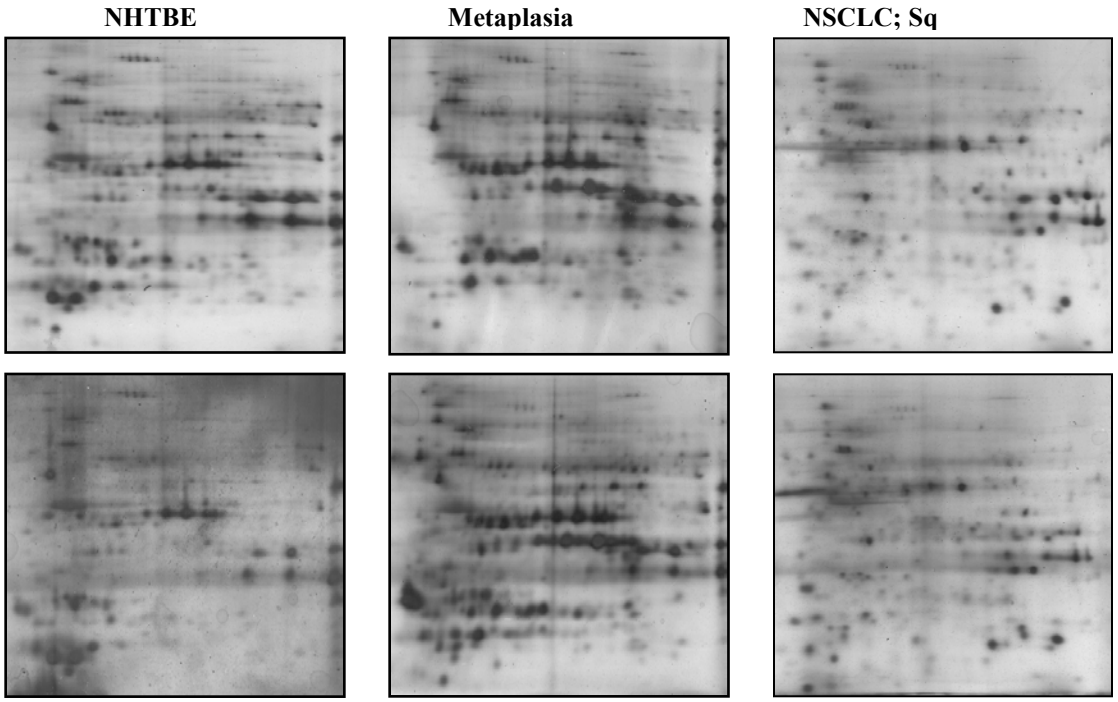

Figure 1: 2-D PAGE using membrane proteins from normal human tracheobronchial epithelial (NHTBE) cells, *in vitro* model of squamous metaplasia, and squamous cell carcinomas of lung (H226, H2170). Isoelectric point: 3 - 10 (from left to right)

left upper: NHTBE from smoker
left lower: NHTBE from non-smoker
center upper: squamous metaplasia from smoker
center lower: squamous metaplasia from non-smoker
right upper: H226 (squamous cell carcinoma of lung)
right lower: H2170 (squamous cell carcinoma of lung)

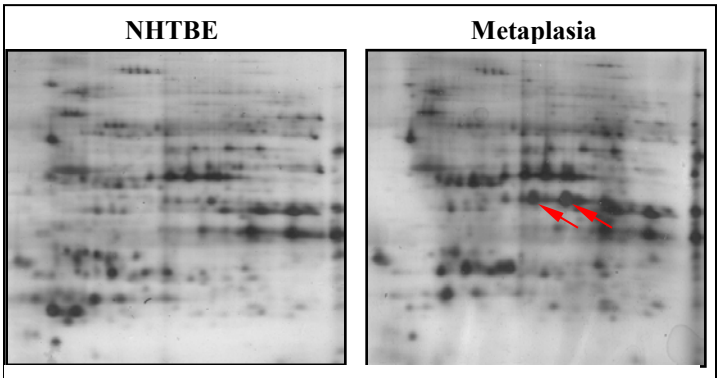

Figure 2: Highly expressed membrane proteins in squamous metaplasia (arrow) compared to NHTBE cells.

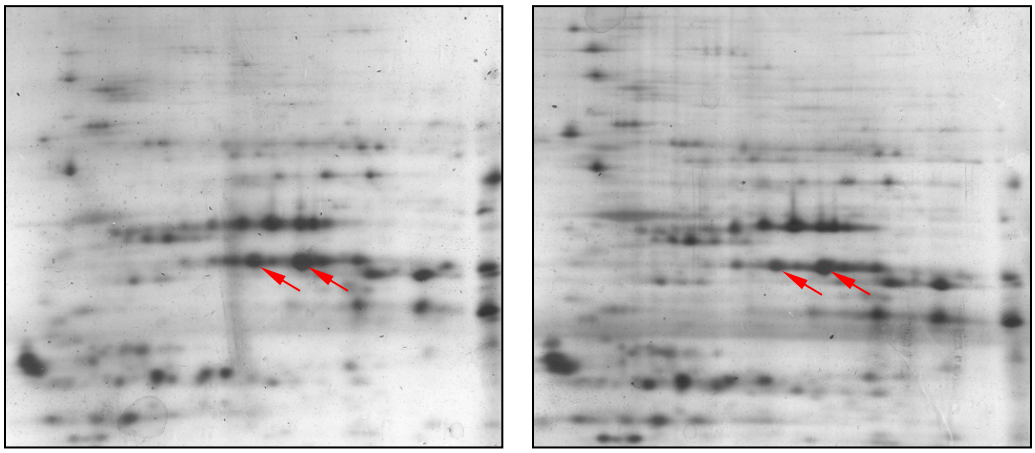

Figure 3: Highly expressed membrane proteins of squamous metaplasia were reproducibly detected in other sample sets.

We compared the expression pattern of membrane proteins of NHTBE cells and squamous metaplasia originating from smokers or non-smokers. There was no significant difference in membrane protein expression on 2-DE between smokers and non-smokers (Fig. 1). We then compared the expression pattern of membrane proteins of NHTBE cells to those of the squamous metaplasia resulting in similar pattern displays. However, some spots had higher expression patterns squamous metaplasia compared to NHTBE cells (Fig. 2). Highly expressed, membrane proteins of squamous metaplasia were reproducibly detected in other sample sets (Fig. 3). Last, we compared expression pattern of membrane proteins of NHTBE cells to those of non-small-cell lung cancer cell lines (H226, H2170; squamous cell carcinoma). Membrane proteins from squamous cell carcinomas displayed very different pattern of expression compared to those from NHTBE cells.

Aim 2 To identify differentially represented proteins using proteomics.

Summary of Research Findings

Feb 2010 Report: The goal of this study is to identify and characterize cell surface markers specific for lung cancer cells, as these proteins have strong potential for novel diagnostic and therapeutic biomarkers.

Our previous attempt to identify membrane proteins specific for cancer cells was not successful. Several technical issues were involved. Here, we repeated 2D-Proteomics Mass spectrometry analysis of the two protein spots (indicated by red arrows in the 2D gel) using optimized new conditions (Figure 20). After extensive

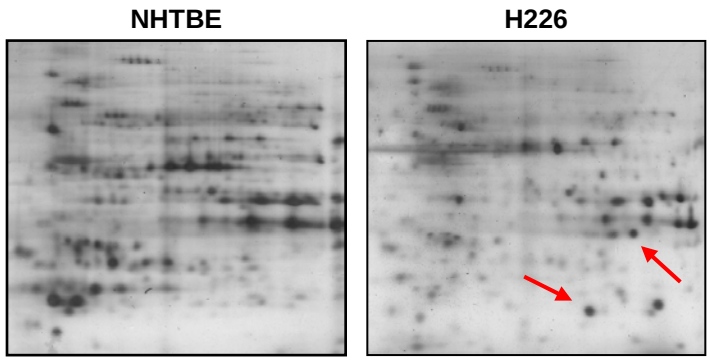

Figure 20. 2-Dimensional electrophoresis analysis of membrane proteins differentially expressed in NHTBE (normal) and H226 squamous cell carcinoma of lung.

database searching, we found that the protein in the lower spot turn out to be an unknown protein and identified the protein in the upper spot as a receptor for activated kinase C (RACK1).

RACK1 is a cytosolic membrane protein and also known as lung cancer oncogene 7 and PIG21 (proliferation-inducing gene 21). Its official gene name is GNB2L1 (guanine nucleotide binding protein (G protein), beta polypeptide 2-like 1).

RACK1 was originally identified as an anchoring protein for protein kinase C β (PKC β), which it stabilizes in the active state and anchors to membranes or functional sites. RACK1 also interacts with several other important signaling proteins including the Src kinase family, integrin β1, - β2, -β3, and β5, beta-spectrin and dynamin, RasGAP, the androgen receptor, insulin-like growth factor 1 receptor (IGF-1r), Epstein-Barr virus trans-activator protein BZLF1, p73, and pRB. This interaction suggests that RACK1 may act as an anchor or adaptor protein, recruiting other proteins to various transmembrane receptors, providing a platform for protein-protein interactions and acting as the focus for several cell-signaling pathways. Accordingly, a number of cellular functions have been attributed to RACK1, such as cell growth, adhesion, protrusion and chemotactic migration. RACK1 may also contribute to angiogenesis and tumor growth, since it was shown to be up-regulated during angiogenesis *in vitro* and *in vivo*, and was also expressed in tumor angiogenesis. RACK1 expression was higher in human non-small cell lung and colon carcinomas than in the corresponding normal tissues.

Recent studies [7] also showed that RACK1 is up-regulated in oral squamous carcinoma, and linked to clinical invasiveness and metastasis. In addition, elevated RACK1 expression predicts poor clinical outcome in oral squamous carcinoma, similar to Ki67 [8]. These studies suggest that RACK1 is a potential biomarker for prognosis and a therapeutic target for squamous carcinoma. We will determine whether RACK1 expression is altered (overexpressed) in lung cancer cells using Western blot analysis. In the meantime, we are collecting samples of various NSCLC cell lines, and the samples will be used for verification of the expression of RACK1. We are aiming to collect samples of at least 30 different genetically certified lung cancer cell lines. Specificity of RACK1 expression will also be determined by immunohistochemical analysis using tissue slides.

Aim 3 To verify the differentially represented proteins using PCR, Western blotting, and immunocytochemistry.

Summary of Research Findings

Feb 2011 Report: To identify cell-surface markers specific for lung cancer cells, as these proteins have strong potential for use as novel diagnostic and therapeutic biomarkers, we performed 2-Dimensional proteomics analysis using membrane fractions isolated from normal human bronchial epithelial (NHBE) cells and non-small-cell lung cancer (NSCLC) cells. We performed the immunoblotting on cell lysates, following by immunohistochemistry and immunofluorescence using the A549, H1355, H1734, H520, H1703, H2228 and H460 cell lines. From this experiment, we conclude that increased expression levels of the receptor for activated kinase C (RACK1) in tumor tissue were observed in tumor but not normal lung cells, and was localized in the tumor cell cytoplasm. The expression of RACK1, which mediates protein–protein interactions for the regulation of cell motility, in NSCLC, and its interaction with several proteins that have important roles in cell growth and survival, makes RACK1 a candidate molecule to target as a potential therapeutic strategy for NSCLC. Details are described below.

*Proteomic identification of RACK1 (*also known as *GNB2L1, guanine nucleotide binding protein, or beta polypeptide 2-like 1) as a lung cancer cell-specific, membrane-associated protein.* Two-dimensional proteomics analysis using membrane fractions isolated from NHBE cells and NSCLC cells. Membrane proteins were isolated from *in vitro* models of squamous metaplastic bronchial epithelial cells and compared with those of normal mucocilliary bronchial epithelial cells by 2-dimensional polyacrylamide gel electrophoresis. Normal human tracheobronchial epithelial (NHTBE) cells from passage 3 were cultured by air-liquid interface method. Cells were harvested at 12 days after air-liquid formation. The NSCLC cell line H226 were grown on plastic plate in RPMI 1640 containing 10% fetal bovine serum. H226 and NHTBE cells were harvested at 80% confluence.

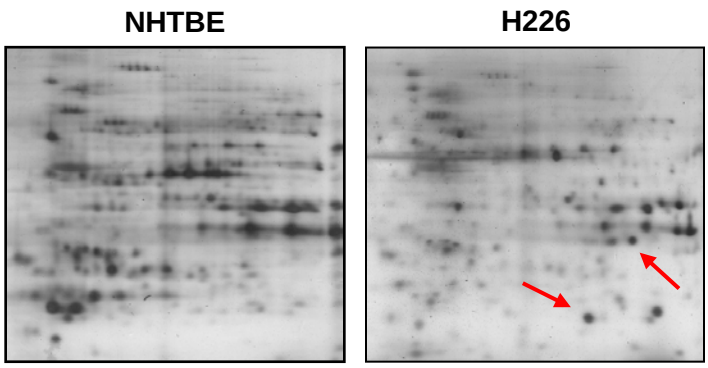

Figure 2. 2-Dimensional electrophoresis analysis of membrane proteins differentially expressed in NHTBE (normal) and H226 squamous cell carcinoma of lung.

Using HPLC-tandem Mass Spectrometer in collaboration with the Proteomics Core facility at MD Anderson, we sequenced and determined the specific identity of the proteins isolated (Arrow marked in Figure 2). After being excised, the silver-stained spots were destained and digested in gel with 200 ng of modified trypsin (Promega). The resulting peptides were analyzed by nano-liquid chromatography-tandem mass spectrometry with on-line desalting with a Famos autosampler, an Ultimate nano-LC module, and a Switchos precolumn switching device (LC Packings/Dionex). Electrospray ion-trap mass spectrometry was done using an LTQ linear ion-trap mass spectrometer (Thermo). The fragment spectra were analyzed using the National Center for Biotechnology Information nonredundant protein database and the Mascot search engine (Matrix Science). After extensive database searching, we found that the protein in the lower spot was an unknown protein and identified the protein in the upper spot as a receptor for activated kinase C (RACK1).

RACK1 is ubiquitously expressed in a wide range of tissues, including the brain, liver, and spleen. Moreover, RACK1 has many other binding partners involved in the organization of adhesions and cell migration, including the cytoplasmic tail of β-integrins and PKC. These interactions support the role of RACK1 as a key scaffolding protein that mediates protein–protein interactions for the regulation of cell motility. Recent studies indicated that RACK1 reduced cell-cycle progression and the growth of colon carcinoma cells by negatively regulating endogenous Src kinase activity, suggesting that RACK1 may be an attractive therapeutic target to treat cancer; thus, we explored its potential utility as a marker in lung cancer.

Expression of RACK1 is detected in NSCLC cells. We studied the expression of RACK1 in H520, H1703, H2228 and A549 NSCLC cell lines by Western blot analysis using the mouse anti-RACK1 antibody as the first antibody and cell lysates from the different cells lines (Figure 3). Proteins resolved by 1-dimensional electrophoresis were blotted onto nitrocellulose membranes (Bio-Rad) in a transfer buffer containing Tris, glycine (MP Biomedical). Membranes were blocked in 5% (wt/vol) skimmed milk in phosphate buffered saline 0.1% tween for 30min and probed with anti-RACK1 monoclonal antibody (Santa Cruz). After washing with phosphate-

buffered saline 0.1% tween (vol/vol), the membranes were incubated with appropriate antibody conjugated with horseradish peroxidase and diluted at 1:1000, that is, anti–mouse immunoglobulin G (BioRad). The blot shows the reactivity of antibody with protein at 33KDa. The staining of RACK1 on cell lysates from H520, H1703 and H2228 appears stronger than the lysates from A549. This data suggests the presence of RACK1 in all the NSCLC cells tested with differences in expression levels.

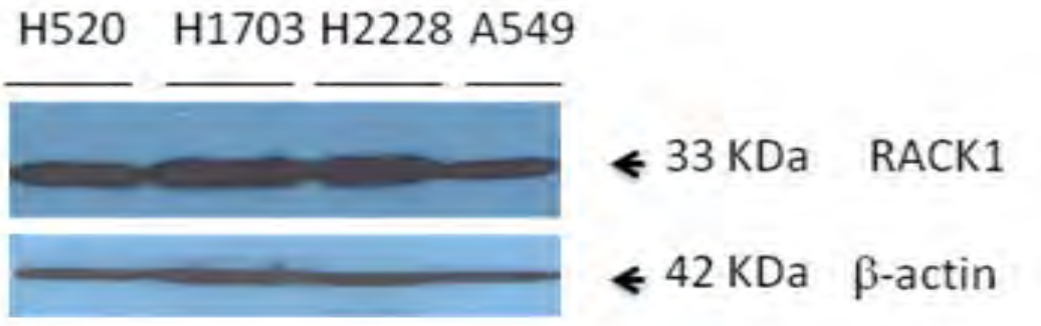

Figure 3. Expression of RACK1 in lung cancer cell line. Immunoblotting analysis of cell lysates from H520, H1703, H2228 and A549 with anti-RACK1 antibody. The mouse anti-RACK1 was used as first antibody followed by secondary antibody coupled with the enzyme horseradish peroxidase.

Immunofluorescence localization of the expression of RACK1. Fluorescence experiments were performed to determine the localization of RACK1. The immufluorescence was started with $2.5x10^4$ cells cultured in chamber slides. Cell lines were fixed for 10 minutes with 4% buffered glutaraldehyde at -20°C, incubated for 30 minutes with 2% bovine serum albumin, and then with Anti-RACK1 antibodies (Santa-Cruz, CA) diluted 1:100 for 1 hour. Antibody binding was detected after 1 hour incubation at room temperature with an anti-mouse antibody Alexa-488 (1:200) (Invitrogen). Cells were imaged using fluorescence microscope equipped with X40 magnification. The staining shown in the cytoplasm of A549, H460, H1355 and H1703 cell lines confirm the presence of RACK1 in the cytoplasm of NSCLC cells (Figure 4). The positive control used shows the similar pattern of staining compare to the RACK1; the negative control shows no artifact of staining. This result confirmed the presence of RACK1 by showing the intense staining observed in cytoplasm of the NSCLC cells.

Immunohistochemical staining. To evaluate the expression of RACK1 as diagnostic marker in the tumor tissue, we studied IHC expression using the tissue of mouse pulmonary carcinomas from *KRAS*-mutant mice. IHC studies were performed on formalin-fixed, paraffin-embedded tissue sections using the streptavidin–biotin–peroxidase complex method. Sections were cut at 4μm thickness and mounted on APES coated slides, dewaxed in xylene, and rehydrated in graded ethanol. The sections were treated with 30% hydrogen peroxide for 10 minutes to inhibit endogenous peroxidase activity and washed in phosphate buffered saline (PBS). To retrieve antigen, the sections were immersed in 0.01M citrate buffer and heated by microwave or on a hot plate for 20 to 25 minutes, following by washing in water. Sections were preincubated with the primary antibody for 60 minutes at room temperature. The biotinylated secondary antibody (Invitrogen) was incubated for 30 minutes at room temperature. The sections were incubated with streptavidin–peroxidase complexes (Invitrogen kit) for 30 minutes at room temperature, followed by washing in PBS.

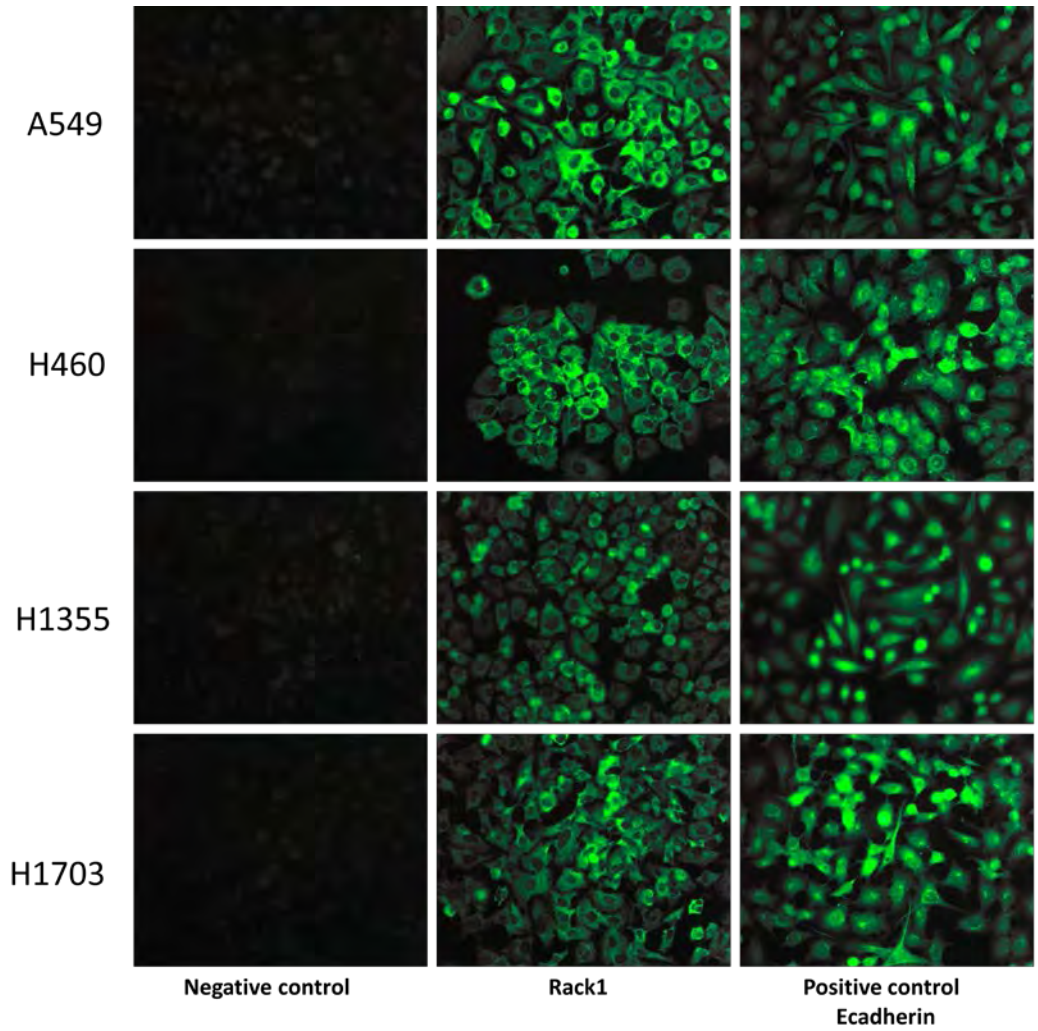

Figure 4. Expression of RACK1 in different NSCLC cell lines. The immunostaining of RACK1 on A549, H460, H1355 and H1703 cell line with RACK1 antibody. Cells were processed for fluorescence microscopy. Cells were fixed and labeled with mouse anti-RACK1 and Alexa 488 conjugated anti-mouse antibodv.

Staining results (Figure 5) show intense expression and localization of RACK1 in the cytoplasm observed in the lung epithelium and adenocarcinoma sections from *KRAS*-mutant mouse, but no obvious staining was observed in the lung sections from wild-type littermate control mice Using mass spectrometry, we were able to identify RACK1 as a protein in plasma membrane fraction. RACK1 is also known as GNB2L1 (guanine nucleotide binding protein, beta polypeptide 2-like 1), lung cancer oncogene 7 or PIG21 (proliferation-inducing gene 21). We verified expression of the RACK1 in lung cancer cells by immunoblotting that demonstrates the staining of protein at 33KDa, in H520, H1703, H2228 and A549. The data confirms the expression of RACK1 in the cell lysates of the different cells lines. Moreover, the fluorescence staining using NSCLC cell line confirms the presence of RACK1 in cytoplasm of these cell lines.

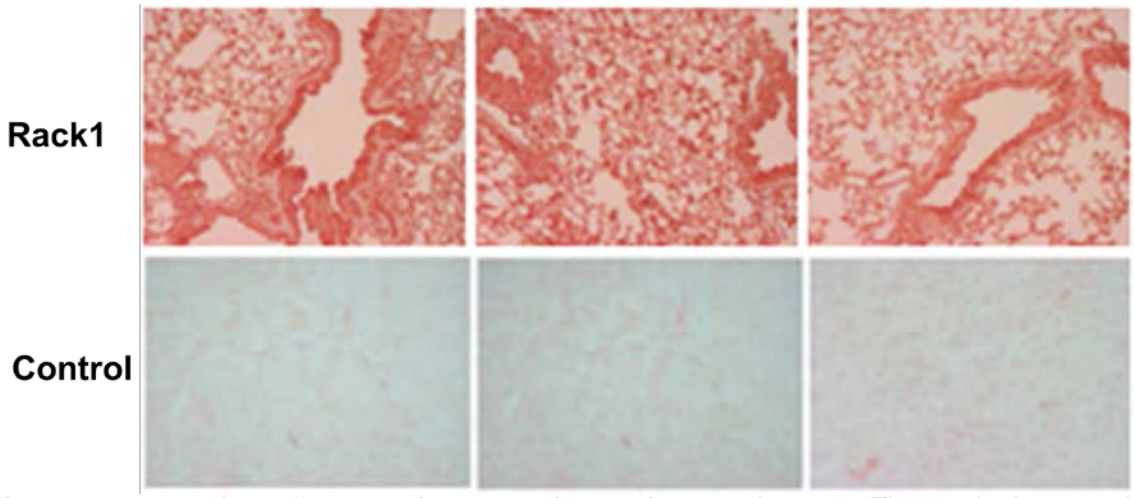

Figure 5. Expression of RACK1 in mouse lung adenocarcinomas. The marked expression of RACK1 was observed in the lung tumor sections from *KRAS*-mutant lung cancer mouse model. The RACK1 staining is not detected in the lungs from normal lung from control mice.

The expression of RACK1 was also verified in mouse tumor tissue obtained from *KRAS* lung cancer mouse model; a high staining and marked level of RACK1 were found in the tumor but not in the normal lung from wild-type mice. Moreover, RACK1 expression level was significantly associated with cell localization within the tumor. Further studies are needed to clarify the relationship between the expression of RACK1 and clinical outcome of adenocarcinoma.

Key Research Accomplishments

- Identified RACK1 as a protein that is uniquely expressed in squamous cell carcinoma cell lines and may be a therapeutic target to treat cancer.

Conclusions

We demonstrated increased expression levels of the RACK1 in tumor tissue in tumor but not normal lung cells, and this increased expression was localized in the tumor cell cytoplasm. RACK1 mediates protein–protein interactions for the regulation of cell motility, in NSCLC, and has interactions with several proteins that have important roles in cell growth and survival, making it a candidate molecule to target as a potential therapeutic strategy for NSCLC. Further extensive studies are warranted to clarify if RACK1 will have utility as a therapeutic target for lung cancer.

KEY RESEARCH ACCOMPLISHMENTS

Project 1: Targeting epidermal growth factor receptor signaling to enhance response of lung cancer to therapeutic radiation.

- Completed patient enrollment to the ID 2005-1023 trial.
- Analyzed biopsy specimens from the phase II clinical trial for biomarkers associated with response to EGFR TKI and tumor's epithelial or mesenchymal status.
- Analyzed the pre-treatment biopsy specimens and correlated findings with response as well as with patterns of failure.

Project 2: Molecular imaging of EGFR expression and activity in targeted therapy of lung cancer

- Completed accrual and treatment of the first cohort of patients (3 females) at 2mCi per patient, and 2 (both male) of the 6 patients planned for the second cohort. Doses of the agent were delivered within 10% of the requested dose (on the high side) as per standard nuclear pharmacy regulations.
- Performed the required statistical analysis following treatment of the first patient cohort to determine the dose level for the next cohort of patients (3.78 mCi per patient).
- Obtained all required regulatory approvals were obtained to move forward with patient screening and accrual to the next cohort of 6 patients (3 males and 3 females); 2 additional patients were accrued.
- Determined a lack of activity of the agent of the current dose level, and unacceptable levels of radiation in the liver, GI and gall bladder of the treated patients.

Project 3: Targeted peptide-based systemic delivery of therapeutic and imaging agents to lung tumors

- Used labeled targeted peptide motifs themselves as imaging tools.
- Demonstrated that AAVP-based molecular-genetic imaging appears to be superior to FDG in side-by-side comparisons for predicting therapeutic response.
- Designed and developed nanotechnology-based (i.e., bottom-up, self-assembled) biocompatible networks of phage-gold as nanotechnology-based molecular sensors and reporters.

Project 4: Inhibition of bFGF Signaling for Lung Cancer Therapy

- Discovered that blocking the FGFR1 signaling by DNFR1 leads to inhibition of cell growth by blocking cells at the G2 phase of the cell cycle through decreased expression, phosphorylation, and kinase function of p34cdc2 combined with increased Wee1, and the cyclin-dependent kinase inhibitors p21 and p27.
- Determined that Geldanamycin inhibits the growth of lung cancer cells by a G2/M block and by a mechanism that in part emulates the blocking of FGFR signaling by DNFR1 expression.
- Demonstrated the ability of bFGF to increase Hsp90 level and the ability of the Hsp90 inhibitor Geldanamycin to inhibit FGF signaling, suggesting that Hsp90 is a positive mediator of FGF effects.

Project 5: Targeting mTOR and Ras signaling pathways for lung cancer therapy

- The combination of RAD001 and BKM120 shows synergistic inhibitory effects on the growth of human NSCLC cells both in vitro and in vivo.
- The finding on BKM120-induced activation of the MEK/ERK signaling provides a scientific rationale for combination of BKM120 and a MEK inhibitor.
- The project entitled “Targeting PI3K and mTOR signaling in lung cancer” in our renewal of P01 grant was re-submitted (01-24-2012).
- A R01 proposal entitled “Therapeutic potential of mTOR kinase inhibitors in lung cancer” was submitted and received a potentially funded score (7 percentile). This grant is pending for funding.

Core B: Biostatistics & Data Management Core

For Project 2, “Molecular Imaging of EGFR Expression and Activity in Targeting Therapy of Lung Cancer,” Core B worked with study investigators in the necessary revisions of the protocol “A Phase I Study of 18F-Fluoro-PEG6-IPQA as a PET Imaging Agent for Active/Mutant EGFR

Expression in Tumors (2009-0832)," completed the analysis of the first cohort accrued to the trial, and completed the final analysis for the trial.

Core C: Pathology Core

- Completed the molecular biomarker analysis on the Project 1 clinical trials using NSCLC tissue specimens from 34 patients enrolled in the clinical trial, and demonstrated that *KDR* CNG and VEGFR-2 overexpression correlated with angiogenesis and patients's outcome when treated with adjuvant chemotherapy.
- Published research findings on the role of NKX2-1 (TITF-1) gene amplification and protein overexpression in lung cancer and its association with EGFR abnormalities NSCLC.
- Published research findings on the molecular abnormalities analysis of TCF21 gene in NSCLC.

DRP-1: Treatment of Malignant Pleural Effusion with ZD6474, a Novel VEGFR and EGFR TK Inhibitor

- Completed patient enrollment to the clinical trial.
- Measured and analyzed all collected plasma and pleural effusion samples using magnetic multiplex bead-based and ELISA assays.

DRP-2: TALK - Teens and Young Adults Acquiring Lung Cancer Knowledge

- Completed all proposed aims.
- Received a Peer Reviewed Medical Research Program award for $3,700,000 for the Project TALK research program.
- Conducted a site visit to Fort Hood, TX to collect data for the new "Escape With Your Life" video game.

CDP1: Identification of Membrane Proteins in Bronchial Epithelia Cells as Biomarkers of Early Detection for Lung Cancer

- Identified RACK1 as a protein that is uniquely expressed in squamous cell carcinoma cell lines and may be a therapeutic target to treat cancer.

REPORTABLE OUTCOMES

Publications:

The following is a list of publications citing this grant:

Manuscripts**:**

1. Behrens C, Lin HY, Lee JJ, Raso MG, Hong WK, Wistuba II, Lotan R. Immunohistochemical expression of basic fibroblast growth factor and fibroblast growth factor receptors 1 and 2 in the pathogenesis of lung cancer. Clinical Cancer Research. 2008 Oct 1;14(19):6014-22.
2. Colella S, Richards KL, Bachinski LL, Baggerly KA, Tsavachidis S, Lang JC, Schuller DE, Krahe R. Molecular signatures of metastasis in head and neck cancer. Head & Neck. 2008 Oct 1;30(10):1273-83.
3. Kong M, Lee JJ. Applying Emax model and bivariate thin plate splines to assess drug interactions. Frontiers in bioscience (Elite edition). 2010;2:279.
4. Kong M, Lee JJ. A generalized response surface model with varying relative potency for assessing drug interaction. Biometrics. 2006 Dec 1;62(4):986-95.
5. Kong M, Lee JJ. A semiparametric response surface model for assessing drug interaction. Biometrics. 2008 Jun 1;64(2):396-405.

6. Lee JJ, Kong M, Ayers GD, Lotan R. Interaction index and different methods for determining drug interaction in combination therapy. Journal of Biopharmaceutical Statistics. 2007 May 1;17(3):461-80.
7. Lee JJ, Lin HY, Liu DD, Kong M. Emax model and interaction index for assessing drug interaction in combination studies. Frontiers in Bioscience (Elite edition). 2010 Jan 1;2:582.
8. Lee JJ, Liu DD. A predictive probability design for phase II cancer clinical trials. Clinical Trials. 2008 Apr 1;5(2):93-106.
9. Ma Y, Yin G. Cure rate model with mismeasured covariates under transformation. Journal of the American Statistical Association. 2012.
10. Massarelli E, Onn A, Marom EM, Alden CM, Liu DD, Tran HT, Mino B, Wistuba II, Faiz SA, Bashoura L, Eapen GA. Vandetanib and Indwelling Pleural Catheter for Non–Small-Cell Lung Cancer With Recurrent Malignant Pleural Effusion. Clinical Lung Cancer. 2014 Sep 30;15(5):379-86.
11. Massarelli E, Varella-Garcia M, Tang X, Xavier AC, Ozburn NC, Liu DD, Bekele BN, Herbst RS, Wistuba II. KRAS mutation is an important predictor of resistance to therapy with epidermal growth factor receptor tyrosine kinase inhibitors in non–small-cell lung cancer. Clinical Cancer Research. 2007 May 15;13(10):2890-6.
12. Nieto-Barajas LE, Yin G. Bayesian semiparametric cure rate model with an unknown threshold. Scandinavian Journal of Statistics. 2008 Sep 1;35(3):540-56.
13. Owonikoko TK, Ramalingam SS, Miller DL, Force SD, Sica GL, Mendel J, Chen Z, Rogatko A, Tighiouart M, Harvey RD, Kim S. A Translational, Pharmacodynamic, and Pharmacokinetic Phase IB Clinical Study of Everolimus in Resectable Non–Small Cell Lung Cancer. Clinical Cancer Research. 2015 Apr 15;21(8):1859-68.
14. Pathak AK, Bhutani M, Saintigny P, Mao L. Heterotransplant mouse model cohorts of human malignancies: A novel platform for Systematic Preclinical Efficacy Evaluation of Drugs (SPEED). Am J Transl Res. 2009 Jan 1;1(1):16-22.
15. Raso MG, Behrens C, Herynk MH, Liu S, Prudkin L, Ozburn NC, Woods DM, Tang X, Mehran RJ, Moran C, Lee JJ. Immunohistochemical expression of estrogen and progesterone receptors identifies a subset of NSCLCs and correlates with EGFR mutation. Clinical Cancer Research. 2009 Sep 1;15(17):5359-68.
16. Richards KL, Zhang B, Baggerly KA, Colella S, Lang JC, Schuller DE, Krahe R. Genome-wide hypomethylation in head and neck cancer is more pronounced in HPV-negative tumors and is associated with genomic instability. PLoS One. 2009 Mar 18;4(3):e4941.
17. Spivey KA, Banyard J, Solis LM, Wistuba II, Barletta JA, Gandhi L, Feldman HA, Rodig SJ, Chirieac LR, Zetter BR. Collagen XXIII: A Potential Biomarker for the Detection of Primary and Recurrent Non–Small Cell Lung Cancer. Cancer Epidemiology Biomarkers & Prevention. 2010 May 1;19(5):1362-72.
18. Tanaka T, Munshi A, Brooks C, Liu J, Hobbs ML, Meyn RE. Gefitinib Radiosensitizes Non–Small Cell Lung Cancer Cells by Suppressing Cellular DNA Repair Capacity. Clinical Cancer Research. 2008 Feb 15;14(4):1266-73.
19. Tang X, Varella-Garcia M, Xavier AC, Massarelli E, Ozburn N, Moran C, Wistuba II. Epidermal growth factor receptor abnormalities in the pathogenesis and progression of lung adenocarcinomas. Cancer Prevention Research. 2008 Aug 1;1(3):192-200.
20. Temam S, Kawaguchi H, El-Naggar AK, Jelinek J, Tang H, Liu DD, Lang W, Issa JP, Lee JJ, Mao L. Epidermal growth factor receptor copy number alterations correlate with poor clinical outcome in patients with head and neck squamous cancer. Journal of Clinical Oncology. 2007 Jun 1;25(16):2164-70.
21. Tian M, Ogawa K, Wendt R, Mukhopadhyay U, Balatoni J, Fukumitsu N, Uthamanthil R, Borne A, Brammer D, Jackson J, Mawlawi O. Whole-body biodistribution kinetics, metabolism, and radiation dosimetry estimates of 18F-PEG6-IPQA in nonhuman primates. Journal of Nuclear Medicine. 2011 Jun 1;52(6):934-41.

22. Wang J, Bhutani M, Pathak AK, Lang W, Ren H, Jelinek J, He R, Shen L, Issa JP, Mao L. ΔDNMT3B variants regulate DNA methylation in a promoter-specific manner. Cancer Research. 2007 Nov 15;67(22):10647-52.
23. Yeh HH, Ogawa K, Balatoni J, Mukhapadhyay U, Pal A, Gonzalez-Lepera C, Shavrin A, Soghomonyan S, Flores L, Young D, Volgin AY. Molecular imaging of active mutant L858R EGF receptor (EGFR) kinase-expressing nonsmall cell lung carcinomas using PET/CT. Proceedings of the National Academy of Sciences. 2011 Jan 25;108(4):1603-8.
24. Yin G, Li H, Zeng D. Partially linear additive hazards regression with varying coefficients. Journal of the American Statistical Association. 2012.
25. Yin G, Yuan Y. Bayesian dose finding in oncology for drug combinations by copula regression. Journal of the Royal Statistical Society: Series C (Applied Statistics). 2009 May 1;58(2):211-24.
26. Yuan P, Temam S, El-Naggar A, Zhou X, Liu DD, Lee JJ, Mao L. Overexpression of podoplanin in oral cancer and its association with poor clinical outcome. Cancer. 2006 Aug 1;107(3):563-9.
27. Zhang S, Schafer-Hales K, Khuri FR, Zhou W, Vertino PM, Marcus AI. The tumor suppressor LKB1 regulates lung cancer cell polarity by mediating cdc42 recruitment and activity. Cancer Research. 2008 Feb 1;68(3):740-8.

Abstracts:

1. Behrens C, Lin H, Lee J, Hong W, Wistuba I, Lotan R. Differential immunohistochemical expression patterns of fibroblast growth factor-2, receptors 1 and 2, and syndecan-1 in squamous cell carcinoma and adenocarcinoma of the lung. Cancer Research. 2007 May 1;67(9 Supplement):190.
2. Behrens C, Wistuba II, Feng L, Lee JJ, Hong WK, Lotan R. Expression of fibroblast growth factor and its receptors in premalignant and malignant human lung tissues. Cancer Research. 2006 Apr 15;66(8 Supplement):1350.
3. Li X, Tang X, Dong W, Woods D, Yin G, ki Hong W, Moran C, Wistuba I. STAT1 protein frequently overexpressed in non-small cell lung carcinoma. Cancer Research. 2008 May 1;68(9 Supplement):2166.
4. Raso M, Behrens C, Liu S, Prudkin L, Woods D, Ozburn N, Moran C, Lee JJ, Wistuba I. Immunohistochemical expression of estrogen and progesterone receptors identifies a subset of non-small cell lung cancers and correlates with EGFR Mutations. Cancer Research. 2008 May 1;68(9 Supplement):2165.
5. Richards KL, Zhang B, Sun M, Dong W, Churchill J, Bachinski LL, Wilson CD, Baggerly KA, Yin G, Hayes DN, Wistuba II. Methylation of the candidate biomarker TCF21 is very frequent across a spectrum of early-stage nonsmall cell lung cancers. Cancer. 2011 Feb 1;117(3):606-17.
6. Silva MP, Liu D, Tchinda J, Woods D, Behrens C, Bekele B, Moran C, Lee C, Aster J, Zhou BB, Wistuba I. NOTCH3/JAGGED1 pathway is involved in non-small cell lung cancer pathogenesis and interacts with EGFR pathway. Cancer Research. 2008 May 1;68(9 Supplement):2168.
7. Sun M, Massarelli E, Ozburn N, Tang X, Prudkin L, Komaki R, Hong WK, Moran C, Aldape K, Varella-Garcia M, Wistuba I. EGFR increased copy number is frequent in non-small cell lung cancer with brain metastasis. Cancer Research. 2008 May 1;68(9 Supplement):2163.
8. Tang X, Liu D, Behrens C, He D, Sun M, Rice D, Lee JJ, Hong W, Wistuba I. Abstract# 3841: TITF-1 and EGFR gene copy variations are associated with prognosis for the patients with non-small cell lung cancer. Cancer Research. 2009 May 1;69(9 Supplement):3841.
9. Tang, X., Sun, M., Behrens, C., Prudkin, L., Ozburn, N., Gazdar, A., Moran, C., Varella-Garcia, M. and Wistuba, I., 2008. TITF-1 gene amplification and protein expression pattern

identify adenocarcinoma of lung with worse prognosis. *Cancer Research*, *68*(9 Supplement), pp.4952.
10. Yuan P, Temam S, Ei-Naggar A, Zhou X, Lee J, Mao L. Podoplanin is overexpressed in head and neck squamous cell carcinomas (HNSCC) and is associated with poor clinical outcome. Cancer Research. 2006 Apr 15;66(8 Supplement):1050.

Patent Application:

Staquicini FI, Pasqualini R, Arap W, inventors; The Board of Regents of The University of Texas System, assignee. Compositions and methods related to DNA damage repair. United States Patent Application US 14/343,943. 2012 Sep 14.

CONCLUSIONS

Project 1: We conclude that the epithelial-to-mesenchymal transition (EMT) plays a significant role in governing not just the intrinsic radiosensitivity of NSCLC cells, but also their sensitivity to inhibitors of the epidermal growth factor receptor (EGFR) and the ability of such inhibitors to radiosensitize these cells. It would be useful to assess the EMT status of patients treated with these combinations. In spite of this finding, results suggest that such combinations might be useful in the clinic. In addition, we conclude that targeting other growth factor receptors such as the c-Met and IG-F1R receptors may be an alternative strategy to using EGFR inhibitors.

Project 2: The first cohort of three patients was completed and evaluated. Based on organ dosimetry, the appropriate dose escalation for the next cohort of 6 patients was determined to be no more than 3.78 (+,- 10%) mCi per patient. All required approvals (IRB, IND, HRPO) were obtained to initiate accrual to the second cohort, and 2 additional patients were consented and treated. Analysis of results on these two patients revealed the lack of tumor targeting as well as unacceptable levels of radiation in the liver, GI and gall bladder of the treated patients, leading to the programmatic decision to terminate the trial.

Project 3: The central working hypothesis in our program is that differential protein expression in the human vascular endothelium associated with lung cancer offers the potential for developing novel diagnostic, imaging, and therapeutic strategies. In essence, combinatorial library selections (peptide- and antibody-based) are leveraged to discover, validate, and exploit the vascular biochemical diversity of endothelial cell surfaces towards a new vascular-targeted pharmacology. Such targeting technologies may lead to the development of ligand-directed agents for application in the treatment of cancer patients. Translational applications, such as first-in-human clinical trials, have now began within the institution, as the Food and Drug Administration (FDA) has recently granted a “safe-to-proceed” status for the first vascular-targeted Investigational New Drug, discovered, developed and being evaluated in patients at MDACC. Such trials will ultimately determine the value of this strategy. Two other drugs are in pre-IND stage and several others in pre-clinical laboratory phase. Long-term, the broader vision of the research is a large-scale mapping of receptors in human vasculature towards a new ligand-directed pharmacology.

Project 4: Our results indicate that the adenoviral vector containing a dominant negative FGFR1 receptor construct, which inhibits FGFR signaling, could potentially be useful for treatment of lung cancer *in vivo.* Studies targeting lung cancer with this adenoviral construct are warranted. Such studies could focus on adenovirus delivery by inhalation using an aerosolized preparation. In terms of understanding FGFR signaling, our studies highlighted an important role for Hsp90 as a downstream mediator of FGF effects. This suggests that combined targeting of FGFR signaling (e.g., by AdVDNFR1) and Hsp90 function (e.g., by Geldanamycin or other Hsp90 inhibitors) could provide additive or synergistic efficacy.

Project 5: Everolimus exerts a measurable, dose-dependent biologic activity in NSCLC tumors. 'Window of opportunity' studies in early stage NSCLC provide strong mechanistic insights and may guide development of novel targeted agents.

Project 6: We performed RNA and DNA profiling on available samples to identify genes and genomic regions that are altered in NSCLC and interrogated additional candidate methylatable genes as potential tumor suppressor genes in NSCLC, to identify their potential as biomarkers. These experiments have generated a list of molecular candidate biomarkers for further investigation in larger sample sets.

Biostatistics Core: Core B provided statistical support for Project 2, including the development of relevant statistical methodologies, and final analysis of the clinical trial.

Pathology Core: The Pathology Core has assisted and collaborated actively with several research projects to perform multiple histopathological, immunohistochemical, and genetic studies in a large series of lung cancer tissue, including the collection and processing of prospectively collected samples from two ongoing clinical trials. In addition, the Pathology Core has managed to complete and publish several research activities, which fully integrate with some of the IMPACT research projects. The Pathology Core has successfully fulfilled the goals proposed for the fifth year of the IMPACT program.

DRP1: The amended single arm, open-label study to evaluate the efficacy of ZD6474 on the management of pleural effusion in NSCLC patients was closed on July 19, 2010, with 28 patients enrolled. Using the pleural effusion specimens collected from the 20 evaluable patients, we performed ELISA assays to determine that several CAFs from plasma and pleural effusions were associated with best responses (therapeutic and radiographic).

CDP1: We demonstrated increased expression levels of the RACK1 in tumor tissue in tumor but not normal lung cells, and this increased expression was localized in the tumor cell cytoplasm. RACK1 mediates protein–protein interactions for the regulation of cell motility, in NSCLC, and has interactions with several proteins that have important roles in cell growth and survival, making it a candidate molecule to target as a potential therapeutic strategy for NSCLC. Further extensive studies are warranted to clarify if RACK1 will have utility as a therapeutic target for lung cancer.